

HEMOZOIN: A TARGET-BASED APPROACH TO ANTIMALARIAL DRUG

DISCOVERY

By

Rebecca D. Sandlin

Dissertation

Submitted to the Faculty of the  
Graduate School of Vanderbilt University  
in partial fulfillment of the requirements

for the degree of

DOCTOR OF PHILOSOPHY

in

Chemistry

May, 2013

Nashville, Tennessee

Approved:

David W. Wright

C. Dave Weaver

Brian Bachmann

Walter Chazin

To Timothy Shane Sandlin

## ACKNOWLEDGEMENTS

This work would not have been possible without the financial support of Vanderbilt University, the Department of Defense (W81XWH-07-ACA-0092), NIH (1R01AI083145), the Bill & Melinda Gates Foundation, and the Medicines for Malaria Venture. Furthermore, several collaborative efforts have played an especially important role in the compilation of this work. The staff of the Vanderbilt University High-Throughput Screening facility, including Dr. Dave Weaver, Dan Dorset and Lisa Wright was each critical in the stages of assay design, implementation and compound management. While Dr. Jens Meiler and Mariusz Butkiewicz were instrumental in developing a computational model based on the results of our high-throughput screening effort. International collaborators including Dr. Marcus Oliveira, Dr. Timothy J. Egan, Aneesa Omar, Kathryn Wicht and Renata Steibler have contributed to both the conception and execution of this work.

I would like to thank all who have served as my educators, labmates and friends throughout my academic career. I began at Volunteer State Community College. I would like to thank Dr. Chuck Snelling for being an excellent mentor. He was the first real scientist I had ever met and was always available to discuss science in general. As an undergraduate at Western Kentucky University, I worked under the advisement of Dr. Kevin Williams. Looking back, Dr. Williams was the most influential mentor in my research career. I was a clueless undergrad. Patiently, he taught me basic laboratory skills and allowed me to work on several research projects. My work in his lab solidified

my desire to continue onto a research career and I am very thankful for that. I would also like to thank Dr. Don Slocum and Dr. Paul Whitley for my research experience at WKU.

My graduate PI, Dr. David Wright, has been the mentor I needed. He never made it easy for me, but because of this, I learned which questions I needed to ask myself while analyzing data. He also taught me not to panic when data doesn't tell me what I expect. I now know that I just need to think a little harder and I will figure things out. He also very patiently read 17 drafts of my first manuscript. During my time in his lab, my coworkers have become my friends. The work environment could not have been better. My first interactions in this lab were with Dr. Melissa Carter. I didn't know what an assay was until I met her. Then I met Dr. Anh Hoang. Anh is now my best friend and we will soon be reunited when I start my postdoc. She has been a great mentor in both my research efforts and more importantly in my personal life. I hope we find faculty positions in close proximity one day. Kim Fong joined the lab less than a year ago and will be my replacement. She was the perfect scientist to begin the complex biological experiments now required to advance our project. Plus she has been a great baymate and friend. Stephen Jackson joined the Wright lab the same year as I did. His criticisms during my practice talks were constructive and extremely helpful. He has also been a great friend. Nick Adams, who along with Stephen and me completes the inner circle, questions every scientific statement that comes out of my mouth. While this can be exhausting, he always asks the questions that I never asked myself. In doing so, he guides me to think more critically about my research project and I am thankful for that. Keersten Davis, Jenny Nesbitt and Chris Gulka have worked near my bench for several years. We have spent countless hours in deep conversations and debates and it has made

my time at Vandy very enjoyable. Though I don't request it, Holly Carrell is always thoughtful enough to bring foods that I will eat and I believe this demonstrates her kindness. She is an excellent baker! Dr. Joseph Conrad, Anna Bitting, Abraham Wang and Adam Ryan Travis are newer additions to our lab and I have enjoyed my time working with each of them.

The primary reason I have had the opportunity to dedicate my time to education is the support of my husband, Shane. He has been willing sacrifice his own career so that he could be close to me. He has supported me both financially and emotionally throughout undergraduate and graduate school. He constantly pushes me to work harder and reminds me to 'focus'. He has also been a great example of how hard work and dedication in your career can pay off. I am fortunate to have met such a supportive partner and I am grateful for the love and patience he has extended to me throughout the past 12 years.

## TABLE OF CONTENTS

	Page
DEDICATION .....	ii
ACKNOWLEDGEMENTS .....	iii
LIST OF TABLES .....	viii
LIST OF FIGURES .....	viii
LIST OF SCHEMES .....	x
Chapter	
I. INTRODUCTION .....	1
Hemozoin: Biomineralization in Disease .....	1
Malaria Overview.....	2
Lifecycle of <i>Plasmodium</i> and the Significance of Hemoglobin Degradation ...	3
Characterization of Hemozoin .....	8
$\beta$ -Hematin, Synthetic Hemozoin.....	10
Hemozoin as a Target for the Development of Antimalarials .....	12
Mechanism of Hemozoin Formation.....	13
II. INVESTIGATIONS INTO THE MECHANISM OF HEMOZOIN FORMATION.....	16
Introduction.....	16
Experimental Methods .....	17
Results and Discussion.....	24
Conclusions.....	33
Acknowledgments.....	34
III. DETERGENT-MEDIATED $\beta$ -HEMATIN FORMATION.....	35
Introduction.....	35
Experimental Methods .....	37
Results .....	40
Discussion.....	51
Acknowledgments.....	54
IV. $\beta$ -HEMATIN AS A TARGET FOR HIGH-THROUGHPUT SCREENING.....	55
Background.....	55

Part I. Validation of the NP-40 $\beta$ -Hematin Formation Assay and Results of High-Throughput Screening Campaign .....	57
Introduction.....	57
Experimental Methods .....	60
Results .....	65
Discussion.....	77
Part II. Preliminary SAR Evaluation of Four Scaffolds Identified in the HTS Campaign.....	79
Introduction.....	79
Results .....	80
Conclusions and Future Directions .....	96
Part III. Identification of $\beta$ -Hematin Inhibitors from <i>In Vitro</i> Antimalarial Compounds Identified in Phenotypic Screens .....	99
Introduction.....	99
Experimental Methods .....	100
Results .....	102
Conclusions and Future Directions .....	108
Acknowledgments.....	108
V. APPLICATION OF MACHINE LEARNING TECHNIQUES REVEALS PATHWAY SPECIFIC INHIBITORS FOR $\beta$ -HEMATIN CRYSTALLIZATION IN <i>PLASMODIUM FALCIPARUM</i> .....	110
Introduction.....	110
Experimental Methods .....	113
Results .....	115
Discussion.....	121
VI. FUTURE DIRECTIONS AND FINAL THOUGHTS .....	124
BIBLIOGRAPHY .....	136
Appendix	
A. Identification of Natural Product Extracts that Inhibit $\beta$ -Hematin Formation.....	145
B. Parasite Culturing Protocol.....	153
C. Malaria SYBR Green-I Assay .....	155
D. Full Results of Hits Identified in the HTS Screen .....	158
E. Gametocyte Culturing Protocol .....	183

F. Top 250  $\beta$ -Hematin Inhibitors Identified in the GSK *In Vitro* Antimalarial Library . 180

CURRICULUM VITAE..... 188

## LIST OF TABLES

### Table

1. List of Triton X-Detergents .....	41
2. Half-Life of Detergent Mediated $\beta$ -Hematin Formation .....	47
3. Avrami Constants for Detergent Mediated $\beta$ -Hematin Formation.....	49
4. Control Drugs in the NP-40 $\beta$ -Hematin Formation Assay .....	66
5. Top Ten Potent $\beta$ -Hematin Inhibitors.....	70
6. Top Ten Potent <i>In Vitro</i> Antimalarial $\beta$ -Hematin Inhibitors .....	73
7. $\beta$ -Hematin Inhibitors Identified in the GSK <i>In Vitro</i> Antimalarial Library.....	102
8. Clusters with Enriched Activity .....	104
9. Prioritization of GSK and Novartis Compounds .....	118
10. Resistance Index Values for Hits.....	128
11. List of Natural Products Screened .....	152

## LIST OF FIGURES

1. The Lifecycle of the Malaria Parasite.....	5
2. Intraerythrocytic Stages of Infection .....	6
3. Hemoglobin Digestion in the Malaria Parasite .....	8



4. The Structure of Hemozoin/ $\beta$ -Hematin .....	10
5. Lipid Emulsion Formed by SNLDs .....	18
6. Confocal Orthogonal Projection of Nile Red-labeled SNLD .....	25
7. Optimization of Nile Red-Labeled SNLDs.....	26
8. pH Dependent Quenching of SNLDs .....	28
9. Characterization of $\beta$ -Hematin .....	29
10. Kinetics and Activation Barrier of Neutral Lipid-Mediated $\beta$ -Hematin Formation....	30
11. Differential Scanning Calorimetry Analysis of Neutral Lipids.....	32
12. Optimal Concentration of Detergents for $\beta$ -Hematin Formation .....	42
13. SEM and TEM Images of Detergent-Mediated $\beta$ -Hematin Crystals .....	44
14. Detergent Micelle Size Distribution .....	46
15. Sigmoidal Growth Profile of the Triton X-Detergents .....	48
16. Overlay of the Kinetics Data Fitted to the Avrami Constants.....	50
17. Solubility of Free Heme in Detergents .....	51
18. $\beta$ -Hematin Assay: Checkerboard of Positive and Negative Controls.....	67
19. Thirteen Scaffolds Identified In the HTS Effort.....	74
20. Preliminary SAR Analysis of Four Scaffolds .....	80
21. Triarylimidazole Identified in the HTS Effort .....	81
22. Triarylimidazole Derivatives.....	83
23. Benzimidazole and Benzoxazole Identified in the HTS Effort.....	84
24. Benzimidazole Derivatives with $\beta$ -Hematin Inhibitory Activity .....	86
25. Mechanisms of $\beta$ -Hematin Inhibition.....	87
26. UV-Vis Spectra of Benzimidazole and Heme.....	88

27. Pyridylbenzamide Identified in the HTS Effort .....	89
28. Pyridylbenzamide Derivatives .....	90
29. Hydroxyquinoline Identified in the HTS Effort .....	91
30. Hydroxyquinoline Derivatives .....	93
31. Speciation of Heme.....	94
32. UV-Vis Spectra of Heme in the Presence of Hydroxyquinoline.....	95
33. Representative Compounds from Clusters with Enriched Activity.....	105
34. Heme Speciation Assay Results .....	107
35. ROC Curve Analysis of the QSAR Model .....	117
36. Experimental Evaluation of Selected GSK and Novartis Compounds.....	120
37. Extraction of Quinine from Cinchona Bark .....	146
38. $\beta$ -Hematin Inhibitory Activity of Actinomycete Extracts.....	149
39. Visualization of Extracts Using the Natural Products Software .....	151
40. Microscope Images of Gametocytes.....	182

#### LIST OF SCHEMES

1. Process of Fluorescently Labeling SNLDs .....	21
2. $\beta$ -Hematin Formation Assay Protocol .....	68

## Chapter I

### INTRODUCTION

#### Hemozoin: Biomineralization in Disease<sup>1</sup>

In nature, biomineralization is observed across the entire biosphere. These biologically synthesized materials can consist of carbonate, phosphate, oxalate, silica, iron, gold and many other diverse compositions of organic or inorganic materials. The most well-known examples of biomineralization are those that lend structural support to a species, including the formation of bones in vertebrates and the shells of eggs. The formation of these biominerals generally occurs under physiological conditions in a highly controlled and organized sequence of events. Another biomineral, hemozoin, is a heme crystal synthesized by the malaria parasite as a survival mechanism to escape heme related toxicity. The discovery of this detoxification biomineral actually precedes the discovery of the malaria parasite itself. Although hemozoin has been studied since the 18<sup>th</sup> century, scientists have only begun to obtain a detailed understanding of the structure and formation of this biomineral in the last 25 years. Hemozoin formation is an important drug target in antimalarial drug discovery and development. In fact, chloroquine, arguably the most successful antimalarial developed to date, acts by disrupting formation of hemozoin. Unfortunately, chloroquine is now ineffective as an antimalarial due to the emergence of multidrug-resistant strains of the parasite, though hemozoin remains a viable drug target in antimalarial drug discovery. In order to

develop new antimalarial compounds that target the formation of hemozoin, it is important to have a sound understanding of the formation of this biocrystal.

## Malaria Overview

Malaria is an ancient disease that has affected mankind throughout human history.<sup>2</sup> Malaria is caused by several species of intracellular protozoan parasites of the *Plasmodium* genus. Of this genus, there have been at least 200 species identified. Four species, including *falciparum*, *vivax*, *malariae* and *ovale*, are known to infect humans. However, the primary causative agent of human malaria, *P. falciparum*, is responsible for the vast majority of deaths that occur as a result of malaria. During the mid-1900s, the WHO proposed an ambitious strategy to eradicate malaria worldwide.<sup>3</sup> This eradication campaign dramatically lowered malarial infections worldwide through a combination of vector control methods and drug treatment using the antimalarial chloroquine. In several areas with seasonal transmission or temperate climates, such as Europe and North America, the elimination was successful. Unfortunately, no significant improvements were made in sub-Saharan Africa where over 90% of malaria deaths occur.

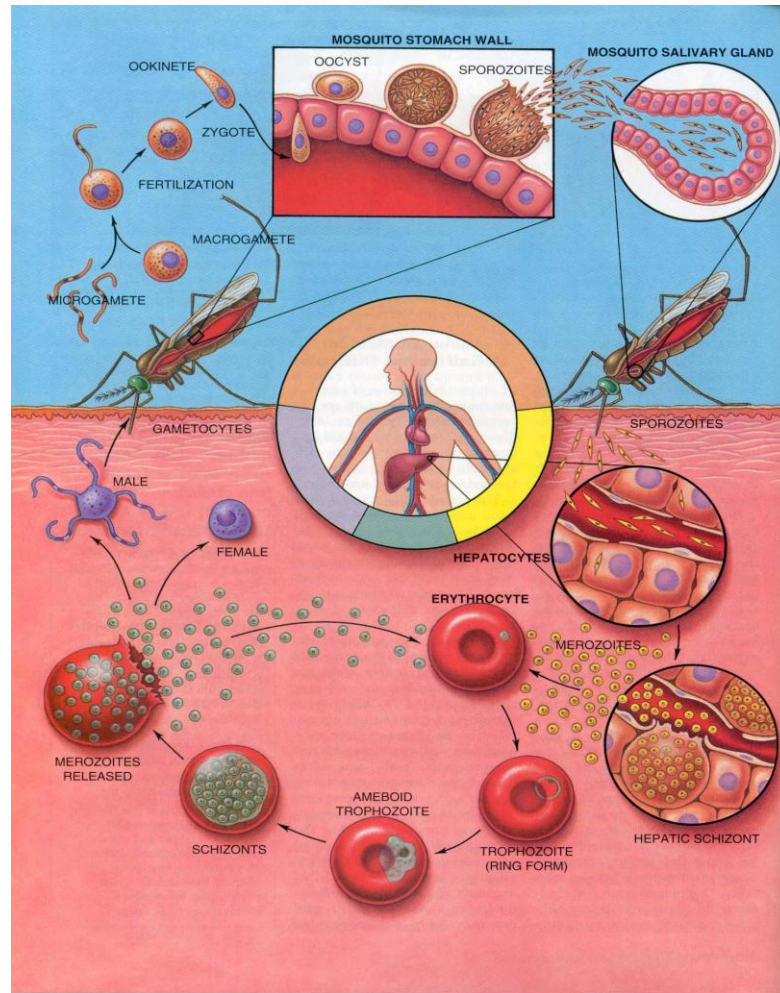
After two decades the focus of these efforts shifted to a less ambitious goal of malaria control due in part to the emergence of chloroquine-resistant parasites and safety concerns with vector control methods. Recently, resurgence in malaria cases has been observed, primarily in underdeveloped, poverty-stricken countries.<sup>4,5</sup> While it has been over 50 years since resistance to chloroquine was first reported, no affordable, widely available replacement has been developed. It is currently estimated that there are over

300 million cases of malaria each year, resulting in nearly one million deaths.<sup>6</sup> The majority of these deaths occur among children under the age of five living in sub-Saharan Africa. The increase of drug-resistant strains of the malaria parasite creates a critical need for the development of new antimalarial treatments.

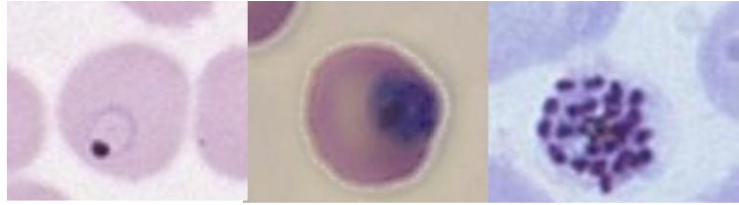
### Lifecycle of *Plasmodium* and the Significance of Hemoglobin Degradation

During the intraerythrocytic stage of infection, the malaria parasite consumes host hemoglobin as a source of amino acids.<sup>7</sup> As a result, toxic free heme is released. In humans, several detoxification mechanisms are in place to protect against the drastic toxic effects of free heme. Primarily, heme detoxification is carried out by the heme oxygenase (HO) systems (HO-1, HO-2 and HO-3), and by extra-HO systems less frequently, including hemopexin and albumin.<sup>8</sup> These HO enzymes play a large role in protecting cells from the oxidative stress caused by free heme by working with NADPH-cytochrome P450 to break down the porphyrin ring into equimolar amounts of free iron, biliverdin, and carbon monoxide.<sup>9</sup> In this process, HO transfers reducing equivalents to the  $\alpha$ -methene bridge of heme from NADPH-cytochrome P-450 reductase to open the tetra-pyrrolic ring, freeing CO and biliverdin. Biliverdin is then converted to bilirubin by biliverdin reductase conjugated to glucuronic acid, and excreted from the body. The HO systems are very efficient at detoxifying free heme and restoring homeostasis in the organisms that have them, but organisms that lack the HO systems have developed alternative mechanisms to protect themselves from free heme toxicity.

One organism lacking a HO system is the parasite responsible for malaria. The lifecycle of the malaria parasite is quite complex (Figure 1). *Plasmodium* sporozoites are transmitted to humans through the saliva of a female *Anopheles* mosquito during a blood meal. Once in the host's bloodstream, sporozoites invade hepatocytes and undergo a phase of growth and differentiation followed by the release of merozoites into the bloodstream. The merozoites then enter host red blood cells, referred to as the intraerythrocytic stage of infection. This stage is characterized by the onset of the symptoms of a malaria infection. Inside the erythrocyte, the parasite goes through three distinct growth phases that can be distinguished under a light microscope (Figure 2). The ring stage is first, lasting about 24 hours. The second stage is the very active trophozoite stage. It is during this stage that most of the erythrocyte cytoplasm is consumed.<sup>7</sup> Third, the parasite undergoes 4-5 cycles of binary divisions, producing merozoites that eventually rupture the red blood cell membrane, and enter the bloodstream to infect new red blood cells. During this intraerythrocytic cycle, the host cytoplasm is consumed, and an estimated 60-80% of available hemoglobin is degraded for use as a nutrient source and to create room for growth.<sup>7</sup> During this degradation process, the amino acids obtained from hemoglobin catabolism are incorporated into *Plasmodium* proteins and used for energy metabolism.<sup>10</sup> The amino acids *Plasmodium* cannot obtain from hemoglobin are readily scavenged from the environment.<sup>11</sup>



**Figure 1.** The lifecycle of the malaria parasite is complex. Upon taking a blood meal, the infected female *Anopheles* mosquito transmits *Plasmodium* into the bloodstream of the human host. The parasite travels to the liver where it matures and differentiates within hepatic cells. Upon rupturing of the hepatic cells, the parasite enters the bloodstream and infects host red blood cells. The parasite can develop into the sexual form (gametocytes) and can be picked up by a feeding mosquito before being transmitted to another human host.<sup>12</sup>

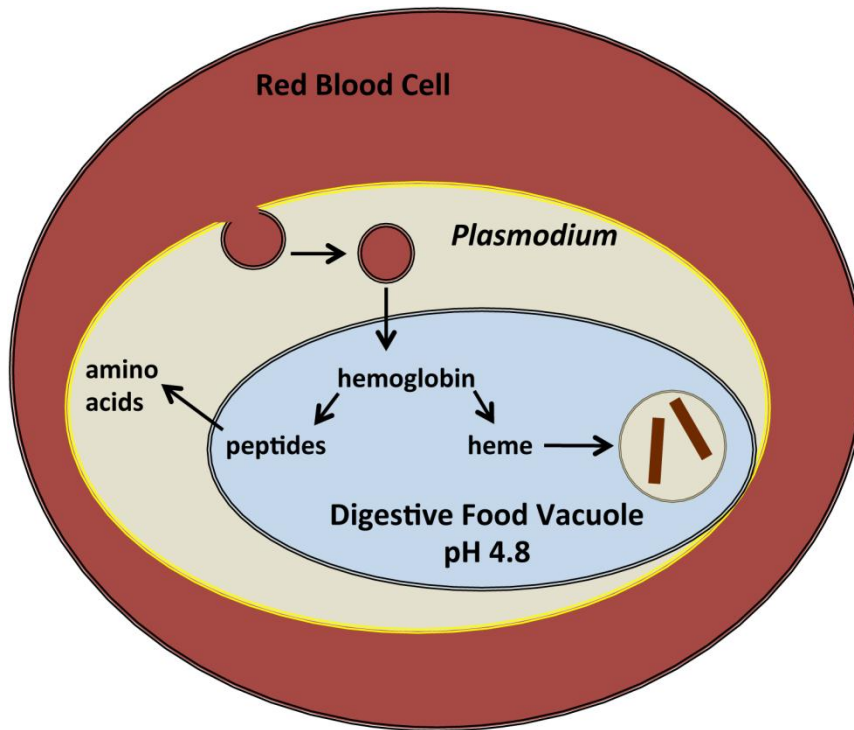


**Figure 2.** During the intraerythrocytic stage of infection, the malaria parasite goes through three distinct growth phases (ring, trophozoite and schizont, respectively) that can be distinguished using a light microscope.

The malaria parasite obtains hemoglobin from the cytosol through invagination of the parasitophorous vacuolar and plasma membrane, creating a double membrane vesicle (Figure 3). These vesicles fuse together, creating a single membrane digestive food vacuole. Once formed, the digestive food vacuole becomes the primary site of hemoglobin digestion. This specialized organelle maintains an acidic environment, estimated pH of 4.8.<sup>11</sup> Inside this organelle, aspartic and cysteine protease activities have been detected that are the primary enzymes responsible for globin proteolysis.<sup>13</sup> Aspartic proteases make up about 60-80% of enzyme activity, while cysteine proteases make up 20-40%. The process of hemoglobin degradation has been found to occur in a specific order, requiring an initial aspartic protease cleavage, followed by secondary aspartic protease and cysteine protease cleavages. Vacuolar degradation produces small polypeptides, but no free amino acids. This suggests that cleavage of the small peptide fragments occurs in the cytoplasm, outside of the digestive vacuole.<sup>14</sup> During this process of hemoglobin degradation, large quantities of free heme are released and can reach concentrations of 400 mM if heme detoxification is prevented.<sup>7</sup> The presence of free heme within the digestive food vacuole has several undesirable consequences. Heme concentrations as low as 10-20  $\mu$ M have been shown to inhibit several proteases present



within the digestive food vacuole including the plasmepsins and falcipains.<sup>15</sup> In addition to inhibiting enzymatic activity, the presence of free heme is detrimental to the stability and deformability of the parasite vacuolar membrane.<sup>16</sup> The resulting hemolysis is likely caused by perturbations to the membrane structure from the insertion of lipophilic heme into the phospholipid bilayer. A further consequence of free heme accumulation is the increase in oxidative stress on the parasite.<sup>17,18</sup> Since the malaria parasite does not have HO like vertebrates, the parasite detoxifies free heme by converting soluble, toxic free heme into an insoluble, nontoxic crystal called hemozoin. This process is essential to parasite survival, as inhibition of hemozoin formation results in parasite death.<sup>7,18</sup> Indeed, the most successful antimalarial ever developed, chloroquine, has been shown to inhibit this detoxification pathway supposedly by binding free heme and preventing its insertion into the growing hemozoin crystal.<sup>19,20</sup> Unfortunately, due to resistance mechanisms developed by the parasite, chloroquine no longer has clinical efficacy. However, hemozoin remains a valid drug target as resistance is a result of efflux, and resistant strains of the parasite still produce hemozoin normally.<sup>21-24</sup> Therefore, it is essential that the formation of this biocrystal is better understood in order to promote the discovery of new antimalarials that target hemozoin formation.

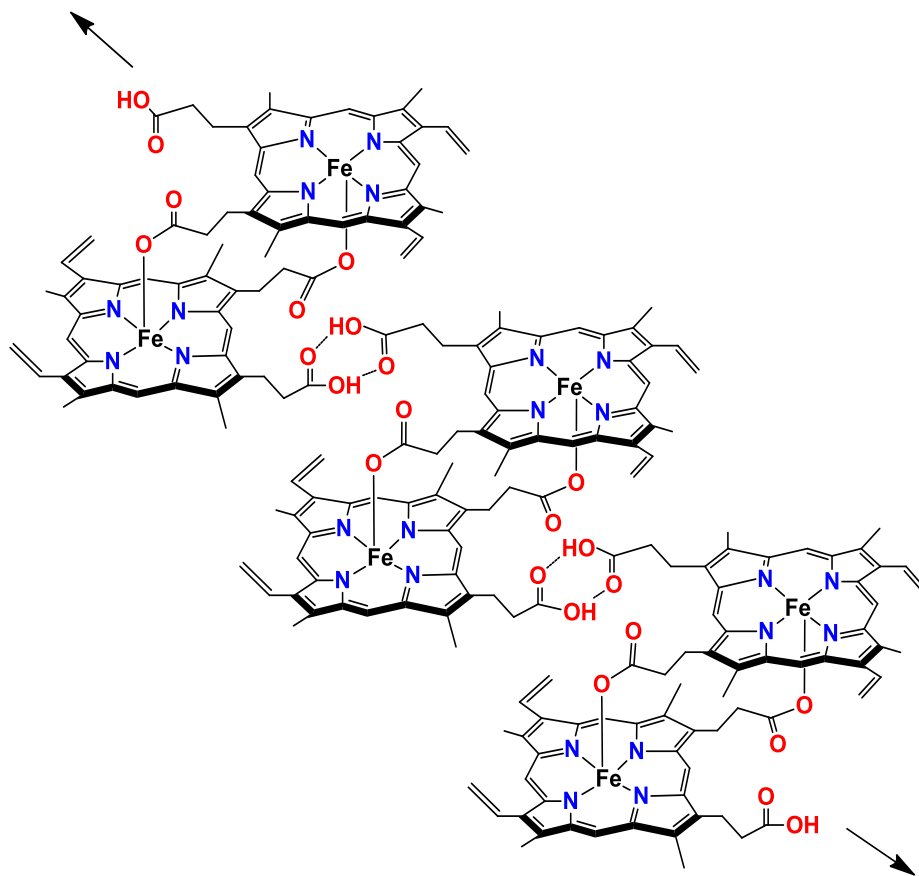


**Figure 3.** Within the erythrocyte, the malaria parasite relies on host hemoglobin as a source of amino acids. Hemoglobin degradation occurs within an acidic organelle known as the digestive food vacuole. Here, hemoglobin is degraded by proteolytic enzymes. As a consequence, toxic free heme is released. In order to survive, the toxic free heme is sequestered into a biomineral known as hemozoin. Hemozoin is shown above as brown rods, encapsulated within a neutral lipid droplet, the suspected site of heme crystallization.

### Characterization of Hemozoin

Lancisi reported the discovery of hemozoin, the dark brown-black malarial pigment, in 1717.<sup>25</sup> As these deposits are quite pronounced in the brains, spleens and livers of malaria victims, the discovery of hemozoin actually precedes the discovery of the malaria parasite itself by over 150 years. For many years, it was hotly contested as to whether or not pigment was the actual cause of malaria, but in 1890, Golgi presented a

photograph of a pigmented parasite in the blood of a malaria patient, forging the connection between hemozoin and malaria.<sup>26</sup> The composition and structure of hemozoin remained a subject of intense debate until 2000 when X-ray powder diffraction methods were used to identify the structure of  $\beta$ -hematin, the synthetic equivalent of hemozoin.<sup>27</sup> Once thought to consist of polymeric strands of O-Fe(III) linked heme units, XRD revealed a centrosymmetric triclinic unit cell comprised of reciprocal head-to-tail dimeric units of heme bound through propionate O-Fe(III) with a bond distance of 1.866(2) Å (Figure 4). The propionic acid groups of the heme dimer then hydrogen bond with other dimers to form the extended crystal. Morphologically,  $\beta$ -hematin and hemozoin crystals are needle-like and vary in size from several hundred nanometers to  $\sim 1 \mu\text{m}$ .



**Figure 4.** The structure of hemozoin/ $\beta$ -hematin. The unit cell is composed of head-to-tail dimers of heme bound through propionate O-Fe(III). The extended crystal is then formed from hydrogen bonding of the propionic acid groups of neighboring dimeric units.

#### Synthetic Hemozoin, $\beta$ -hematin

Understanding the mechanism by which the parasite converts soluble, toxic free heme into an insoluble and non-toxic crystal is valuable for antimalarial drug-discovery, as perturbations to this crystallization process can result in parasite death. However, studying the formation of hemozoin *in vivo* has proven challenging to researchers.  $\beta$ -hematin, the abiological version of hemozoin, has been utilized as a tool to study

hemozoin formation *in vitro*. For such comparisons to be meaningful, it had to be unequivocally established that these entities are isostructural. Chemical, spectroscopic, and crystallographic evidence have been used to conclude the similarity of these two materials.

Chemically, both hemozoin and  $\beta$ -hematin are composed of insoluble, head-to-tail dimers of Fe(III)PPIX (Figure 4).<sup>27-29</sup> Spectroscopically, the similarity of hemozoin and  $\beta$ -hematin dimeric units can be confirmed from the infrared spectrum, that exhibits fingerprint vibrations around 1664 and 1211  $\text{cm}^{-1}$  corresponding to the C=O and C-O stretching from coordination of the propionate O atom to the Fe(III) metal center of the neighboring heme molecule.<sup>29</sup> Furthermore, the Fe(III) spin state of each species is identical, confirmed by variable temperature EPR that has shown that both  $\beta$ -hematin and hemozoin exist in the high spin  $S=5/2$  state, a paramagnetic complex.<sup>30</sup> This observation is in agreement with Mössbauer data where the isomer shift and quadrupolar splitting values suggest that the Fe(III) exists in a high-spin state. Morphologically, SEM images reveal that both BH and hemozoin are composed of needle-like crystals with tapered habits. The crystal structure of each species is nearly identical. Synchrotron x-ray powder diffraction patterns have demonstrated that the crystal structure of hemozoin is identical to its synthetic counterpart. However, a more recent study suggests hemozoin may contain slightly more disorder in the Fe-O bonds than  $\beta$ -hematin formed under nonaqueous equilibrium conditions.<sup>31</sup>

## Hemozoin as a Target for the Development of Antimalarials

The malaria parasite contains several unique metabolic pathways that may be exploited for the discovery of new antimalarials. These include targeting the synthesis of DNA precursors, fatty acid synthesis, glycolysis, and de novo heme biosynthesis, among others.<sup>32-34</sup> Of relevance here, however, is inhibition of the formation of hemozoin. One of the earliest effective treatments for malaria dating from the 17<sup>th</sup> century was prepared from bark of *Cinchona* spp.<sup>35</sup> The most active component of “Jesuit’s bark” was later identified as quinine, a potent inhibitor of  $\beta$ -hematin formation. Chloroquine, arguably the most successful antimalarial developed to this day, is an analogue of quinine and is thought to share a similar mechanism of action: inhibition of hemozoin formation.<sup>36</sup> Unfortunately, the efficacy of chloroquine has widely diminished in endemic areas due to rampant drug resistance. These resistant strains of *P. falciparum* exhibit several mutations in the *Plasmodium falciparum* chloroquine resistance transporter (PfCRT), a transmembrane vacuolar protein.<sup>22</sup> In resistant strains the accumulation of chloroquine within the digestive food vacuole is significantly less than in wild-type strains, as it is actively transported out of the digestive food vacuole.<sup>37</sup> Nevertheless, hemozoin formation remains a valid drug target, as resistance is the result of diminished vacuolar accumulation of chloroquine, rather than changes to the hemozoin formation pathway itself. Importantly, the interactions of hemozoin and antimalarial inhibitors of this pathway have been studied in great detail, lending a wealth of information that can facilitate the drug discovery process. In utilizing hemozoin formation as a drug target, it

is important to gain insights regarding the mechanism of hemozoin formation utilized by the parasite.

### Mechanism of Hemozoin Formation

The identification of the biological mediator responsible for hemozoin formation has been a topic of intense debate. Proteins, membrane lipids and neutral lipids extracted from the *Plasmodium* parasite have each shown to mediate  $\beta$ -hematin formation *in vitro*. Indeed, many biological components within parasite lysates are quite capable of promoting the formation of  $\beta$ -hematin *in vitro*. One of the earliest studies of these lysates was conducted by Slater and Cerami who examined trophozoite extracts.<sup>38</sup> The formation of  $\beta$ -hematin in the presence of these extracts was dependent on pH, time and concentration. The authors concluded that the presence of an enzyme, a heme polymerase, was responsible for mediating the formation of  $\beta$ -hematin, as activity of these lysates was sensitive to both heat and treatment with 1% SDS. However, subsequent work contradicted this hypothesis, demonstrating that heat treated parasite lysates retained activity and therefore are not dependent on the presence of an enzyme.<sup>39</sup> It was suggested that  $\beta$ -hematin formation in these experiments was actually due to the presence of hemozoin crystals within the lysates. In fact, the authors showed that preformed  $\beta$ -hematin crystals were sufficient to seed the process of crystallization *in vitro*. While these studies demonstrated that an enzyme is not necessary for hemozoin formation, the mechanism of hemozoin crystallization remained unanswered.

Polar membrane lipids were also implicated as a possible mediator of hemozoin formation. Bendrat *et al.* first implicated these polar lipids when acetonitrile extracts of authentic hemozoin were found to promote the formation of  $\beta$ -hematin.<sup>40</sup> MS analysis of these extracts identified the presence of the methyl esters of oleic, palmitic and stearic acids and low yields of phospholipids within the active fractions. Further, it seemed that these studies were in agreement with a previously published TEM image of an intact parasite showing aligned parallelepiped crystals of hemozoin present within the digestive food vacuole of the parasite. These observations supported the hypothesis that crystallization occurs via epitaxial nucleation of hemozoin at the lipid layer of the vacuolar membrane.<sup>41</sup> Despite the strength of this argument, it was later revealed that axenic parasite cultures lacking a parasitophorous vacuolar membrane still produce hemozoin, ruling out any role for these membrane lipids in the parasite's mechanism of heme detoxification.<sup>42</sup> While these polar membrane lipids are capable of promoting  $\beta$ -hematin formation *in vitro*, they are not responsible for the *in vivo* formation of hemozoin.

More recently, the focus has shifted to the role played by neutral lipids in the process of hemozoin formation. Neutral lipid droplets (also called neutral lipid particles, bodies or nanospheres) can be found concentrated within the digestive food vacuole of the parasite and are located in close proximity to crystals of hemozoin.<sup>43,44</sup> These lipid droplets were subsequently extracted from the parasite by Sullivan and coworkers and found to consist of a mixture of mono and di-acylglycerols.<sup>43</sup> Further, molecular dynamic simulations have demonstrated that the lipophilic environment of the lipid body would serve to stabilize the hemozoin precursor dimer and that formation of hemozoin



would be favored at the lipid/aqueous interface.<sup>45</sup> However, the precise details regarding the mechanism of hemozoin formation have yet to be determined.

## Chapter II

# INVESTIGATIONS INTO THE MECHANISM OF HEMOZOIN FORMATION<sup>122</sup>

### Introduction

The mechanism by which the parasite converts soluble, toxic free heme into an insoluble, inert crystal has been the topic of intense debate. Although hemozoin has been studied since the 18<sup>th</sup> century, scientists have only begun to obtain a detailed understanding of the structure and formation of this biomineral in the last 25 years. Hemozoin formation is an important drug target in antimalarial drug discovery and development. Therefore, understanding the mechanism by which hemozoin formation occurs within the parasite is valuable for the development of new antimalarials that target this parasite-specific pathway.

Proteins, membrane lipids and neutral lipids extracted from the *Plasmodium* parasite have each shown to mediate  $\beta$ -hematin formation *in vitro*.<sup>39,40</sup> Indeed, many biological components within parasite lysates are quite capable of promoting the formation of  $\beta$ -hematin *in vitro*. Recently, the focus has shifted to a role for neutral lipid droplets (NLDs, also known as neutral lipid particles/bodies or neutral lipid nanospheres) in the process of hemozoin formation. TEM images have revealed that these NLDs are concentrated within the digestive food vacuole of the parasite and are located in close proximity to crystals of hemozoin.<sup>44</sup> These NLDs were extracted from the parasite and characterized by Sullivan and coworkers in 2007.<sup>43</sup> Analysis of these lipid droplets by

mass spectrometry identified a specific blend of monostearic, monopalmitic, dipalmitic, dioleic and dilinoleic glycerols in a 4:2:1:1:1 ratio, referred to as the “lipid blend”. *In vitro* studies have further shown that a solution containing these neutral lipids support the conversion of free heme to  $\beta$ -hematin.<sup>43,46</sup>

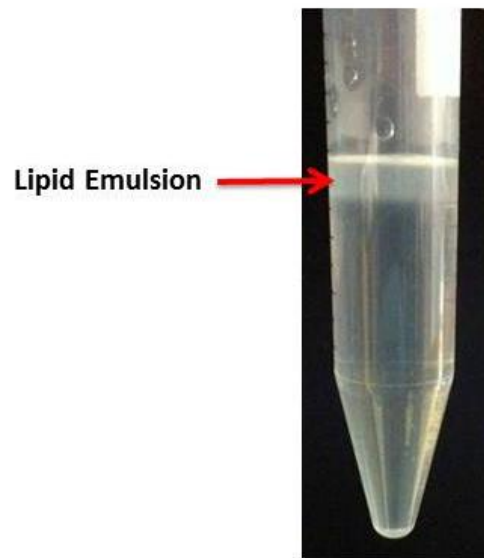
Many lipophilic mediators of *in vitro*  $\beta$ -hematin formation have been identified including lipophilic extracts from the parasite as well as lipophilic detergents and solvents.<sup>40,47,48</sup> It has been estimated that the maximum half-life required for hemozoin formation must be no more than 40 minutes in order for the parasite to escape free heme toxicity.<sup>49</sup> Therefore, if the NLD is the site of hemozoin formation, then it must be capable of promoting the formation of hemozoin at a kinetically competent rate. Here, a system of studying synthetic NLDs (SNLDs) is utilized in a physiologically relevant context to 1) examine the interactions that occur between SNLDs with free heme and 2) determine if SNLDs are a kinetically competent site for  $\beta$ -hematin formation.

## Experimental Methods

### Preparation of SNLDs

A 50 mM citric acid buffer was prepared. The pH was adjusted to 4.8 using sodium hydroxide pellets. Five lipid components were obtained for these studies: *rac* 1-monopalmitoylglycerol (MPG), *rac* 1-monostearoylglycerol (MSG), 1,3-dioleoylglycerol (DOG), 1,2-dipalmitoylglycerol (DPG) and 1,3-dilinoleoylglycerol (DLG). Each lipid was prepared at a 16.2 mM stock concentration by solubilizing the lipid in a 1:9 acetone/methanol solvent system. The “lipid blend” refers to the biological lipid

components found to comprise the NLDs within the digestive food vacuole of the parasite (4:2:1:1:1 ratio of MSG:MPG:DOG:DLG:DPG prepared at final concentration of 16.2 mM lipid content). Citric buffer (5 mL) was added to 15 mL Falcon polypropylene conical tubes and allowed to equilibrate in a water bath for 15 min. A 200  $\mu$ L aliquot of stock lipid was then carefully deposited onto the surface of the citric buffer using a 22.5 gauge needle. The tubes were not disturbed following addition of the lipid. If deposited carefully and correctly, the lipids will form an emulsion (Figure 5). As the lipids' environment becomes dominantly aqueous, the molecules aggregate in the form of solid particles. As the organic solvent system becomes primarily aqueous, the solubilized neutral lipids spontaneously form SNLDs in order to maximize lipophilic interactions.



**Figure 5.** The lipid emulsion (red arrow) containing SNLDs is formed after carefully depositing solubilized neutral lipids in acetone/methanol onto the aqueous surface in a 5 mL Falcon tube.

### Kinetics of $\beta$ -Hematin Formation

Fe(III)PPIX (heme) stock was prepared by solubilizing 2 mg of heme in 0.4 mL of 0.1 M NaOH. This solution was then vortexed thoroughly to solubilize free heme. Next, 0.6 mL of a 1:9 acetone:methanol solution was added so that the final concentration of heme stock was 2 mg/mL. To generate a lipid:heme stock, 2  $\mu$ L of heme stock is added to 200  $\mu$ L of lipid stock followed by vortexing for 5 sec. This “premix” is then pre-warmed and carefully added to the surface of the citric buffer as described above.  $\beta$ -hematin formation was analyzed using the pyridine-ferrochrome method developed by Egan and coworkers.<sup>50</sup> A solution of 50% pyridine, 20% acetone, water and 200 mM HEPES buffer (pH 7.4) was added to each tube followed by vortexing. The final concentration of pyridine was 5%. Each tube was then centrifuged at 3500 rpm for 10 min to remove precipitated lipids. 200  $\mu$ L was then transferred to a clear bottom microtiter plate and was then read at 405 nm on a Biotek H4 plate reader.

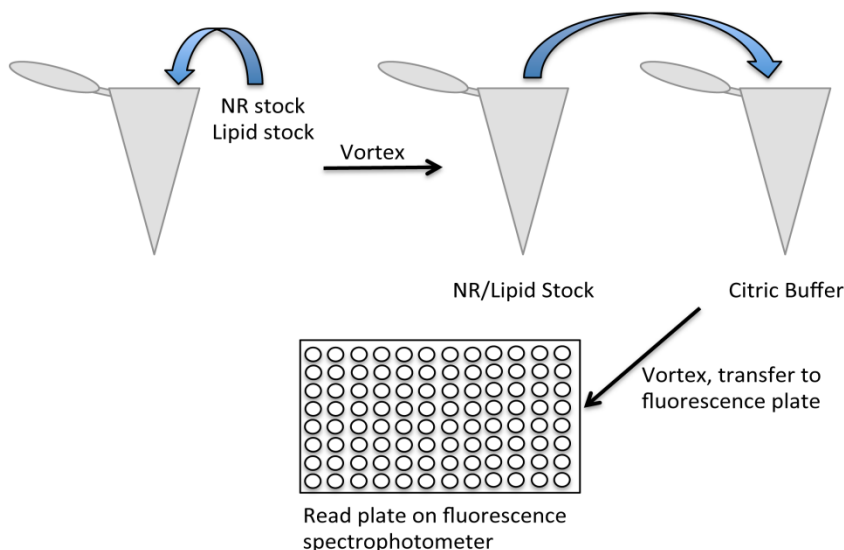
### Linear Range of Nile Red

The linear range of Nile Red (NR) signal in acetone was established using a Varian Cary Eclipse fluorescence spectrophotometer. Excitation/emission wavelengths of 545/605 were used with 10 nm slit widths. A stock concentration of 20  $\mu$ M NR in acetone was prepared in a 5 mL falcon tube placed in an ice bath in order to limit the evaporation of acetone. NR was added to a 96-well black fluorescence plate in a concentration range from 0-20  $\mu$ M. Acetone was used to correct for volume differences. The plate was quickly read to establish the linear range of NR signal. An optimal concentration of 3.3  $\mu$ M NR was established.

### *Interactions Occurring Between Heme and Nile Red*

A stock of 3.3  $\mu\text{M}$  NR was prepared in acetone and added to a black fluorescence plate as described above. A 2 mg/mL solution of heme was prepared in 2:3 ratio of 0.1M NaOH:acetone. This heme stock was titrated into the microtiter plate (0-500  $\mu\text{M}$ ) containing NR. The plate was allowed to sit on ice for 2 minutes then quickly read to quantitate NR signal quenching as a function of free heme concentration.

This procedure was then adapted to incorporate SNLDs into the system (Scheme 1). A solution of 100:1 neutral lipid blend: NR was prepared (as suggested by literature methods) and briefly vortexed. This stock (60  $\mu\text{L}$ ) was then added citric buffer and vortexed briefly before adding the solution to a 96-well fluorescence plate. Since NR fluorescent signal is quenched by water, the only signal observed in this sample is SNLD-associated NR. Next, the wells were titrated with free heme stock in a concentration range from 0-500  $\mu\text{M}$ . Since the NR signal is associated with SNLDs, then any quenching of the fluorescent signal would suggest heme is in close proximity with the SNLDs.



**Scheme 1.** SNLDs were labeled with NR and combined with a pH 4.8 citric buffer then added to a fluorescence plate. Following addition of the NR-labeled SNLDs to the plate, a heme titration was performed to monitor interactions occurring between heme and the SNLDs (heme was shown to quench NR signal).

### Characterization of SNLDs using Confocal Microscopy

The morphology of the SNLDs was observed using confocal microscopy. A 1 mL solution of NR-labeled SNLDs was prepared in a 100:1 ratio of lipid blend: NR as described above. The stock was briefly vortexed and 168.5  $\mu\text{L}$  was transferred and diluted with citric buffer (50 mM, pH 4.8) to 1 mL total volume and vortexed briefly. The final concentration of lipid in this solution was 300  $\mu\text{M}$ . From this NR-labeled lipid blend stock, 180  $\mu\text{L}$  was transferred to a glass bottom microwell dish (MatTek Corporation, 14 mM microwell dish). Confocal measurements were made using a Zeiss LSM 510META upright confocal microscope with a 63x oil immersion objective. A 488 nm argon laser with 505-550 nm band pass filter was used for imaging. Z-stacking was

performed to examine the interior of the SNLDs to ensure that they were continuous throughout.

#### *Partitioning of Free Heme into SNLDs*

A confocal microscope was used to analyze the interactions that occur between the SNLDs and free heme in real-time. SNLDs were labeled with NR and transferred to a microwell dish in the manner described in the previous section. Next, 20  $\mu\text{L}$  aliquots of heme stock were carefully added every 30 seconds to the surface of the microwell dish containing the NR-labeled lipid blend until quenching was observed. Extreme care was taken to not disturb the SNLDs in the focal plane. A time series application was used to monitor changes in NR fluorescence every ten seconds. Z-stacking was used at the beginning and end of the experiment to ensure that the lipids had not been displaced as a result of heme titration. Proper controls were utilized to ensure photobleaching did not play a major role in NR quenching.

#### *Characterization of SNLDs using Dynamic Light Scattering*

Dynamic Light Scattering (DLS) was used in order to establish the size distribution of SNLDs. Following deposition of the lipid stock onto the surface of the citric buffer, the system was allowed to equilibrate for a period of time (5, 20, 40, and 60 min, 37°C) resulting in the formation of a lipid emulsion (Figure 5). A pipette was then used to carefully transfer 500  $\mu\text{L}$  of the lipid emulsion to a cuvette and analyzed using a Malvern Zetasizer with a lower limit of 0.1 nm and an upper limit of 6  $\mu\text{m}$ . Each



measurement was repeated in triplicate to monitor the stability and size distribution of these SNLDs as a function of incubation time.

#### Differential Scanning Calorimetry

Each lipid was weighed with a microbalance (2.4 – 3.2 mg samples). Samples were sealed in aluminum capsules and analyzed over a temperature range from 80° to -80°C using a TA Instrument DSC Q200. A cooling rate of 10°C/min and heating rate of 15°C/min was used to measure exothermic and endothermic peaks.

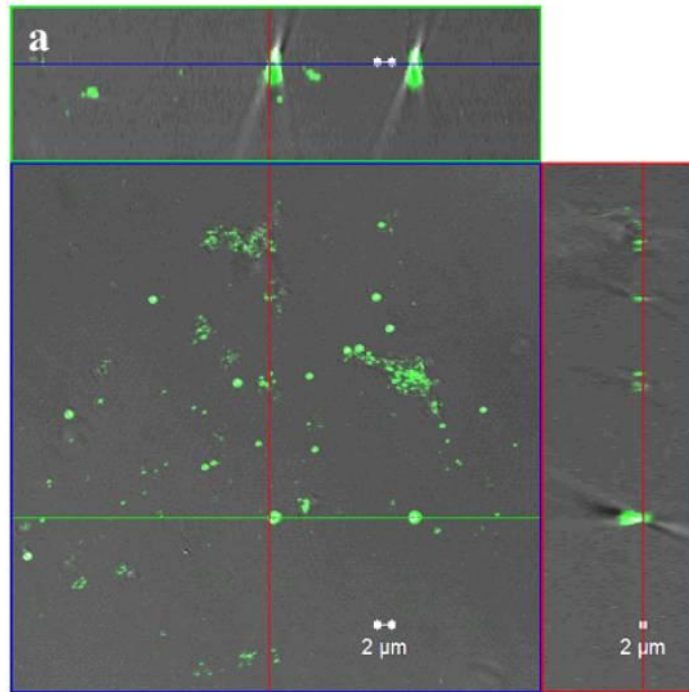
#### Characterization of $\beta$ -Hematin

Product obtained from the kinetics experiments was characterized to confirm that the product formed was  $\beta$ -hematin. Prior to characterization, the product was washed thoroughly with 5% pyridine to remove free heme contamination. pXRD was conducted using Cu K $\alpha$  radiation ( $\lambda = 1.541 \text{ \AA}$ ), with data collection on a Philips PW1050/80 vertical goniometer in the  $2\theta$  range of 5–40°. Scanning electron microscope (SEM) images were obtained using a Hitachi S-4200 instrument to confirm the crystal habit of the product was similar to hemozoin.

## Results and Discussion

### Characterization of SNLDs

The SNLDs were produced by depositing solubilized neutral lipids onto the surface of a buffer under physiologically relevant pH (4.8) and temperature conditions (37°C) in order to mimic the NLDs observed within the digestive food vacuole of the parasite. Under these conditions, a lipid emulsion spontaneously forms (Figure 5). The resulting emulsion was characterized to establish the size, stability and morphology of the SNLDs. Upon generating the lipid emulsion, particle size was measured using DLS for 1 h in 20 min intervals. The DLS measurements revealed two distinct populations of particles - the largest population of SNLDs was ~50-200 nm in diameter, with a smaller population of ~1-10  $\mu\text{m}$  in diameter. The stability of this size distribution was found to be stable. Confocal imaging of the Nile Red (NR) labeled SNLDs visually confirms the presence of spherical particles that range from approximately one hundred nanometers to a few micrometers in diameter. Orthogonal projections reveal that the particles have a spherical morphology and are continuous (not hollow) (Figure 6). These observations are in agreement with the characterization of the NLDs found within the digestive food vacuole of the parasite.<sup>44</sup>

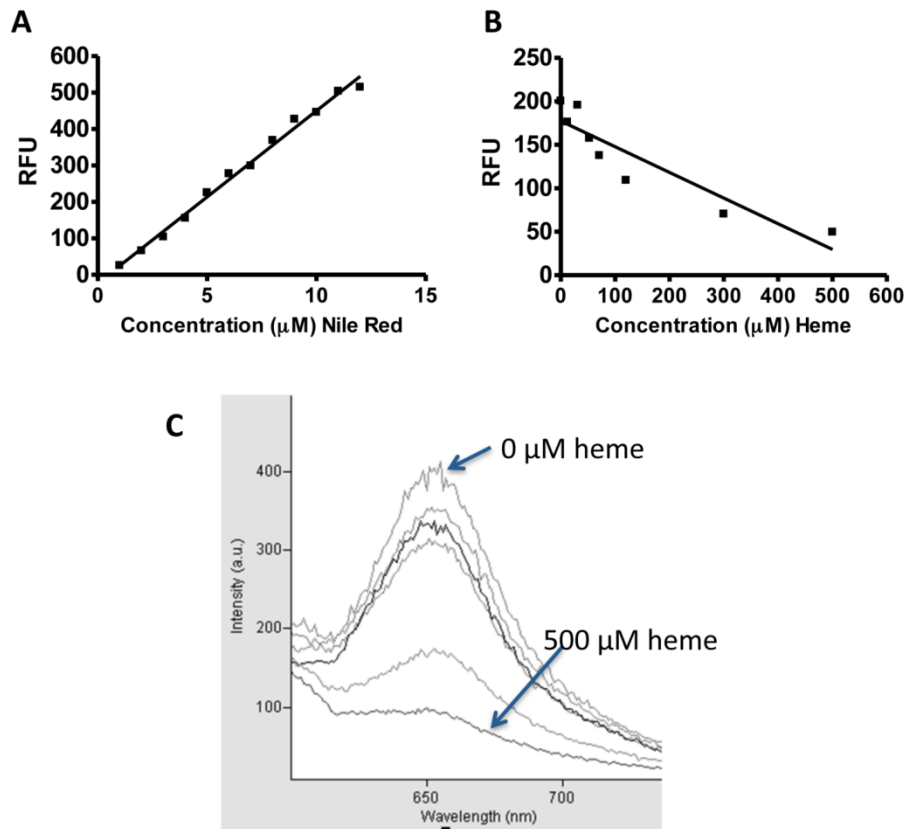


**Figure 6.** Orthogonal projections of NR-labeled SNLDs reveals the presence of spherical, continuous particles.

#### *Interactions Occurring Between Free Heme and Nile Red*

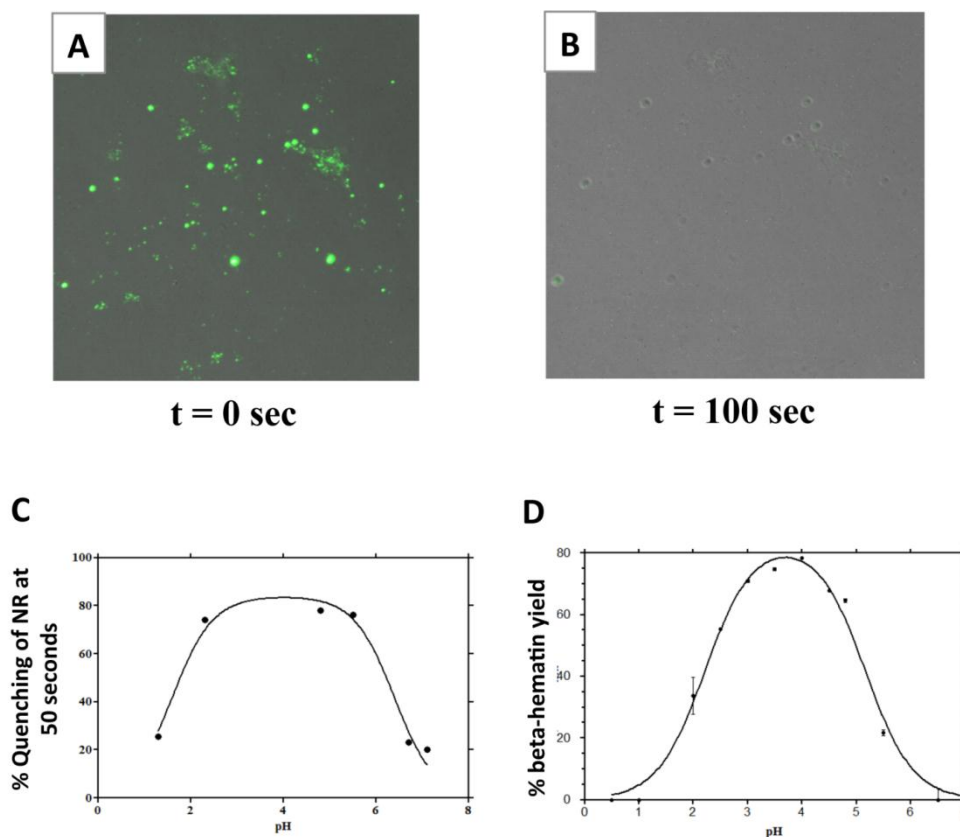
If the digestive vacuole-associated NLDs are indeed the mediator of hemozoin formation utilized by the parasite, then it would follow that free heme would interact with these lipids. To examine these interactions, the fluorescent probe, NR, was utilized. Fluorescence calibration measurements revealed a linear relationship between the concentration of NR and measured fluorescence intensity (Figure 7A) and revealed the linear range of NR signal intensity. Using this fluorescent property, we then explored the interactions that occur between free heme (in a lipophilic solvent) and NR and revealed that heme quenches NR in a concentration-dependent manner (Figure 7B). Addition of  $\beta$ -hematin did not quench the NR signal. Next, NR-labeled SNLDs were generated under

physiologically relevant pH conditions and titrated with free heme (Scheme 1). Under these conditions, NR that exists in the bulk aqueous solution is quenched, and the observed fluorescent signal is a result of NR enveloped within the SNLDs. Upon addition of free heme, the NR signal is quenched, indicating the association of heme with the SNLDs (Figure 7C).



**Figure 7.** (A) Fluorescence calibration measurements revealed a linear relationship between the concentration of NR and measured fluorescence intensity. (B) A 3.3  $\mu\text{M}$  solution of NR in acetone was titrated with heme. Fluorescence quenching was observed. (C) NR-labeled SNLDs were titrated with free heme. Fluorescence quenching of NR was observed as a function of increasing heme concentration.

To further examine NR/heme interactions in real-time, confocal microscopy was employed to visualize the transport and partitioning of free heme into the SNLDs. We observed that upon careful addition of 20  $\mu$ L aliquots of heme, the fluorescent signal of the SNLDs are rapidly quenched throughout (Figure 8A,B). Z-stacking measurements confirmed that the quenching not only occurred on the surface of the SNLDs, but occurred within the interior of the lipid droplet as well. As crystals of hemozoin have no effect on NR signal, these observations would suggest that free heme rapidly partitions into the SNLDs *prior* to crystallization. The partitioning of heme into the SNLDs was pH dependent in a manner that mirrors the pH-dependence of  $\beta$ -hematin formation (Figure 8C,D). The notion that NLDs serve as a reservoir for free heme are supported by previous reports that indicate these lipids may help protect heme from peroxide degradation, which would lead to parasite toxicity.<sup>43</sup> In the absence of these lipids, a 50 mM H<sub>2</sub>O<sub>2</sub> solution degraded 50% of dilipidated hemozoin, while a 90 mM concentration of peroxide was necessary to reduce encapsulated hemozoin by 50%, suggesting that the lipids serve as a protective reservoir for free heme preceding its incorporation into the nontoxic hemozoin crystal.

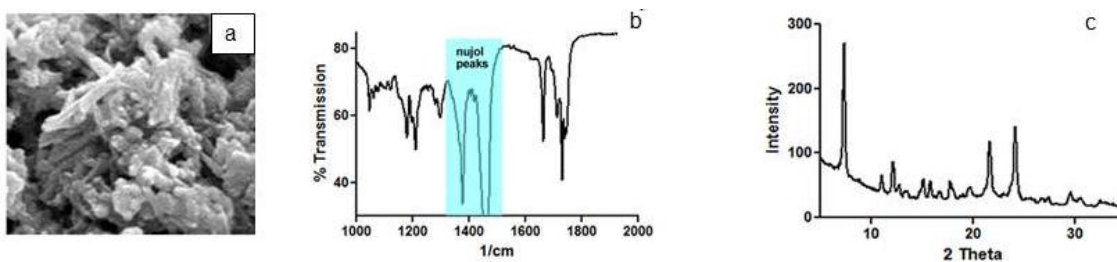


**Figure 8.** (A) NR-labeled SNLDs (B) Fluorescence/DIC overlay of NR-labeled SNLDs demonstrate that heme-quenching is observed throughout the lipid bodies. (C) Fluorescence quenching of NR-labeled SNLDs occurs in a pH dependent process, mirroring the observed (D) pH dependence of  $\beta$ -hematin formation. *Data in (D) was obtained by Dr. Anh Hoang*

### Characterization of $\beta$ -Hematin

Morphological and structural analysis of the product collected from depositing a solution of the lipid blend and heme to an aqueous surface confirmed the formation of  $\beta$ -hematin. SEM imaging of the product obtained revealed needle-like crystals resembling hemozoin in their crystal habit (Figure 9a). Infrared spectra (Fig 9b) of the product displayed prominent IR peaks at  $1662\text{ cm}^{-1}$  and  $1210\text{ cm}^{-1}$ , indicating the formation of the C=O stretching vibration and the C-O stretching vibration of hematin linked dimers.

These findings are confirmed by XRD (Fig 9c) showing the expected diffraction peaks of  $\beta$ -hematin.



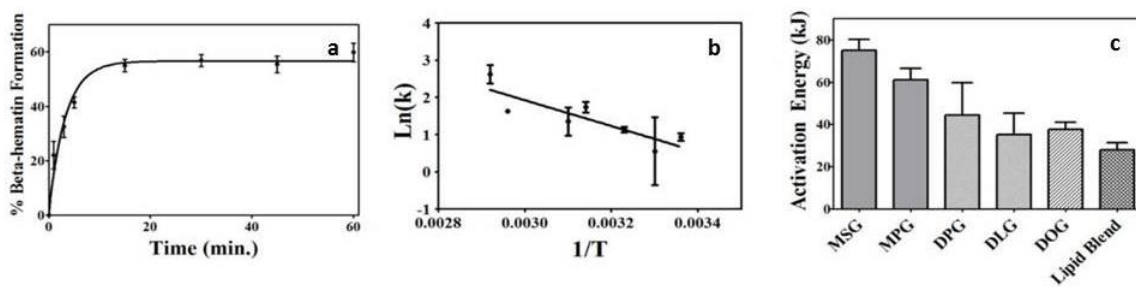
**Figure 9.** Data obtained by former lab member Dr. Anh Hoang. (a) The crystal habit of SNLD-mediated  $\beta$ -hematin crystals are similar to that observed for hemozoin. (b) Characteristic IR peaks are observed at  $1662\text{ cm}^{-1}$  and  $1210\text{ cm}^{-1}$ , indicating the formation of the C=O stretching vibration and the C-O stretching vibration of hematin linked dimers. (c) XRD shows the expected diffraction peaks for  $\beta$ -hematin.<sup>51</sup>

#### Kinetics of $\beta$ -Hematin Formation Mediated by SNLDs

It has been estimated that in order to escape heme-associated toxicity, the parasite must convert free heme to hemozoin with a half-life of less than 40 min.<sup>49</sup> Therefore if NLDs are the mediator of *in vivo* hemozoin formation, crystallization would be expected to occur rapidly. Here, SNLDs have been utilized to determine if these lipids serve as a kinetically competent site for  $\beta$ -hematin formation. Each individual lipid component, as well as the biological lipid blend was examined as a mediator of  $\beta$ -hematin formation under physiologically relevant conditions (pH 4.8, 37°C). The half-life for each reaction was determined.  $\beta$ -hematin formation in the presence of the individual lipid components as well as the neutral lipid blend all revealed half-lives of <5

min (Figure 10a). To examine this system further, the activation energy of  $\beta$ -hematin formation was determined for each component as well as the lipid blend.

The formation of  $\beta$ -hematin as mediated by SNLDs follows Arrhenius behavior (Figure 10b). Half-lives of crystallization were examined at 25, 37, 45 and 60°C for individual lipid components and the lipid blend. This analysis revealed that the monoglycerides exhibit higher energy barriers than the diglycerides. MSG and MPG have calculated values of  $74.8 \pm 5.3$  and  $60.4 \pm 7.1$  kJ/mol, respectively, while DLG, DPG, and DOG exhibited lower values of  $44.5 \pm 15.4$ ,  $35.2 \pm 9.4$ , and  $37.7 \pm 3.3$  kJ/mol, respectively (Figure 10c). When the lipid blend is utilized, a lower activation barrier of  $27.8 \pm 3.4$  kJ/mol is calculated.



**Figure 10.** (a) The half-life of  $\beta$ -hematin formation mediated by the neutral lipid blend is  $1.9 \pm 0.01$  min. (b) SNLD-mediated  $\beta$ -hematin formation follows Arrhenius behavior. (c) The activation energy of  $\beta$ -hematin formation was calculated for each individual component as well as the neutral lipid blend.<sup>51</sup> *Data obtained in collaboration with Dr. Anh Hoang.*

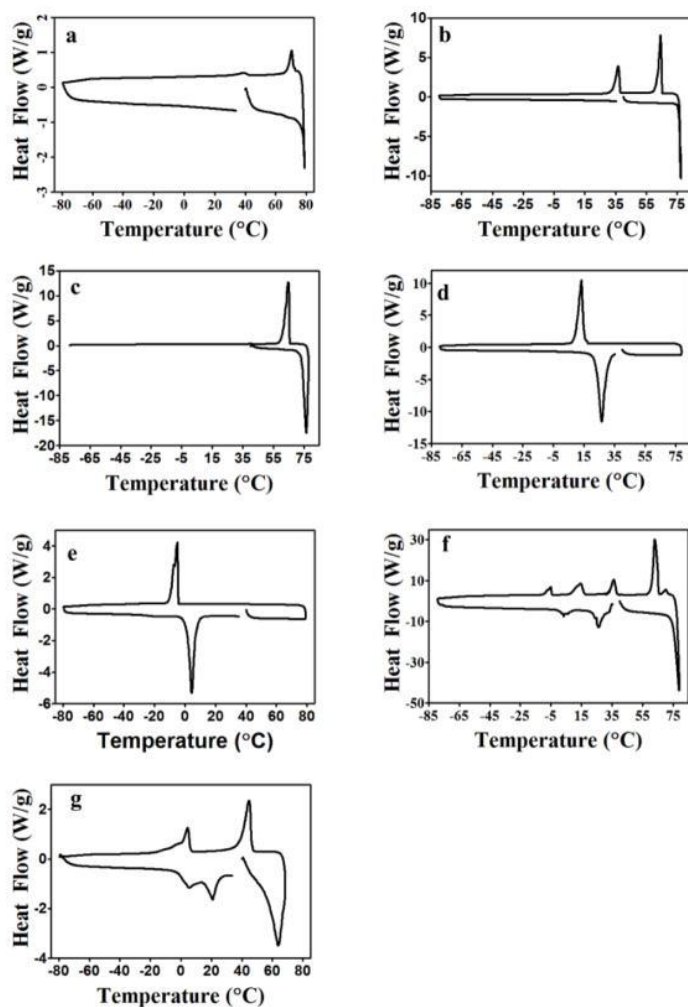


### Differential Scanning Calorimetry Measurements of the Lipids

The activation barrier for  $\beta$ -hematin formation is reduced by utilizing the lipid blend compared to the individual lipid components. This would suggest that the lipid blend provides a unique environment for crystallization to occur compared to the lipid components. One explanation for this observation is that the heterogeneous lipid composition of the neutral lipid blend would facilitate better packing of lipid molecules through unique intermolecular interactions that are not observed between homogeneous lipid components. These new interactions would result in a detectable change in heat flux necessary to break these new interactions. Therefore, differential scanning calorimetry (DSC) was employed to measure the phase transition peaks of the neutral lipid components compared to the lipid blend. MSG, MPG and DPG (saturated lipids) had higher melting points than DLG and DOG (Figure 11). Specifically, negative heat flow peaks were observed at 76, 74 and 74°C MSG, MPG and DPG when the samples were heated. When these samples were cooled, a positive heat flow at 69, 63 and 63°C was observed corresponding to crystallization peaks of MSG, MPG and DPG, respectively. For the unsaturated diglycerides, different phase transition measurements were observed. For DOG and DLG, melting temperatures of 25 and 4°C were measured. Positive heat flow peaks at 14 and -5°C were measured upon cooling the samples.

Each of these resultant plots were overlaid (Figure 11f, normalized to their biologically relevant ratio) for comparison to the phase transitions observed for the neutral lipid blend obtained experimentally (Figure 11g). When comparing these two plots, there are distinct differences. In the experimental DSC plot, the lipid blend exhibits three melting peaks at 5, 20, and 63°C that are not observed in the overlay.

Further, only two crystallization peaks (5 and 45°C) are observed in the blend compared to four crystallization peaks in the overlay. These data suggest that unique intermolecular interactions, not present within the individual lipid components, exist in the blend of lipids located in the parasitic digestive food vacuole.



**Figure 11.** DSC measurements of (a) MSG, (b) MPG, (c) DPG, (d) DOG, (e) DLG, (f) an MSG/MPG/DOG/DLG/DPG overlay with components normalized to the lipid blend ratio of 4:2:1:1:1, and (g) the lipid blend.<sup>51</sup>

## Conclusions

If heme-associated toxicity is to be avoided, the malaria parasite must convert free heme to hemozoin with a half-life of less than 40 min. Recent evidence has implicated neutral lipids in the formation of hemozoin. If these neutral lipids are indeed the biological mediator of hemozoin formation, we expect 1) the lipids to support rapid formation of  $\beta$ -hematin and 2) free heme to interact with the neutral lipids. Here, we have utilized SNLDs as a mediator of  $\beta$ -hematin formation under physiologically relevant conditions to examine the partitioning of heme and kinetics of crystallization. By adding heme to a solution containing SNLDs, we have confirmed that crystals of  $\beta$ -hematin that are chemically, spectroscopically and morphologically identical to authentic hemozoin are formed. Further, we have shown that SNLDs support formation of  $\beta$ -hematin with a half-life of less than 5 min. Additionally, we have revealed that the lipid blend found within the digestive food vacuole of the parasite has a lower activation barrier for  $\beta$ -hematin formation compared to the individual lipid components. This data suggested that the lipid blend offers a unique intramolecular environment not supported by the individual lipid components. We examined these interactions using DSC and confirmed that new phase transitions are observed for the lipid blend that are not seen in the individual lipid components, indicative of unique molecular interactions that exist in the heterogeneous lipid blend. Finally, using NR-labeled SNLDs, we have demonstrated that not only does free heme interact with the surface lipids, but rapidly partitions throughout the lipid. This would suggest that the neutral lipids serve as reservoirs for lipophilic,

toxic free heme. Taken together, these data support a role for neutral lipid bodies in the process of hemozoin formation.

### Acknowledgments

This work was performed in collaboration with Dr. Anh Hoang in the Wright lab. I would like to acknowledge the Vanderbilt Engineering Dept. for so kindly allowing me to use the differential scanning calorimeter. This work was performed in collaboration with Timothy Egan and Aneesha Omar (University of Cape Town, South Africa).

## Chapter III

### DETERGENT-MEDIATED FORMATION OF $\beta$ -HEMATIN<sup>123</sup>

#### Introduction

During the intraerythrocytic stages of malarial infection, *Plasmodium* spp. catabolizes 60-80% of the red blood cell hemoglobin content to serve as a source of amino acids and to create space for growth.<sup>7</sup> This process of hemoglobin degradation occurs within an acidic compartment (pH ~ 4.8) known as the digestive food vacuole. As a consequence of hemoglobin degradation, toxic amounts of free heme are released. Lacking an enzymatic method of detoxification, the parasite has developed a mechanism by which it converts the toxic, free heme into a nontoxic, insoluble biomineral known as hemozoin. Once thought to consist of polymeric strands of O-Fe(III) linked heme units, XRD revealed a centrosymmetric triclinic unit cell comprised of reciprocal head-to-tail dimeric units of heme bound through propionate O-Fe(III) with a bond distance of 1.866(2) Å (Figure 4).<sup>27</sup> The propionic acid groups of the heme dimer then hydrogen bond with other dimers to form the extended crystal. Though this dark brown-black material was discovered in the tissues of malarial victims as early as 1717, the precise mechanism by which hemozoin formation occurs is not yet fully understood.<sup>25</sup>

Current evidence indicates a role for digestive vacuole-associated neutral lipids in the process of hemozoin formation (Chapter II).<sup>43-46,51-53</sup> Specifically, neutral lipid droplets (also known as particles, nanospheres) present within the digestive food vacuole

of the parasite have been imaged in close proximity to crystals of hemozoin. The composition of these lipids were identified by mass spectrometry and found to consist of a specific blend of neutral lipids in a 4:2:1:1:1 ratio of monostearic, monopalmitic, dipalmitic, dioleic and dilinoleic glycerols. Synthetic neutral lipid droplets (SNLDs) consisting of this biologically relevant blend of lipids support the rapid conversion of free heme to  $\beta$ -hematin (half-life of  $1.9 \pm 0.01$  min), the synthetic equivalent of hemozoin.<sup>46,51</sup> Furthermore, heme has been shown to rapidly localize within these lipid droplets in a pH dependent manner that mirrors the pH dependence of  $\beta$ -hematin biomineralization.

In addition to neutral lipids, several lipophilic abiological mediators of  $\beta$ -hematin formation have been identified including detergents, solvents, alcohols and acids.<sup>54-57</sup> Data obtained from these studies indicate that the lipophilicity of the abiological mediators facilitate the solubilization of free heme, the rate limiting step in  $\beta$ -hematin formation.<sup>56,58</sup> As heme itself is quite hydrophobic and insoluble in aqueous solution, it would be expected that heme solubility would increase as a function of increasing hydrophobicity of the surrounding environment.

Detergents possess a hydrophobic head group and a lipophilic tail, similar to lipids. If the concentration of a detergent is above a certain threshold (CMC, critical micellar concentration), the detergent will spontaneously organize into spherical nanostructures known such as micelles or vesicles. Here, we aim to investigate the ability of detergent nanostructures to serve as a surrogate for neutral lipid bodies in the process of  $\beta$ -hematin formation. Eleven detergents were examined in their ability to solubilize free heme and competently facilitate formation of  $\beta$ -hematin.

## Experimental Methods

### Materials

Nonidet P-40 (NP-40) was purchased from Pierce Biotechnology, Rockford, IL. Flat bottom, 384-well plates (3680, Corning) were purchased from Fisher. Hemin ( $\geq 98\%$ , Fluka), amodiaquine, sodium acetate trihydrate, Tween-20, Tween-80, Sodium dodecyl sulfate and pyridine were obtained from Sigma-Aldrich, St. Louis, MO. All Triton X-detergents (45, 114, 165, 305, 102 and 100) were also purchased from Sigma-Aldrich.

### Determination of Optimal Detergent Concentration

The optimal concentration that promotes maximum product formation was determined for each detergent. The range of concentrations tested varied from 0-400 $\mu$ M. Each detergent was solubilized in water (800  $\mu$ M) and added in the appropriate volume to a 384-well flat bottom clear microtiter plate. The total volume in each well was then adjusted to 25  $\mu$ L using water. A 25 mM stock solution of hematin was prepared by dissolving hemin chloride in DMSO followed by one minute of sonication. The heme solution was then filtered through a 0.22  $\mu$ M PVDF membrane filter unit. From this solution, the heme suspension (100  $\mu$ M) was added to a 2 M acetate buffer at pH 4.9 and vortexed for  $\sim 5$  sec to make the 'heme stock' solution. 25  $\mu$ L of this heme stock was rapidly added to each detergent well. The plate was then incubated in a shaking water bath for 24 hours at 37°C at 45 rpm. Following incubation, the microtiter plate was removed from the water bath and the assay was analyzed using the pyridine-ferrochrome

method developed by Egan and coworkers.<sup>50</sup> Following the addition of 15  $\mu\text{L}$  of acetone to each well of the plate, 7  $\mu\text{L}$  of pyridine solution (50% pyridine, 20% acetone, water and 200 mM HEPES, pH 7.4) was added so that the final concentration of pyridine was 5% (v/v). Following a 30 minute interval of shaking to facilitate the solubilization of free heme, the absorbance of the resulting complex was measured at 405 nm on a BioTek H4 plate reader.

#### *Kinetics of Detergent Mediated $\beta$ -Hematin Formation*

The half-life of  $\beta$ -hematin formation was determined for each detergent. Stock solutions of each detergent were prepared at 2x the optimal concentration determined previously (all Triton X-detergents were analyzed at 50  $\mu\text{M}$  concentration). To 1.5 mL eppendorf tubes, 400  $\mu\text{L}$  of the detergent stock was added. The tubes were pre-incubated at 37°C for 15 minutes, followed by the addition of 400  $\mu\text{L}$  of a 100  $\mu\text{M}$  heme stock in 2M acetate buffer (pH 4.9) was added to each tube. The tubes were shaken at 45 rpm. Triplicate sample tubes were removed from the water bath at regular intervals and  $\beta$ -hematin formation was analyzed using the heme-ferrochrome method of quantification described above.<sup>50</sup>

#### *Characterization of Detergent Nanostructures*

Dynamic Light Scattering (DLS) was used in order to establish the size distribution of detergent nanostructures. Each detergent was prepared in 1 M acetate buffer at the optimal concentration of detergent to determine whether or not detergent micelles or vesicles were present at this concentration (each of the Triton X-detergents



was analyzed at 50  $\mu\text{M}$ ). The detergents were equilibrated for 15 min at 37°C. A pipette was then used to carefully transfer the solution to a cuvette and analyzed using a Malvern Zetasizer with a lower limit of 0.1 nm and an upper limit of 6  $\mu\text{m}$ . Triplicate samples were prepared to ensure the detergent nanostructure size distribution was stable.

#### Characterization of $\beta$ -Hematin Product

Product obtained from the kinetics experiments was characterized to confirm the product was  $\beta$ -hematin. Prior to characterization, the product was washed thoroughly with 5% pyridine to remove free heme contamination. pXRD was conducted using Cu K $\alpha$  radiation ( $\lambda = 1.541 \text{ \AA}$ ), with data collection on a Philips PW 1050/80 vertical goniometer in the  $2\Theta$  range of 5-40°. Scanning electron microscope (SEM) images were obtained using a Hitachi S-4200 instrument to confirm the crystal habit of the product was similar to hemozoin.

#### Data Analysis

The kinetics of  $\beta$ -hematin formation were analyzed using linear least-squares fitting methods with Graphpad Prism 5.0. The data were fit to the Avrami equation<sup>59</sup>:

$$Y = c * (1 - e (-zX^n))$$

where Y is the mass percentage of  $\beta$ -hematin formed, c is the maximum percentage of  $\beta$ -hematin formed at the end of the reaction, z is the rate constant, X is time and n is the Avrami constant. Kinetics data were fit to n = 1, 2, 3 and 4. The curve that represented

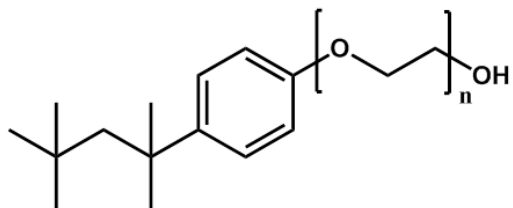
the best fit based on the  $r^2$  value was reported as the appropriate Avrami constant that represents the crystallization process.

## Results

### Selection of Detergents

A collection of five detergents were initially selected for this study based on cost, availability and structural diversity. These detergents include: NP-40, Tween-20, Tween-80, sodium dodecyl sulfate (SDS) and 3-[(3-cholamidopropyl)dimethylammonio]-1-propanesulfonate (CHAPS). Ionic SDS and the zwitterionic detergent CHAPS were obtained to examine the effects of charge on  $\beta$ -hematin formation. Tween-20 and Tween-80 are both nonionic detergents with identical polyoxyethylene hydrophilic head groups. These two detergents can be distinguished by the length of the fatty acid ester moiety. The 11 carbon hydrophobic tail of Tween-20 is saturated, while the 17 carbon tail of Tween-80 contains a double bond. The detergent NP-40 (Nonidet P-40) was selected due to the polyethylene oxide hydrophilic portion, which is similar to the glycerol hydrophilic portion of neutral lipids. After examining each of these detergents, we noted that NP-40 behaved most similarly to the biological blend of neutral lipids found within the malaria parasite. Based on these observations, six additional detergents were selected so that a systematic analysis of the NP-40 polyethylene oxide portion of the detergent could be examined in relation to formation of  $\beta$ -hematin. These detergents, known as the Triton X- detergents, vary with NP-40 based on the size of the polyethylene oxide side chain (Table 1).

### Triton X-detergents



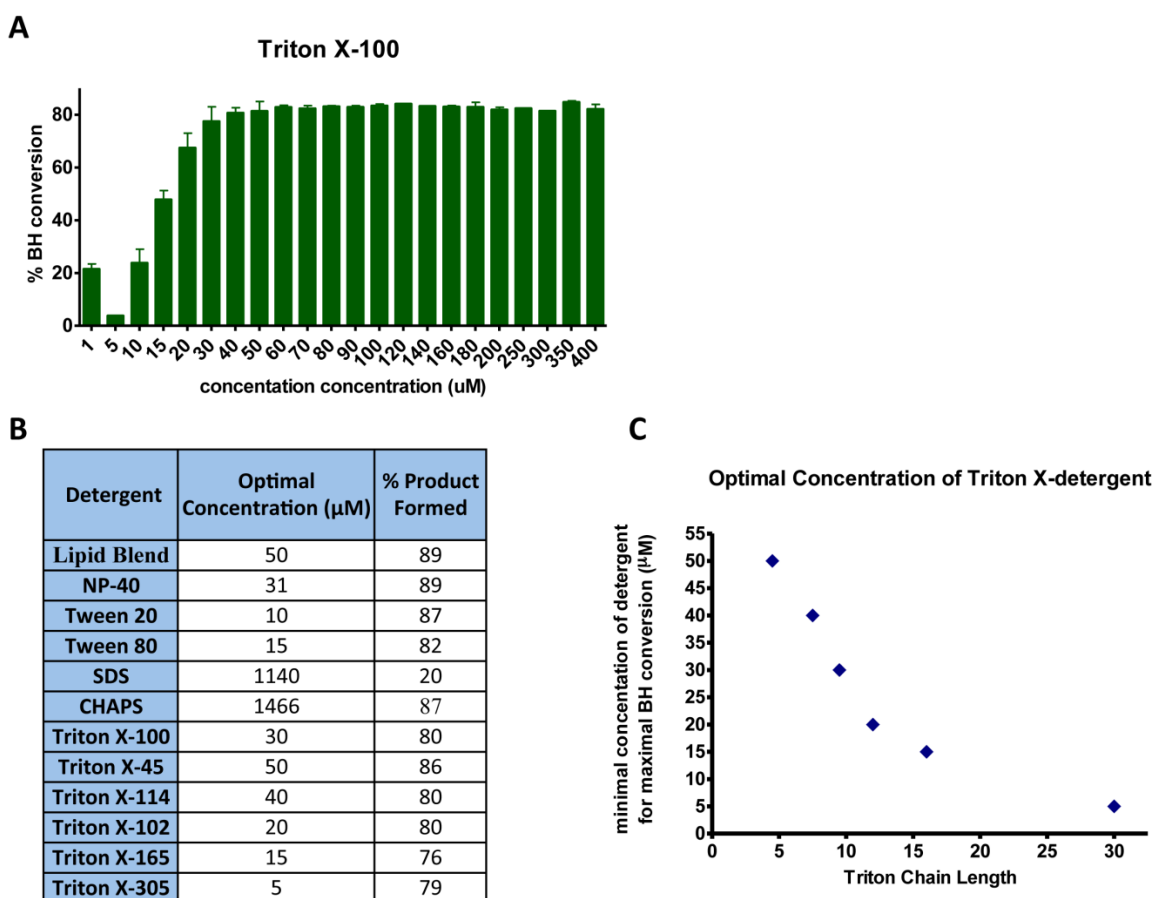
Detergent	n = Average Polyethylene Oxide Repeats
NP-40	9.0
Triton X-45	4.5
Triton X-114	7.5
Triton X-100	9.5
Triton X-102	12
Triton X-165	16
Triton X-305	30

**Table 1.** Structurally, the Triton X-detergents contain an 8 carbon hydrophobic portion and varying sizes of polyethylene oxide repeats.

#### Determination of Optimal Detergent Concentration

The minimum concentration at which maximum  $\beta$ -hematin formation is observed was determined using a range from 1-400  $\mu$ M for each of the detergents, as well as the blend of neutral lipids (Figure 12). This concentration is referred to as the ‘optimal’ detergent concentration. Within this concentration range, all detergents except SDS and CHAPS produced 80-90% formation of  $\beta$ -hematin. SDS and CHAPS are ionic and zwitterionic, respectively, while all other detergents (including the lipid blend) are neutral. As micelles or vesicles, the ionic surfaces of SDS and CHAPS are exposed to water. This observation suggests that the presence of a neutral surface facilitates more efficient  $\beta$ -hematin formation, in agreement with previously published reports exploring

the role of charge on lipid surfaces.<sup>51,60</sup> A closer examination of the Triton X-detergents (Figure 12C) reveals the optimal concentration of detergent varies based on the size of the polyethylene oxide (PEO) chain length. Specifically, as the PEO chain length increases, the optimal concentration of detergent necessary for  $\beta$ -hematin formation decreases

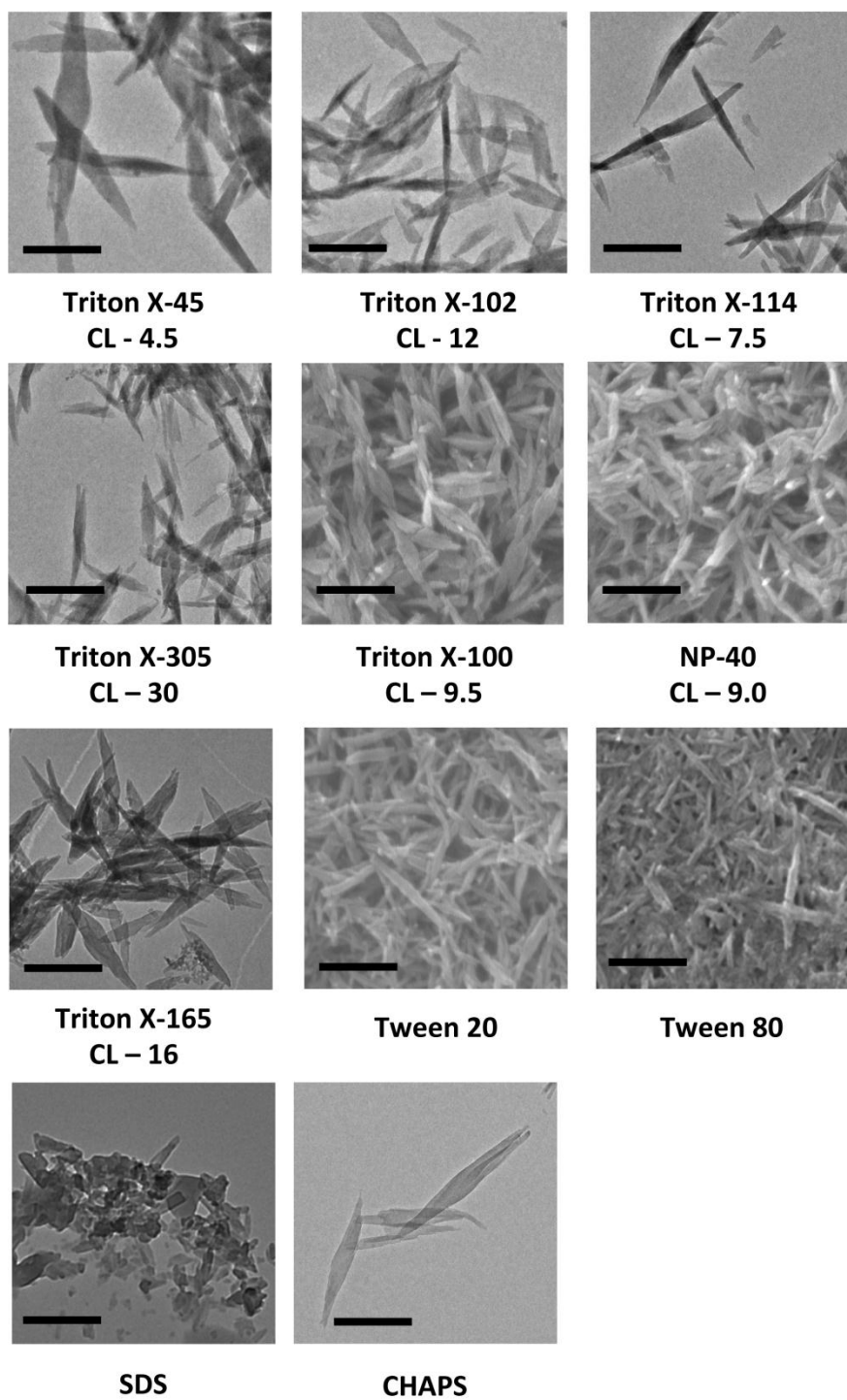


**Figure 12.** (A) The minimum concentration of Triton X-100 detergent was found to be 30  $\mu$ M. (B) The minimum concentration of mediator necessary to promote maximal formation of  $\beta$ -hematin (the ‘optimal’ concentration) was determined for each detergent. (C) The optimal concentration of Triton X-detergent as a function of increasing PEO chain length reveals a trend.

### Characterization of $\beta$ -Hematin Product

Morphological and structural analysis of the product obtained upon incubation of free heme with the optimal concentration of each detergent confirmed the presence of  $\beta$ -hematin for all detergents except SDS and CHAPS. Infrared spectra of the products of neutral detergents displayed prominent IR peaks at  $1662\text{ cm}^{-1}$  and  $1210\text{ cm}^{-1}$ , indicating the formation of the C=O stretching vibration and the C-O stretching vibration of hematin linked dimers. In the case of SDS and CHAPS, the product was heavily degraded as a result of the 5% pyridine washes. This would suggest that the majority of the product obtained is likely comprised primarily of heme aggregates rather than  $\beta$ -hematin.

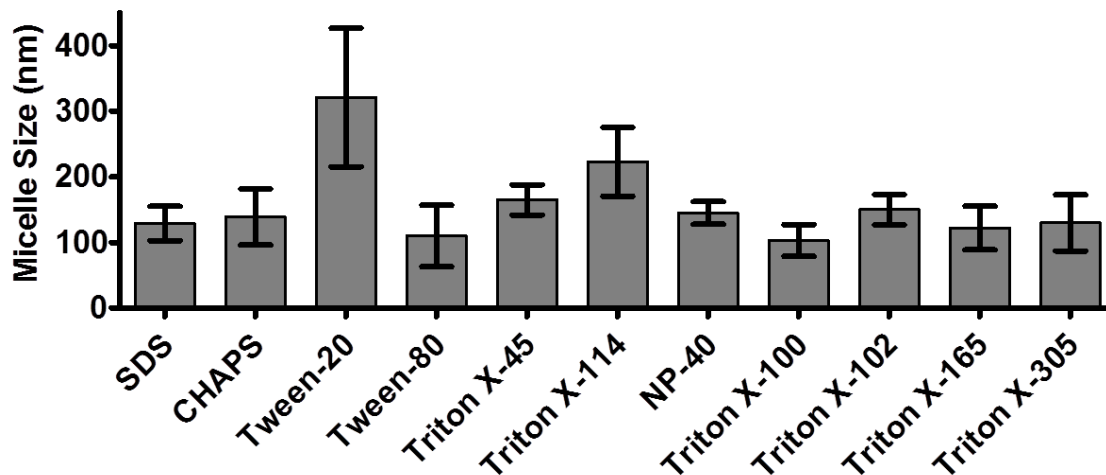
SEM and TEM imaging were used to examine the morphology of the  $\beta$ -hematin crystals produced by different detergents. Well-formed crystals resembling hemozoin were observed in the presence of all detergents except SDS (Figure 13).



**Figure 13.** SEM and TEM of the  $\beta$ -hematin product obtained using the indicated detergent mediator. Scale bar = 500 nm, CL = PEO chain length

### Characterization of Detergent Nanostructures

SNLDs have been shown to serve as a lipophilic reservoir for free heme and support the rapid formation of  $\beta$ -hematin, likely occurring at the lipid/aqueous interface.<sup>51</sup> Similar to lipids, most detergents will spontaneously form organized particles above a certain concentration known as the CMC (specific to each detergent). These nanostructures are generally spherical in shape with the CMC being influenced by the temperature, pressure and the presence of other substances in solution (such as electrolytes). Since these nanostructures are similar in shape and composition to the SNLDs that support  $\beta$ -hematin formation, we wanted to determine if they are present for the detergent mediators examined in this study under assay conditions. DLS studies have previously shown that under assay conditions, SNLDs exist in two size populations - the largest population of SNLDs was ~50-200 nm in diameter, with a smaller population of ~1-10  $\mu\text{m}$  in diameter.<sup>46</sup> The size and stability of the nanostructures was determined for Tween-20, Tween-80, SDS, CHAPS and NP-40 using the optimal detergent concentration. For the Triton X-detergents, a concentration of 50  $\mu\text{M}$  was used. The particle diameter observed within this set of detergents under assay conditions ranged from ~100 – 300 nm (Figure 14). As micelles are typically 5-10 nm in diameter, it is likely that the detergent exists as vesicles under assay conditions.



**Figure 14.** Average size of vesicles measured at the optimal concentration of detergent under assay conditions.

#### Kinetics of Detergent-Mediated $\beta$ -Hematin Formation

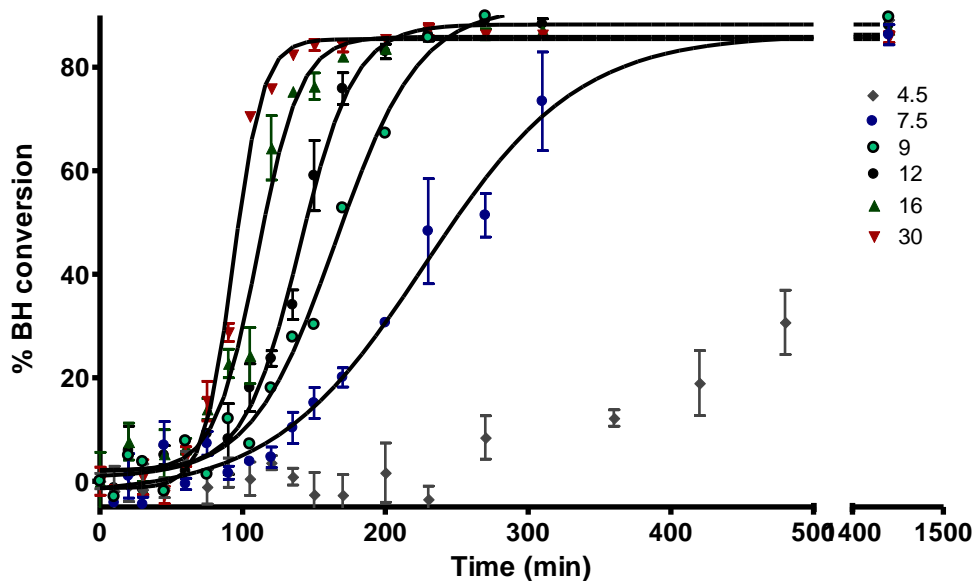
The kinetics of  $\beta$ -hematin formation was determined in the presence of each of the detergents. CHAPS, Tween-20, Tween-80 and NP-40 were each examined at the optimal detergent concentration (Table 2). Tween-20 and Tween-80 both facilitated rapid formation of  $\beta$ -hematin with half-lives of 5 and 7 min, respectively. The half-life of CHAPS was 630 min, though the product produced was not stable and easily degraded when washed with 5% pyridine. The product obtained from the SDS detergent was very unstable and a half-life could not be determined. The half-life of  $\beta$ -hematin formation in the presence of NP-40 exhibited a half-life of 53 min. All detergents exhibited sigmoidal growth profiles.



Detergent	Concentration ( $\mu\text{M}$ )	Half-life (min)	% $\beta$ -hematin formation
Tween-20	14	5	86
Tween-80	15	7	80
CHAPS	1400	630	84
NP-40	31	53	88
Triton X-45	50	550	89
Triton X-114	50	228	86
Triton X-100	50	165	90
Triton X-102	50	140	88
Triton X-165	50	111	87
Triton X-305	50	93	86

**Table 2.** The half-life of  $\beta$ -hematin formation was determined in the presence of each of the detergent mediators.

The kinetics of  $\beta$ -hematin formation in the presence of each of the Triton X-detergents was determined using a concentration of 50  $\mu\text{M}$  (Table 2) detergent. This analysis reveals that the half-life of  $\beta$ -hematin formation is influenced by the PEO chain length. Specifically, the longer the PEO chain length, the more rapid  $\beta$ -hematin formation is observed (Figure 15). Additionally, Triton X-mediated  $\beta$ -hematin formation exhibits a sigmoidal shaped growth curve, consistent with previous reports of solvent-mediated  $\beta$ -hematin formation.<sup>57,58</sup>



**Figure 15.** The kinetics of detergent-mediated  $\beta$ -hematin formation were monitored over the course of 24 hours. Shown here are the Triton X-detergents, identified based on the number of repeating polyethylene oxide units. BH =  $\beta$ -hematin

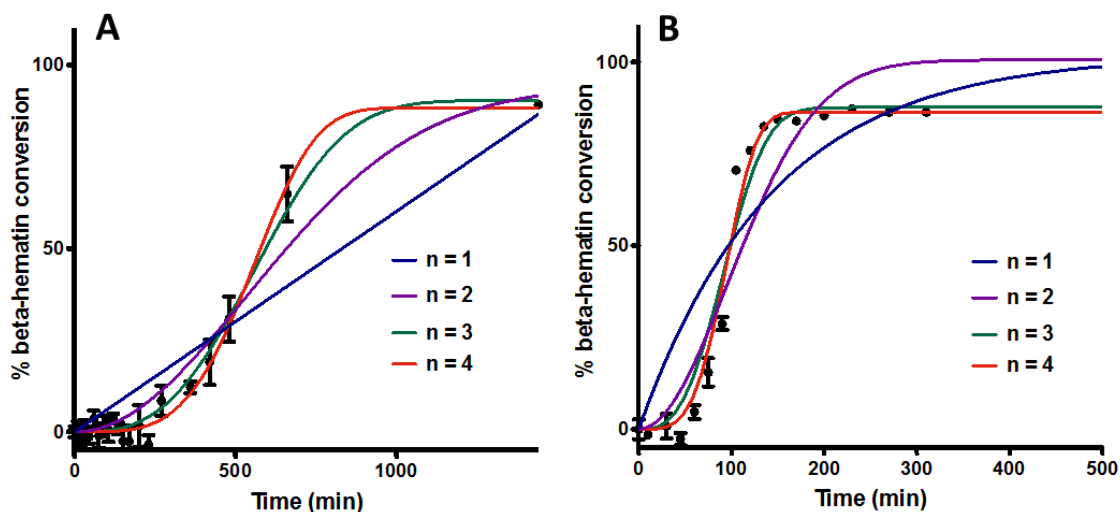
The sigmoidal growth profile observed for detergent-mediated  $\beta$ -hematin formation is typical of a crystallization process. Specifically, this type of curve is reflective of a nucleation and growth phase where an initial induction phase of  $\sim 20$  minutes is observed followed by rapid product formation. The Avrami equation is frequently used to model this nucleation and growth process (see methods).<sup>59</sup> In this equation, the Avrami constant,  $n$ , represents the type of nucleation and dimensionality of the growth process and typically takes an integer value where  $n = 1, 2, 3$  or  $4$ . The kinetics data were fitted to the Avrami equation and constrained to each of the four integer values of  $n$ . Table 3 lists the best fit value of  $n$  obtained from each of the detergent mediators.

Detergent	$n$	$r^2$	$z$ (min <sup>-n</sup> ) <sup>a</sup>
Triton X-45	4	0.989	$7.52 \pm 0.57 \times 10^{-12}$
Triton X-114*	4	0.973	$2.68 \pm 0.34 \times 10^{-10}$
Triton X-100	4	0.989	$9.65 \pm 0.77 \times 10^{-10}$
Triton X-102	4	0.991	$1.87 \pm 0.13 \times 10^{-9}$
Triton X-165	4	0.982	$4.92 \pm 0.52 \times 10^{-9}$
Triton X-305	4	0.985	$9.11 \pm 0.95 \times 10^{-9}$
NP-40*	4	0.973	$7.26 \pm 1.34 \times 10^{-8}$
Tween-80	1	0.958	$0.11 \pm 0.01$
Tween-20	1	0.936	$0.12 \pm 0.02$
CHAPS*	4	0.973	$6.30 \pm 0.87 \times 10^{-12}$

**Table 3.** The best-fit value of the Avrami equation was determined for each of the detergents. \*These detergents had slightly better fits for  $n = 3$ . <sup>a</sup>The rate constant calculated based on the indicated Avrami constant,  $n$ .

Tween-20 and Tween-80 had excellent fits for  $n = 1$  but deviated significantly for all other values of  $n$ . This fit indicates that crystal growth follows instantaneous nucleation and rod-like growth in one dimension. All other detergents conform to  $n = 3$  and 4. Figure 16 represents the fit for the Avrami constants to the kinetics data obtained from Triton X-45 and 305. Since there is almost no difference in fit, we chose to use the value of  $n = 4$  to describe the kinetics of these detergents since this is consistent with

other systems that have been described previously.<sup>57,58,61</sup> Specifically, an Avrami constant of  $n = 4$  describes a system where nucleation is sporadic and spherical growth occurs in three dimensions.

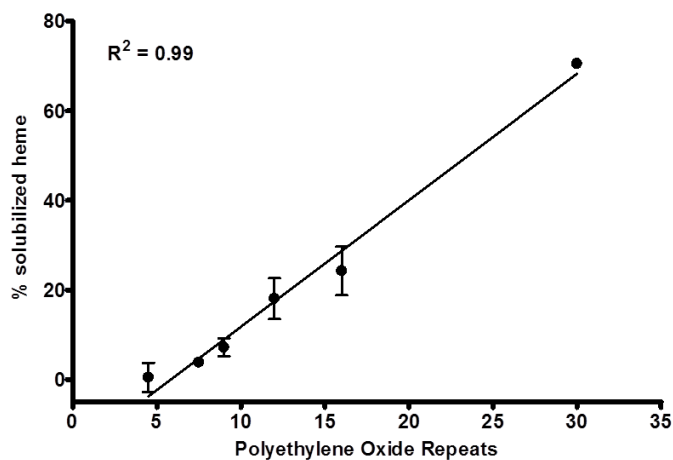


**Figure 16.** The kinetics data was fit to the Avrami equation.  $\beta$ -hematin formation mediated by (A) Triton X-45 and (B) Triton X-305 exhibit best fits to  $n = 4$ .

#### Solubility of Heme in the Presence of Triton X-Detergents

There is clearly a correlation between PEO chain length and the half-life of  $\beta$ -hematin formation mediated by the Triton X-detergents (Figure 15). In an effort to explain this correlation, we examined the solubility of heme in the presence of each of the Triton X-detergents since this is the rate-limiting step in  $\beta$ -hematin.<sup>48,58</sup> Solubilized heme was measured at 105 minutes under assay conditions at 50  $\mu$ M of each of the Triton X-

detergents. Figure 17 reveals as the PEO chain length size increases, more efficient solubilization of heme is achieved.



**Figure 17.** The solubility of heme increases as a function of increasing PEO chain length.

## Discussion

Though the precise mechanism of hemozoin formation is not yet fully understood, current evidence indicates that neutral lipid droplets located in the digestive food vacuole of the parasite play an important role in hemozoin formation. Previous investigations have demonstrated that SNLDs serve as a reservoir for free heme and are a kinetically competent site for  $\beta$ -hematin formation.<sup>46,51</sup> Here, our aim was to determine whether detergents could serve as surrogates for SNLDs in the process of  $\beta$ -hematin formation. Since detergents are similar to lipids in molecular structure (hydrophilic head groups and

hydrophobic tails) and in the spontaneous organization into spherical structures when present at concentrations above the detergent-specific CMC values, we hypothesized that detergent vesicles would support the formation of  $\beta$ -hematin.

Each of the nine *neutral* detergents examined in this study were efficient mediators of  $\beta$ -hematin formation. On the other hand, the ionic and zwitterionic detergents SDS and CHAPS produced material that was unstable and likely consists primarily of heme aggregates rather than  $\beta$ -hematin. This observation substantiates the importance of utilizing a neutral mediator for  $\beta$ -hematin formation.

The optimal concentration which promoted maximal  $\beta$ -hematin formation was determined for each detergent. For all detergents except SDS and CHAPS, the product obtained at this concentration of mediator was confirmed to be  $\beta$ -hematin. Further, DLS confirmed that detergent vesicles are present for each of the detergents under these conditions ranging in size from ~100-300 nm. This size distribution is consistent with SNLDs examined under assay conditions (the largest population of SNLDs was ~50-200 nm). Current evidence indicates that  $\beta$ -hematin formation readily occurs at interfacial regions of lipids or solvents.<sup>58,60</sup> Based on this data, it is reasonable to hypothesize that detergent-mediated  $\beta$ -hematin formation would occur at the surface of vesicle particles present in solution.

The kinetics of detergent-mediated  $\beta$ -hematin formation was shown to follow a sigmoidal growth profile typical of a crystallization process that involves an initial nucleation phase followed by a rapid growth phase. The Avrami equation was used to determine the type of nucleation and dimensionality of the growth. Tween-20 and Tween-80 had excellent fits for  $n = 1$ , indicating that crystal formation occurs as a result

of instantaneous nucleation and rod-like growth in one dimension. The remaining detergents conformed to  $n = 3$  and 4 but since there was almost no difference in fit, we chose the value of  $n = 4$  to describe the kinetics of these detergents since this is consistent with other systems that have been described previously.<sup>57,58,61</sup> Therefore, the crystallization process for these detergents occurs as a result of sporadic nucleation and spherical growth occurs in three dimensions.

Though the neutral detergent mediators efficiently support the formation of  $\beta$ -hematin, there are clear differences in half-lives. Derivatives of NP-40, the Triton X-detergents, were analyzed to facilitate a direct comparison of the PEO chain length in the process of  $\beta$ -hematin formation. We observed a clear correlation where the longer the PEO chain length, the more rapid  $\beta$ -hematin formation was observed. In an effort to understand this relationship, the solubility of heme in the presence of each detergent was analyzed since this is the rate-limiting step in  $\beta$ -hematin formation. At 105 min, a linear relationship was revealed between PEO chain length and the amount of free heme that was solubilized ( $r^2 = 0.99$ ). This relationship clearly indicates that the longer PEO chain length facilitates quicker formation of  $\beta$ -hematin as a result of more rapid solubilization of free heme.

Here, we have demonstrated that neutral detergent vesicles can serve as surrogates for SNLDs in  $\beta$ -hematin formation. This observation allows the digestive food vacuole conditions where hemozoin formation occurs to be recapitulated without the need of obtaining expensive neutral lipids. Consequently, one of the neutral detergents discussed here, NP-40, has been utilized as a  $\beta$ -hematin mediator in a high-throughput screening

assay. In the next chapter, the optimization, validation and use of the NP-40  $\beta$ -hematin formation assay will be described.

### Acknowledgments

This work was completed in collaboration with Renata Stiebler who visited our laboratory from Universidade Federal do Rio de Janeiro, Rio de Janeiro, Brazil. Dr. Timothy J. Egan from the University of Cape Town, in South Africa assisted in the analysis of the Avrami kinetics and Jenny Nesbitt from Vanderbilt University completed the vesicle stability and size measurements. Chris Gulka from Vanderbilt University obtained all TEM images presented in this Chapter.



## Chapter IV

### $\beta$ -HEMATIN AS A TARGET FOR HIGH-THROUGHPUT SCREENING<sup>54</sup>

#### Background

With antimalarial drug resistance on the rise, there is a pressing need for the discovery of novel chemical scaffolds that are active against *Plasmodium* spp. One discovery technique is high-throughput screening (HTS), where thousands to millions of small molecules are rapidly tested for activity in assay. An HTS suitable assay is generally formatted for use in 384- or 1536-well microtiter plates in order to test a large number of compounds in a short amount of time. Furthermore, an HTS amenable assay must involve minimal processing steps, be highly robust and should be comprised of easily accessible reagents at a minimal cost. Assays can be either phenotypic or target-based in nature. In antimalarial HTS, phenotypic assays are those that seek to identify small molecules that are capable of killing the parasite itself in *P.falciparum* infected erythrocytes. The disadvantage to this approach is that the mechanism of action of inhibitors is unknown, and can be quite difficult to elucidate. In target-based assays, a specific cellular process, such as hemozoin formation, is used to identify potential antimalarials. Inhibitor/target interactions can be studied immediately after identifying hits, an advantage over phenotypic screening. An additional advantage is the option to select pathways that are specific to the parasite. The disadvantage to target-based screening is that activity does not necessarily confer to the whole-cell assay.

The use of HTS in antimalarial drug discovery has been utilized in recent years for both target-based and phenotypic assays.<sup>50,54,62-68</sup> Of the target based assays, several have been developed for the purpose of identifying inhibitors of  $\beta$ -hematin formation.<sup>50,54,69,70</sup> One of the first successful assays developed for use in HTS utilized radioactive  $^{14}\text{C}$ -labeled hematin to quantitate  $\beta$ -hematin formation using scintillation counting.<sup>65</sup> Crystallization was mediated by the addition of lipid-rich extracts from parasite lysates. The semi-automated assay tested over 100,000 compounds in 96-well plates and identified 45 nonquinoline hits. Of these 45 compounds, the structural classes of compounds identified included triarylcarbinols, piperazines, benzophenones, imides, hydrazides, indoles and isoxazoles. The non-quinoline hits were then tested in a secondary whole-cell assay consisting of cultures of CQ-sensitive and CQ-resistant *P. falciparum*. Four compounds were identified to have activity in both strains at concentrations of  $<5\ \mu\text{M}$  (the  $\text{IC}_{50}$  of CQ in sensitive strains of *P. falciparum* is  $\sim 25\ \text{nM}$ ). Though few of the compounds identified in the  $\beta$ -hematin inhibition screen were active against parasite cultures, the ability of HTS to identify novel pharmacophores supported the utility of this approach. However, this assay was not utilized to its full potential due to deficiencies in design. The semi-automated use of 96-well plates would be considered a medium-throughput method compared to the more often used 384- and 1536- well plates. Further, the need for trophozoite lysates and radioactive hematin limits the use of this assay to laboratories capable of maintaining parasite cultures and open to the restrictions imposed by utilizing radioactive substrates. Superior  $\beta$ -hematin formation assays should boast increased throughput of compound screening, incorporating more

readily available substrates, and using improved methods of quantification that do not require the use of radio-labeled heme.

## **Part I. Validation of the NP-40 $\beta$ -Hematin Formation Assay and Results of a High-Throughput Screening Campaign<sup>54</sup>**

### Introduction

*Plasmodium falciparum*, the most virulent species of the malaria parasite, is responsible for nearly one million deaths each year.<sup>71</sup> The overwhelming majority of these deaths occur among young children residing in sub-Saharan Africa. Alarming, the parasite has developed resistance mechanisms to nearly all affordable, widely-available antimalarials.<sup>72,73</sup> It is therefore critical to enrich the antimalarial drug discovery pipeline with lead probe candidates. Fortunately, several unique pathways have been identified that serve as drug targets including inhibition of DNA synthesis, de novo heme biosynthesis, glycolysis and hemozoin inhibition.

During the intraerythrocytic stages of infection, the malaria parasite consumes upwards of 80% of the infected red blood cells hemoglobin content to serve as a source of amino acids.<sup>7</sup> This process of hemoglobin degradation occurs within the parasite's digestive food vacuole, an acidic organelle (pH ~4.8-5.2). As a consequence of hemoglobin degradation, toxic free heme is liberated. Lacking an enzymatic method of heme detoxification, the malaria parasite has evolved a method by which it converts

soluble free heme into an insoluble, nontoxic biomineral called hemozoin, the malarial pigment.<sup>48</sup> Though hemozoin has been studied since the 18<sup>th</sup> century, it was not until 1999 that XRD revealed hemozoin consists of a centrosymmetric triclinic unit cell comprised of reciprocal head-to-tail dimeric units of heme bound through propionate O-Fe(III).<sup>27</sup> The propionic acid groups of the heme dimer then hydrogen bond with other dimers to form the extended crystal. The *in vivo* mechanism of hemozoin formation has been contested for many years, though emerging evidence concerning the mechanism of hemozoin formation implicates the involvement of neutral lipids present within the digestive food vacuole as the site of crystal nucleation and growth (Chapter II).<sup>45,52,53</sup> Analysis of the digestive food vacuole concentrated neutral lipid particles by mass spectrometry identified a specific blend of neutral lipids in a 4:2:1:1:1 ratio of monostearic, monopalmitic, dipalmitic, dioleic and dilinoleic glycerols.<sup>43,44</sup> Synthetic neutral lipid droplets (SNLDs) that consist of this biologically relevant blend of neutral lipids successfully promote the rapid formation of  $\beta$ -hematin (half-life of  $1.9 \pm 0.01$  min) under physiologically realistic pH and temperature conditions (Chapter II). Further, soluble free heme was shown to rapidly partition in the SNLDs in a pH-dependent manner. The pH profile of heme partitioning resembles that of  $\beta$ -hematin formation.<sup>46,51,60</sup> Collectively, this evidence substantiates a role for neutral lipid particles in the process of hemozoin formation.

As perturbations to hemozoin formation lead to parasite death, understanding the mechanism of hemozoin formation is useful. Chloroquine (CQ), one of the most successful antimalarials ever developed, owes its activity to inhibition of hemozoin formation.<sup>19,74</sup> Unfortunately, the parasite has developed resistance to the use of this

quinoline-based antimalarial. However, this resistance is not due to changes in the hemozoin formation pathway, but rather arises from mutations in *PfCRT*, a membrane protein localized to the digestive food vacuole.<sup>22,24,37</sup> Mutations are thought to be responsible for reduced accumulation of CQ within the digestive food vacuole, thereby preventing CQ-heme interactions from occurring. This efflux mechanism is seemingly specific for quinoline-based antimalarials. In the case of CQ, resistance can be overcome by synthetically altering the side chain, as derivatives of this quinoline scaffold retain activity against resistant strains.<sup>75,76</sup> Consequently, hemozoin formation remains an important drug target for the development of new antimalarials.

Recently, the NP-40  $\beta$ -hematin formation assay was validated for use in screening.<sup>77</sup> This assay utilizes the lipophilic detergent, NP-40, to serve as a surrogate for *in vitro*  $\beta$ -hematin formation under physiologically relevant assay conditions (Chapter III). This detergent mediator is low cost and requires no special handling steps in assay setup.<sup>54</sup> Here, the  $\beta$ -hematin formation assay has been utilized to screen a library of 144,330 commercially available compounds in the Vanderbilt University High-Throughput Screening Facility. Each of the target-specific hits was analyzed for *in vitro* antimalarial activity in *in vitro* cultures of *P. falciparum*. Follow-up dose-response data was collected for each *in vitro* antimalarial compound. Those that exhibited nanomolar activity against the parasite were further examined in a multi-drug resistant strain of *P. falciparum*.

## Experimental Methods

### Materials

Nonidet P-40 (NP-40) was purchased from Pierce Biotechnology, Rockford, IL. Flat bottom, 384-well plates (3680, Corning) and optical bottom plates (142761, Nunc) were purchased from Fisher. Minimum Essential Medium (MEM) and 3-(4,5-dimethylthiazol-2-yl)2,5-diphenyltetrazolium bromide (MTT) were purchased through Fisher. Hemin ( $\geq 98\%$ , Fluka), amodiaquine, sodium acetate trihydrate, and pyridine were obtained from Sigma-Aldrich, St. Louis, MO. SYBR Green I nucleic acid gel stain (10,000X) was supplied by Invitrogen. The screening library consisted of compounds originating from ChemBridge and ChemDiv.

### Detergent-mediated NP-40 $\beta$ -hematin formation assay

The  $\beta$ -hematin formation assay was adapted for use in a 384-well microtiter plate as previously described.<sup>54</sup> Solutions were added to the microtiter plate in the order of water (20  $\mu$ L), NP-40 stock solution (5  $\mu$ L), acetone (7  $\mu$ L) and heme suspension (25  $\mu$ L). The NP-40 stock solution (348  $\mu$ M) was prepared in water. It is important to note that there are two different detergents, both called NP-40. A 25 mM stock solution of hematin was prepared by dissolving hemin chloride in DMSO followed by one minute of sonication. The heme solution was then filtered through a 0.22  $\mu$ m PVDF membrane filter unit. From this solution, the heme suspension (228  $\mu$ M) was added to a 2 M acetate buffer at pH 4.9 and vortexed for  $\sim$  5 sec. The plate was then incubated for four hours in a shaking water bath at 45 rpm and 37°C. Following incubation, the microtiter plate was

removed from the water bath and the assay was analyzed using the pyridine-ferrochrome method developed by Egan and coworkers.<sup>50</sup> Following the addition of 15  $\mu$ L of acetone to each well of the plate, 8  $\mu$ L of pyridine solution was added (50% pyridine, 20% acetone, water and 200 mM HEPES, pH 7.4) so that the final concentration of pyridine was 5% (v/v). Following a 30 minute interval of shaking to facilitate the solubilization of free heme, the absorbance of the resulting complex was measured at 405 nm on a SpectraMax M5 plate reader.

#### Identification of $\beta$ -hematin Inhibitors

Test compounds in the Vanderbilt University High-Throughput Screening Facility originated from ChemBridge and ChemDiv. A Labcyte Echo 550 non- contact acoustic liquid delivery system was used to deliver all control and test compounds to the 384-well assay plate. Positive controls consisted of a 100  $\mu$ M final concentration of amodiaquine (dissolved in DMSO) and negative controls consisted of DMSO only. Controls were added to the first and last two columns of each plate in an alternating, checkerboard pattern. All test compounds (10 mM in DMSO) were added so that the final test concentration was 19.3  $\mu$ M (320 total compounds tested per plate). Following addition of controls and test compounds, the reagents of the  $\beta$ -hematin formation assay described above were added using a Thermo Scientific Multidrop Combi Bulk Reagent Dispenser. Inhibition of  $\beta$ -hematin was assessed relative to the positive and negative controls on each plate. Compounds inhibiting >80%  $\beta$ -hematin formation were considered hits. This stringent threshold for identifying  $\beta$ -hematin inhibitors facilitated the identification of a set of potent inhibitors of crystallization. Each hit was then tested in duplicate in a dose-

response assay to identify false-positives and establish IC<sub>50</sub> values using a range of concentrations of test compound from 0.5 – 110 µM. Sigmoidal dose-response curves were generated using GraphPad Prism v5.0 (March 7, 2007).

#### Determination of Drift, Z' and Edge Effects

For the purpose of assay validation, positive controls of the IC<sub>100</sub> of AQ, and negative controls with no drug were added to the plate in an alternating, 'checkerboard' pattern. The quality of the assay was measured by the Z' statistical test proposed by Zhang.<sup>78</sup> The assay was analyzed for drift and edge effects using established guidelines of the NCGC (*Assay Guidance Manual Version 5.0, 2008*, Eli Lilly and Company and NIH Chemical Genomics Center. Available online at: [http://www.ncgc.nih.gov/guidance/manual\\_toc.html](http://www.ncgc.nih.gov/guidance/manual_toc.html) (last accessed [October 26, 2010])).

#### Cytotoxicity Test Using the RAW 264.7 Murine Cell Line

The murine macrophage-like cell line RAW 264.7 (American Type Culture Collection TIB-71, Monassas, VA) was used for testing the cytotoxicity of select compounds confirmed active in the parasite assay.<sup>79</sup> A concentration range from 0-20 µM was tested in a 96-well flat bottom tissue culture treated assay plate. Cells were delivered at a concentration of 2 X10<sup>4</sup> cells/well in a solution of minimum essential medium (MEM) supplemented with 10% fetal bovine serum and incubated overnight at 37°C and 5% CO<sub>2</sub>. The following morning, drugs (diluted using MEM) were added to the culture plates. After 30 hours, media was replaced in each well. The cells were returned to incubation and allowed to recover overnight. The following day, a solution



of MTT (3-(4,5-dimethylthiazol-2-yl)2,5-diphenyltetrazolium bromide) was prepared at 1.5 mg MTT/1 mL of MEM. The wells were then emptied and 180  $\mu$ L of MEM and 30  $\mu$ L of MTT solution were added and incubated for one hour. The wells were emptied and the purple precipitate was allowed to dry completely. A 200  $\mu$ L solution of acidified isopropanol was added and mixed then analyzed at 590 nm on the SpectraMax M5 plate reader.

#### *P. Falciparum Culture Conditions*

*P. falciparum* strains D6 and C235 were maintained using a modification of methods described by Trager and Jensen.<sup>80</sup> RPMI 1640 medium supplemented with 25 mM HEPES, 11 mM glucose, 0.24% sodium bicarbonate, 10% human A(+) plasma (heat-inactivated) and 29  $\mu$ M hypoxanthine was prepared weekly. Cultures were maintained at 5% hematocrit in A(+) blood (washed two times with RPMI medium and used no longer than one week). Culture medium was routinely exchanged and subcultured upon reaching 5% parasitemia (every 3-4 days). Cultures were incubated at 37°C in a gas mixture of 5% O<sub>2</sub>, 5% CO<sub>2</sub> and nitrogen.

#### *Malaria SYBR Green I Fluorescence Assay*

Inhibitors of  $\beta$ -hematin formation were tested in the CQ-sensitive, D6 strain of *P. falciparum* using a modification of literature methods.<sup>81</sup> Briefly, test compounds were prescreened at a concentration of 23  $\mu$ M at 0.3% starting parasitemia (2% hematocrit) in duplicate in 384-well optical bottom microtiter plates. Positive and negative controls consisted of a kill concentration of CQ (400 nM in water) and water, respectively. Dose-

response curves were established for each active compound from a concentration of 0-23  $\mu\text{M}$ . Sigmoidal dose-response curves were generated using GraphPad Prism v5.0 (March 7, 2007)

Clustering Analysis (kindly provided by Mariusz Butkiewicz)

$\beta$ -hematin active compounds were analyzed by means of hierarchical clustering with Average Linkage as cluster distance measure.<sup>82</sup> The similarity calculation among all compound pairs was based on common occurring molecule fragments. The fragment library was established by determining the largest common substructure between pairs of molecules keeping ring systems intact. Each fragment had a minimum of four atoms. The resulting library contained 165 unique molecule fragments. Pairwise distances were calculated based on molecule fragment overlap using tanimoto coefficients between molecular fragment sets.<sup>83</sup> All atoms were considered equivalent. Bonds were compared by order, ring membership, and aromaticity. A cluster linkage cutoff of 0.65 was chosen to find a balance between number of clusters and the scaffold purity in each cluster.

The analysis yielded a total of 47 clusters including 17 singletons (clusters containing 3 or fewer compounds). A careful analysis of each of the clusters resulted in the identification of 13 primary scaffolds that represent 51% of the entire set of  $\beta$ -hematin inhibitors. Some of the scaffolds are found within more than one cluster, reflecting the structural diversity associated with that particular scaffold.

## Results

### Primary NP-40 Detergent Mediated $\beta$ -Hematin Formation Screen

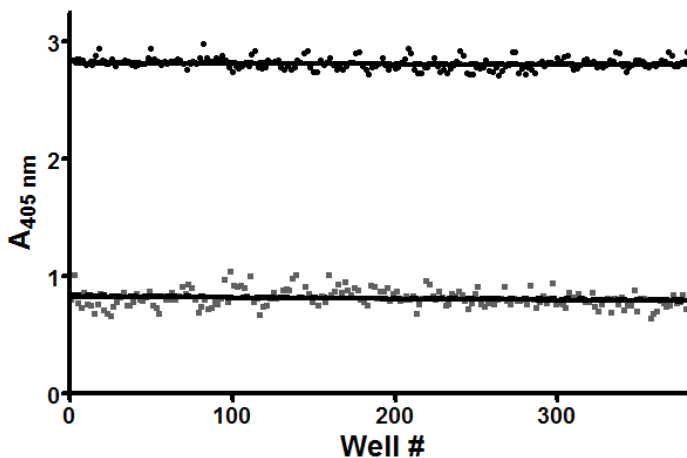
The NP-40 detergent mediated  $\beta$ -hematin formation assay originally reported for use in 96-well plates was modified and validated for suitability in high-throughput 384-well plate screening (Scheme 2).<sup>77</sup> While the chemistry of the assay remained unchanged, the processing of the assay was deemed unsuitable for HTS. In the original protocol, after incubation, the plate was centrifuged for one hour and the supernatant removed. The differential solubility of non-aggregated heme and  $\beta$ -hematin in sodium bicarbonate was used to isolate product by centrifugation. Subsequently, treatment with sodium hydroxide allowed quantification of  $\beta$ -hematin formation. The original method required over two hours of centrifugation, and multiple manual solution removal and additions to achieve a readable sample. The assay was simplified by implementing the colorimetric pyridine ferrochrome method described by Egan and coworkers.<sup>84</sup> A 50% pyridine solution in 20% acetone/water was added to each well, resulting in a final concentration of 5% v/v pyridine. The pyridine complexes free heme (absorbance at 405 nm), but not  $\beta$ -hematin, allowing for the rapid quantification of hemozoin formation. To ensure that the drug-response of this assay was preserved in this modified 384-well format, the  $IC_{50}$ 's of AQ and CQ were determined for comparison to the neutral lipid mediated assay. The  $IC_{50}$  using the NP-40 assay was 21.0  $\mu$ M for AQ and 53.0  $\mu$ M for CQ. This compares nicely to the assay mediated by the biological neutral lipid composition present within the parasite's digestive food vacuole where the  $IC_{50}$ 's of AQ and CQ were 23.1  $\mu$ M and 85.3  $\mu$ M. To further assess the drug response of the NP-40

assay, a series of known drugs were evaluated for  $\beta$ -hematin inhibition at a 100  $\mu$ M concentration (Table 4). Positive controls consisted of the antimalarials CQ, AQ and quinacrine, all known inhibitors of hemozoin formation. Negative controls were compounds that do not inhibit formation of hemozoin including pyrimethamine (antimalarial), indomethacin (antipyretic) and 8-hydroxyquinoline (a non-antimalarial quinoline). The results in Table 4 indicate the successful inhibition of  $\beta$ -hematin formation in the presence of positive controls, while only negligible crystal inhibition is observed in the presence of negative control drugs.

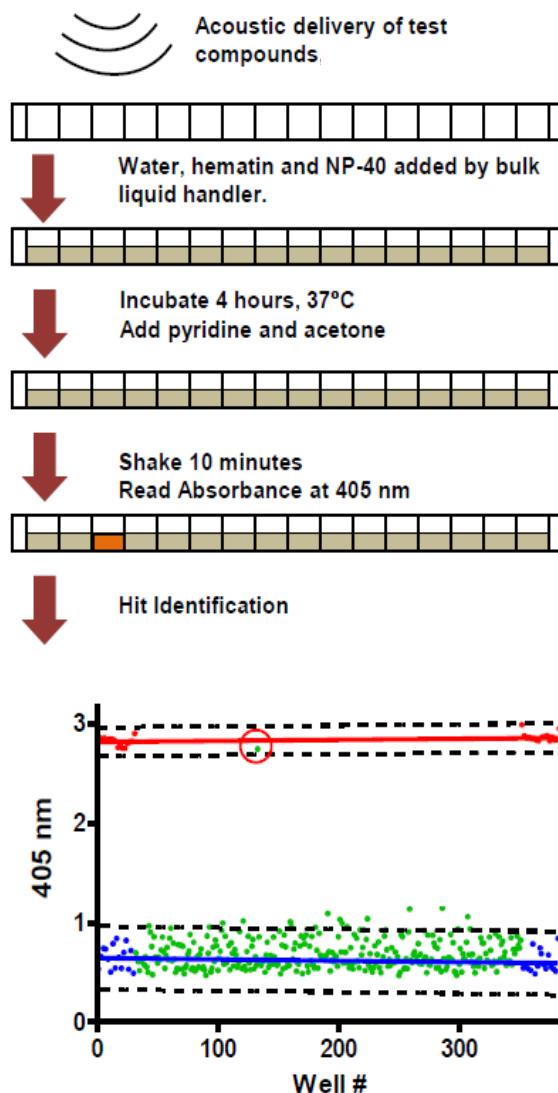
Drug	Known $\beta$ -Hematin Activity	% Inhibition
Pyrimethamine	-	1
Indomethacin	-	4
8-Hydroxyquinoline	-	5
Chloroquine	+	98
Amodiaquine	+	100
Quinacrine	+	100

**Table 4.** A panel of known inhibitors of  $\beta$ -hematin formation were tested in the NP-40 assay at a concentration of 100  $\mu$ M. The known inhibitors of  $\beta$ -hematin formation (indicated by a (+)) successfully prevented crystallization. The (-) drugs which are known as non-inhibitors of  $\beta$ -hematin formation were inactive in this assay.<sup>54</sup>

The quality of the assay was assessed by determining  $Z'$  using a 384-well plate of positive and negative controls consisting of wells with the  $IC_{100}$  of AQ and wells with an equal volume of DMSO distributed across the plate in an alternating, 'checkerboard' pattern (Figure 18).<sup>78</sup> Here, a favorable  $Z'$  of 0.82 is observed, well above the often reported 0.5 threshold value. The assay was also analyzed for drift and edge effects using the methods suggested by the NCGC. The maximal drift of the positive control was <2%, while the maximal drift of the negative control was <4% (maximal drift was observed when plotting well number by column, then by row). The assay was repeated on different days using freshly prepared solutions to ensure reproducibility of these results.



**Figure 18.** A 'checkerboard' pattern of positive and negative controls was utilized to analyze the  $Z'$ , drift and edge effects of the NP-40 detergent mediated assay prior to screening.<sup>54</sup>



**Scheme 2.** Steps in the NP-40  $\beta$ -hematin formation assay in HTS.<sup>54</sup>

### Identification of $\beta$ -Hematin Inhibitors

A total of 144,330 compounds from the Vanderbilt University HTS library were tested in the NP-40  $\beta$ -hematin formation assay (Scheme 2). This screening effort resulted in the identification of 729 compounds exhibiting >80% inhibitory activity relative to controls (0.5% hit rate). This threshold for identifying hits ensured that only potent  $\beta$ -hematin inhibitors were identified in addition to providing a manageable number of

compounds for follow-up dose response testing. Each preliminary hit was cherry-picked and tested in a dose-response assay (0.5 – 110  $\mu\text{M}$ ) to identify false-positives and to establish the potency of each hit against  $\beta$ -hematin formation. Compounds exhibiting  $\text{IC}_{50}$  values  $< 27 \mu\text{M}$  were confirmed as hits. Using this approach, a total of 530 hits was confirmed (0.14% false-positive hit rate, see Appendix D for full hit list). Of these, all had more potent  $\text{IC}_{50}$  values than CQ (53.0  $\mu\text{M}$ ) and 457 were more potent than AQ (21.0  $\mu\text{M}$ ) in this assay. The top ten most potent  $\beta$ -hematin inhibitors identified in this screen are shown in Table 5 to demonstrate the level of structural diversity resulting from this screening effort.

Identifier	Structure	$\beta$ -hematin IC <sub>50</sub> ( $\mu$ M)	D6 IC <sub>50</sub> ( $\mu$ M)
VU0014981		0.5	Inactive
VU0063871		0.5	Inactive
VU0015078		1.1	0.81
VU0020967		1.5	Inactive
VU0042031		1.7	3.52
VU0000264		2.0	0.59
VU0099210		2.2	Inactive
VU0123869		2.4	Inactive
VU0358176		2.4	1.72
VU0094619		2.4	0.70

**Table 5.** The top ten most potent  $\beta$ -hematin inhibitors identified in the screening effort.



### Activity of $\beta$ -hematin inhibitors in cultures of *P. falciparum*

While the  $\beta$ -hematin formation assay successfully identified over 500 highly potent inhibitors of heme crystallization, it was vital to establish whether or not these compounds retained activity in *in vitro* cultures of *P. falciparum*. As such, the malaria SYBR green I-based fluorescence assay described by Johnson and coworkers was used to establish the activity of each of the 530  $\beta$ -hematin inhibitors against parasitized red blood cells.<sup>81</sup> Each  $\beta$ -hematin inhibitor was prescreened at a concentration of 23  $\mu$ M. Percent inhibition was determined relative to positive (kill concentration of CQ) and negative (DMSO only) controls. Test compounds that exhibited >90% inhibition of parasitemia were considered hits. Using these criteria to identify hits, 171 of the  $\beta$ -hematin inhibitors identified in the primary screen were also active against the parasite cultures. This high hit rate (32%) was quite surprising, as previous analysis of HTS libraries against cultures of parasitized red blood cells have resulted in hit rates of ~1% when compounds were tested at a similar concentration and similar activity thresholds were considered.<sup>68</sup> The considerable increase in *in vitro* antimalarial activity observed within the  $\beta$ -hematin inhibitors would suggest that many of these compounds are indeed reaching their proposed target, hemozoin.

Follow-up dose-response analysis of the 171  $\beta$ -hematin inhibiting *in vitro* antimalarial compounds revealed that many highly potent compounds were present within this subset of the screening library. Specifically, 73 compounds exhibited < 5  $\mu$ M activity against *P. falciparum*, including 25 compounds with nanomolar activity. The ten most potent *in vitro* antimalarial  $\beta$ -hematin inhibitors identified in this screen are shown in Table 6. Furthermore, each compound exhibiting nanomolar activity against the D6

strain was also tested against the multidrug-resistant C235 strain of *P. falciparum* to determine the resistance index associated with each of the most potent in vitro antimalarial  $\beta$ -hematin inhibitors. For 21 of the 25 nanomolar potent in vitro antimalarials identified, the resistance indices were between 0.2 - 3, suggesting that the majority of these compounds may serve as valuable starting points for lead probe optimization.

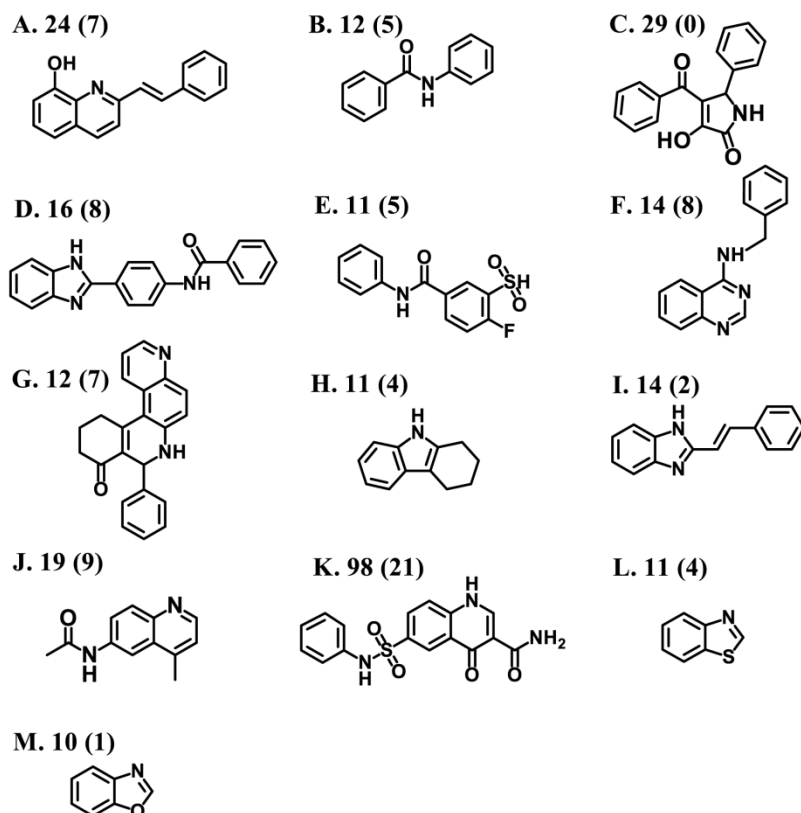
Identifier	Structure	$\beta$ -hematin IC <sub>50</sub> ( $\mu$ M)	D6 IC <sub>50</sub> ( $\mu$ M)	C235 IC <sub>50</sub> ( $\mu$ M)	RI
VU0098755		12.6	0.106	0.127	1.2
VU0073687		6.3	0.185	0.551	2.9
VU0001281		5.9	0.194	0.174	0.9
VU0065708		16.2	0.198	0.184	0.9
VU0096505		8.8	0.238	0.217	0.9
VU0107282		16.9	0.290	0.54	1.9
VU0114785		13.4	0.346	4.817	13.9
VU0002101		14.3	0.348	0.412	1.2
VU0028177		13.3	0.350	0.465	1.3
VU0063971		8.9	0.384	0.833	2.2

**Table 6.** The top ten most potent in vitro antimalarial  $\beta$ -hematin inhibitors identified in the HTS effort.

### Structural characterization of hits

In an effort to assess the chemical diversity of compounds exhibiting activity against  $\beta$ -hematin formation, a clustering analysis was performed using hierarchical

clustering with Average Linkage as a cluster distance measure. This analysis yielded a total of 47 clusters including 17 singletons (a cluster containing three or fewer compounds). The resultant clusters were then carefully scrutinized to identify scaffolds present within the data set of  $\beta$ -hematin inhibitors. Figure 19 shows the 13 predominant scaffolds identified in this analysis. The number of  $\beta$ -hematin inhibitors associated with each scaffold (as well as the number of those  $\beta$ -hematin inhibitors that also showed in vitro antimalarial activity) is shown above each scaffold. These 13 scaffolds represent 51% of the total number of  $\beta$ -hematin inhibitors identified.



**Figure 19.** The 13 scaffolds that represent 52% of the  $\beta$ -hematin inhibitors identified in the screening effort.

### *Quinoline-Based (scaffolds A, G, J and K)*

Quinoline-based compounds are among the most successful and widely used antimalarials developed to date. Though most strains of the parasite have developed resistance to CQ, several classes of quinoline derivatives that evade the mechanism of resistance have been developed including ferroquine which is currently in clinical development.<sup>75,76</sup> The ability to overcome quinoline resistance suggests that creative medicinal chemistry could perpetuate quinolines as a valid scaffold. Of the 530  $\beta$ -hematin inhibitors identified, several quinoline-based scaffolds were noted. Scaffolds A, B, J and K represented 12, 12, 19 and 98 of the total number of  $\beta$ -hematin inhibitors identified, respectively. Further, approximately one-third of these quinoline-based  $\beta$ -hematin inhibitors were also active against the parasite. While scaffold A was previously reported in the results of the pilot screen (38,000 compounds were screened), scaffolds G, J and K were only identified after completion of screening the entire HTS library of 144,330 compounds.<sup>54</sup> Derivatives of both scaffold G and J have previously been reported in the PubChem database (<http://pubchem.ncbi.nlm.nih.gov/>) as having activity against *P. falciparum* targets M18 aspartyl aminopeptidase (AID 1822), plastid activity (AID 504834) and glucose-6-phosphate dehydrogenase activity (AID 504690). No previously reported activity for scaffold K was found.

### *Phenyl benzamides (scaffolds B, D and E)*

Several phenyl benzamides were also identified from the clustering analysis. Benzamides have previously been investigated for their activity against *P. falciparum*

(AID 2306) and have also been identified as inhibitors of the *P. falciparum* pyrimidine biosynthetic enzyme dihydroorotate dehydrogenase PfDHODH.<sup>54,64,85,86</sup> Scaffolds B, D and E contained 12, 16 and 11  $\beta$ -hematin inhibitors, respectively. Surprisingly, nearly half (46%) of these phenyl benzamide  $\beta$ -hematin inhibitors were also active in parasite cultures.

#### *Benzylethene (scaffolds A and I)*

Scaffolds A and I contain an ethene-bridged phenyl group to either a quinoline or benzimidazole. Though A is an 8-hydroxyquinoline (and by structural definition is a quinoline), the quinoline portion of this scaffold does not explain its activity. Previous analysis of 8-hydroxyquinoline has demonstrated that this compound is not active against  $\beta$ -hematin formation. Therefore, the activity of scaffold A must be related to the addition of the ethane-bridged phenyl group. As such, it is more accurate to group scaffold A with scaffold I than to associate it strictly as a quinoline. The two scaffolds, A and I, containing this structural motif have previously been reported to have in vitro antimalarial activity (AID 2306).<sup>64</sup> Scaffolds A and I contained 12 and 14 compounds, respectively. 58% of scaffold A  $\beta$ -hematin inhibitors were active against the parasite while 14% of the  $\beta$ -hematin inhibitors from cluster I were active against the parasite.

#### *Miscellaneous Compounds:*

In addition to the 13 scaffolds identified in this effort, a large number of interesting compounds were not associated with a specific scaffold type, or only accounted for a very small percentage of the overall hit rate. Specifically, 261  $\beta$ -hematin

inhibitors that did not fall into a specific scaffold were identified including 90 *in vitro* antimalarial compounds. The structural diversity of these compounds include pyridines, amides, indoles, acridinediones, amides, ethers and thiols, among others.

## Discussion

Utilizing the biologically relevant conditions under which hemozoin formation occurs within the digestive food vacuole of the parasite, 144,330 compounds were screened to identify those that inhibit  $\beta$ -hematin formation. As a result of this effort, 530 potent  $\beta$ -hematin inhibitors were identified, 32% of these hits were further shown to have *in vitro* antimalarial activity. Previous successful attempts to identify *in vitro* antimalarial compounds in HTS libraries have resulted in hit rates of ~1% when compounds were tested at a similar concentration and similar activity thresholds were considered.<sup>68</sup> Therefore, by utilizing an assay that successfully recapitulates biological conditions within the digestive food vacuole of the parasite, a higher percentage of compounds retained activity against *in vitro* cultures of *P. falciparum*. Further, this strong correlation between target-specific and *in vitro* antimalarial activity suggests that many of these compounds are indeed acting on their proposed target, hemozoin.

Examination of the structures that were identified as having activity against  $\beta$ -hematin formation screen reveals 13 distinct scaffolds that represent 269 of the total number of compounds identified in this screen (Figure 19). The remaining 261 compounds that were not associated with one of the 13 scaffolds encompass a wide range of structural diversity. It is important to note that the overwhelming majority of these

compounds have not previously been reported as having activity against  $\beta$ -hematin formation.

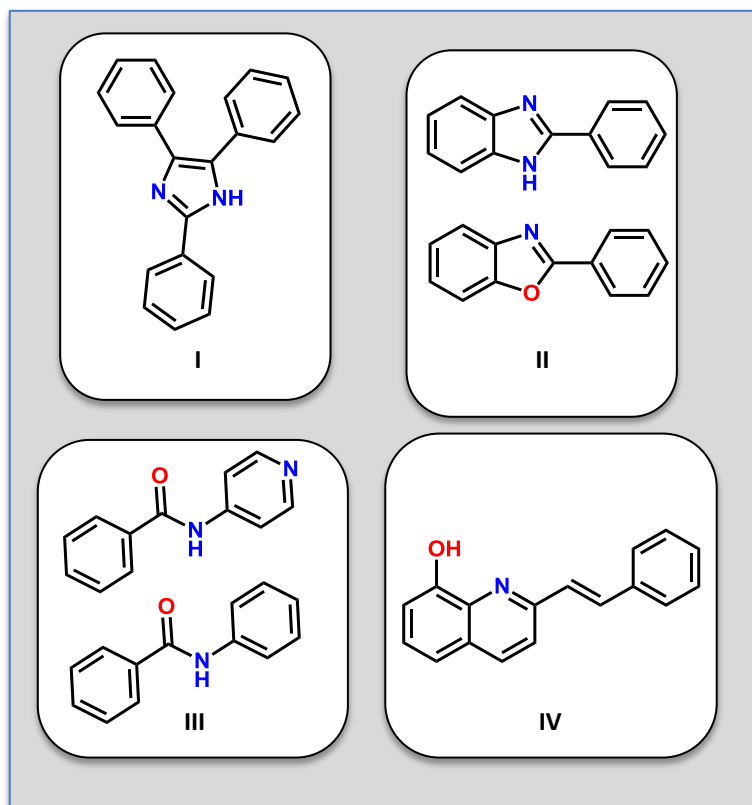
HTS has become a valuable technique to rapidly identify *in vitro* antimalarial compounds. Notably, GlaxoSmithKline (GSK), St. Jude Children's Research Hospital and Novartis have screened millions of compounds against *P. falciparum*.<sup>62-64</sup> Though these efforts have resulted in the identification of thousands of chemical starting points, the optimization of the lead compounds into useful drugs may prove challenging since the targets of these *in vitro* antimalarial compounds are unknown. The reductionist approach reported herein facilitates the prioritization of HTS *in vitro* antimalarial compounds based on their activity against a specific antimalarial target, hemozoin formation. The next stage of this work will be to validate hemozoin as the *in vivo* target for each of the compounds exhibiting nanomolar activity against *P. falciparum*.<sup>74</sup> Compounds that are confirmed to inhibit hemozoin formation in parasite cultures will then be tested further in terms of solubility, permeability and metabolic stability. With such a diverse library of compounds, the probability of identifying multiple lead candidates for further development is likely.



## **Part II. Preliminary SAR Evaluation of Four Scaffolds Identified in the HTS Campaign**

### **Introduction**

The NP-40  $\beta$ -hematin formation assay was successfully utilized to screen a library of 144,330 compounds (Part I). The screening campaign resulted in the identification of 530 inhibitors of  $\beta$ -hematin formation (see Appendix D for complete list of active compounds and their respective activities activity). With hundreds of chemical starting points available, four scaffolds (Figure 20, triarylimidazole, benz-azole, pyridyl- and phenyl- amide, and hydroxyquinoline) were selected for a preliminary structure-activity analysis (SAR). The goal of this effort was to obtain a more detailed understanding of the activity of each scaffold in order to determine if a more rigorous and expensive SAR analysis is warranted. These four scaffolds were selected based on 1) the chemical tractability for synthetic chemistry 2) commercial availability and 3) in vitro antimalarial activity.



**Figure 20.** Preliminary SAR analysis of four scaffolds was explored. (I) triarylimidazole (II) benzimidazole and benzoxazole (III) phenylbenzamide and pyridylbenzamide (IV) hydroxyquinoline

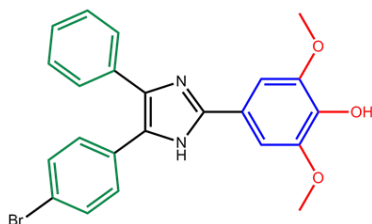
## Results

### I. Triarylimidazole

The triarylimidazole scaffold exhibits a wide range of biological activity including antibacterial and analgesic activity and has previously been shown to inhibit  $\beta$ -hematin formation.<sup>54,87</sup> Though potent in vitro antimalarial compounds containing this core scaffold have been identified, the mechanism of interaction with the putative target, heme, has not previously been explored. The NP-40  $\beta$ -hematin formation assay

identified a particularly potent compound that is also a potent in vitro antimalarial ( $IC_{50} = 310$  nM, Figure 21). A literature review revealed that this scaffold has not previously been explored for use as an antimalarial. A set of eleven derivatives were therefore selected with the guidance of the Chemical Synthesis Core at Vanderbilt. The derivatives were selected in order to examine the significance of three structural components of the original hit (Figure 22):

- 1) determine the importance of O-rich substituents on the phenyl ring (red)
- 2) determine if the phenyl ring can be replaced with a pyridine ring<sup>36</sup> (blue)
- 3) determine the consequences of substitution on the phenyl rings (green)

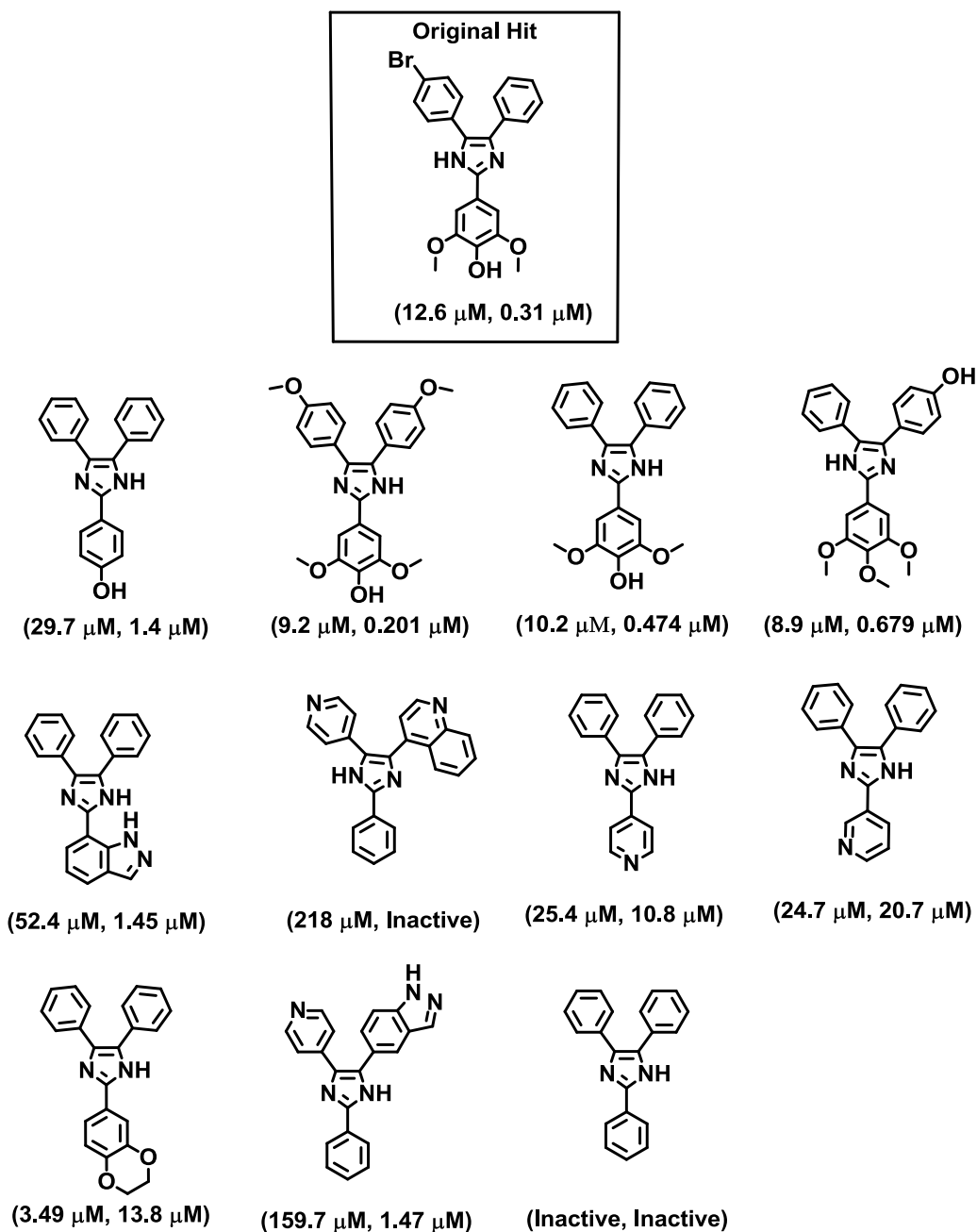


**Figure 21.** The original hit identified in the HTS screen exhibited an  $IC_{50}$ 's of  $12.6\mu\text{M}$  in the  $\beta$ -hematin formation assay and  $310$  nM in the MSF assay.

Of the eleven derivatives obtained, ten retained activity in the  $\beta$ -hematin formation assay. The compound that lost activity is the triarylimidazole that contains no substituents on the phenyl rings. Concentration-response data reveals  $IC_{50}$  potencies for the ten actives ranging from  $3.49 - 218 \mu\text{M}$ . When tested against in culture of *P. falciparum*, nine compounds exhibited activity with  $IC_{50}$  values ranging from  $201$  nM –  $20.7 \mu\text{M}$ . A careful structural examination reveals that the compounds in the second row

(Figure 22) are the most active against the malaria parasite. The common feature in this subset of compounds is the presence of oxygen-containing functional groups at the 2-phenyl position. Though the precise molecular interactions that are responsible for this increased activity are not yet understood, two hypotheses are considered:

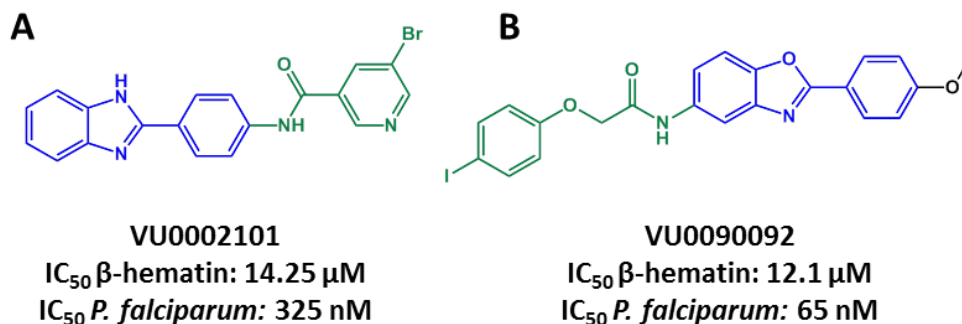
- 1) The oxygen atoms, as electron donating groups, could increase the electronegativity of the phenyl ring. The increased negative charge on the phenyl ring could then facilitate pi-cation interactions between the phenyl ring and the Fe(III) center of heme.
- 2) As is observed for the antimalarial halofantrine, an oxygen atom could coordinate directly to the Fe(III) center of heme, thereby preventing the formation of the reciprocal heme-propionate dimeric species that is incorporated into the hemozoin crystal.<sup>88</sup>



**Figure 22.** A set of eleven triarylimidazoles were obtained/synthesized in order to further explore the activity of this scaffold. Parenthesis denote: (IC<sub>50</sub>  $\beta$ -hematin inhibitory activity, IC<sub>50</sub>  $\mu\text{M}$  in vitro antimalarial activity)

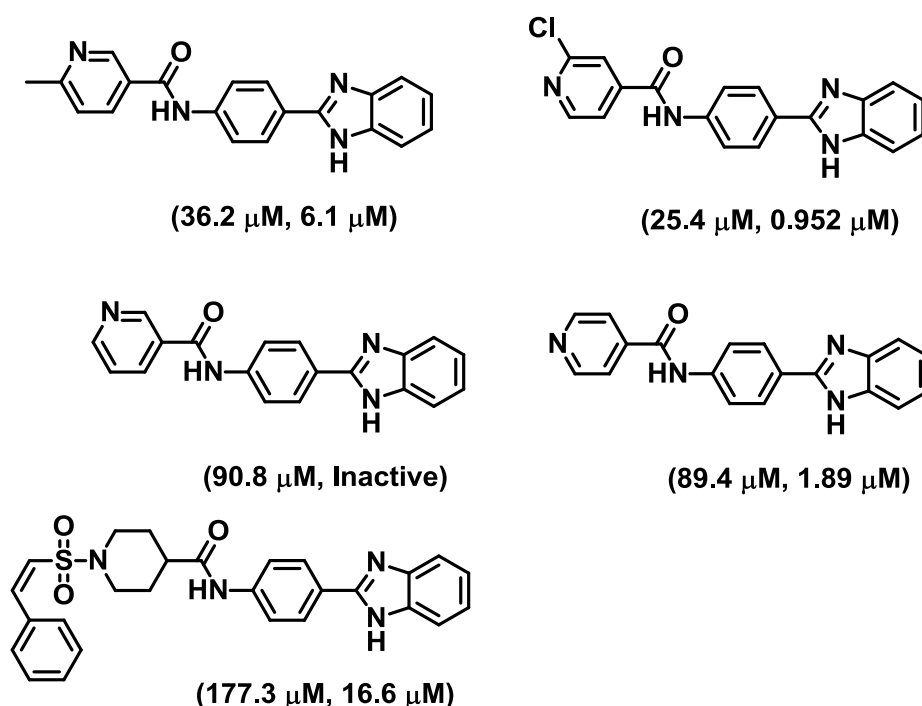
## II. Benz-azole

The benzimidazole scaffold is an important pharmacophore and privileged structure exhibiting a broad range of biological activity. Benzimidazoles have been widely used in both humans and livestock as broad spectrum anthelmintics (i.e. albendazole, mebendazole).<sup>89</sup> The benzimidazole and benzoxazole scaffolds have previously been identified as antimalarial inhibitors of  $\beta$ -hematin formation.<sup>54,64,90</sup> A literature evaluation reveals a range of benz-azoles have inhibitory activity against  $\beta$ -hematin formation; however this scaffold has not previously been optimized for use as an antimalarial. In the HTS analysis (Part I), 49 benz-azoles were identified that exhibited potent  $\beta$ -hematin inhibitory activity. A careful examination of these hits prompted a further investigation based around two specific benz-azole scaffolds (Figure 23).



**Figure 23.** Analysis of the hits identified in the HTS effort revealed several interesting benz-azole scaffolds including a benzimidazole (VU0002101) and a benzoxazole (VU00090092). Both compounds contain a 2-phenyl benz-azole scaffold (blue). The green highlighted portion indicates the region of the molecule that was altered in the derivatives obtained.

The common feature of both benz-azole scaffolds is the presence of the phenyl substituent in the 2 position. Furthermore, each scaffold also contains an amide group, though the location of this group differs for each of the scaffolds. For the benzimidazole, VU0002101, the focus was to obtain derivatives that preserved the core scaffold (blue) while altering the pyridyl amide (green) portion of the molecule. For the benzoxazole (VU0090092), the derivatives obtained preserved the core scaffold (blue) while substituting the phenoxyacetamide portion of the molecule (green). A total of 13 benz-azole derivatives were obtained. Six derivatives of the benzoxazole scaffold (VU0090092) were obtained but none of these retained  $\beta$ -hematin inhibitory or in vitro antimalarial activity, suggesting that modifications to the 5 position are not trivial. For the benzimidazole scaffold (VU0002101), seven derivatives were selected, with five exhibiting activity against  $\beta$ -hematin formation and four with in vitro antimalarial activity (Figure 24).

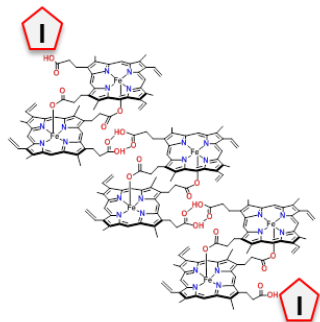


**Figure 24.** A set of 13 benz-azoles were obtained in order to further explore the activity of this scaffold. The two original compounds that prompted exploration of these scaffolds are shown at the top of the figure. Parenthesis denote: ( $\text{IC}_{50}$   $\beta$ -hematin inhibitory activity,  $\text{IC}_{50}$   $\mu\text{M}$  in vitro antimalarial activity)

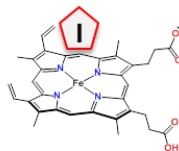
There are three mechanisms by which  $\beta$ -hematin inhibitory activity can be observed (Figure 25). First, the inhibitor can bind directly to the  $\beta$ -hematin crystal. As a result of this capping mechanism, heme cannot be incorporated into the growing  $\beta$ -hematin crystal.<sup>41</sup> Alternatively,  $\beta$ -hematin inhibition can be the result of interactions between the inhibitor and free heme, as is thought to be the case for many antimalarial hemozoin inhibitors.<sup>41,91</sup> In this assay  $\beta$ -hematin inhibition can also be the result of interactions between the inhibitor and NP-40 detergent, compromising the ability of the NP-40 detergent to mediate crystallization.



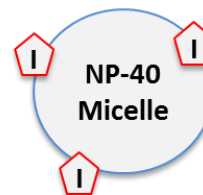
### I. Crystal Capping



### II. Interaction With Free Heme



### III. Interaction with Detergent Micelle

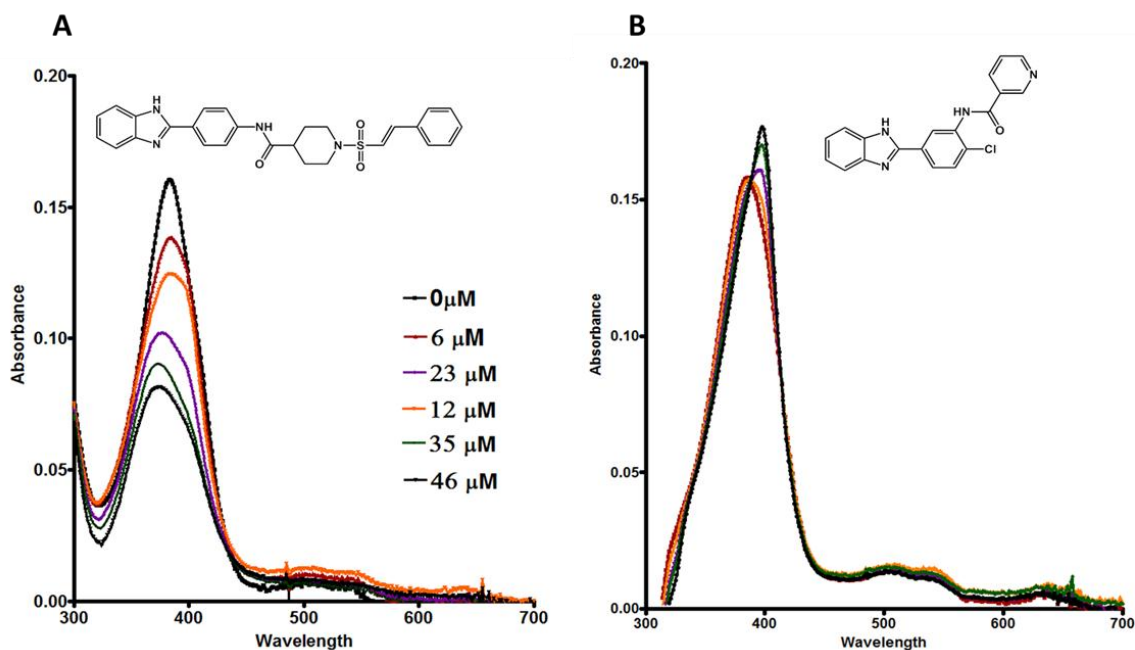


 = Inhibitor

**Figure 25.** There are multiple modes by which a compound could potentially inhibit  $\beta$ -formation in the assay. (I) Interaction with the  $\beta$ -hematin crystal (II) Interaction with free heme (III) Interaction with mediator

Here, we wanted to determine if the benzimidazole scaffold interacts with free heme. This interaction can be observed by monitoring the heme Soret band using UV-Vis spectrophotometry.<sup>88</sup> Figure 26A reveals that upon titration of the heme solution with benzimidazole  $\beta$ -hematin inhibitor, a hypochromic shift occurs in the Soret band. This type of shift has been observed with other  $\beta$ -hematin inhibitors such as chloroquine and halofantrine and is indicative of  $\pi$ - $\pi$  interactions with heme.<sup>88</sup> Therefore, this evidence clearly demonstrates that the benzimidazole does indeed interact directly with heme, leading to inhibition of  $\beta$ -hematin formation. As a control, one of the benzimidazole derivatives that did not exhibit  $\beta$ -hematin inhibitory activity was analyzed

under the same conditions. No significant change in the heme Soret band was observed (Figure 26B).

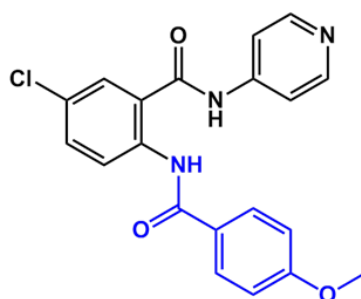


**Figure 26.** Solutions of free heme were titrated with (A) a benzimidazole  $\beta$ -hematin inhibitor and (B) a control benzimidazole that does not inhibit  $\beta$ -hematin formation. This analysis confirms that the benzimidazole  $\beta$ -hematin inhibitor directly interacts with free heme, leading to the inhibitory activity observed for this compound.

### III. Pyridylbenzamides

Benzamides have previously been investigated for their activity against *P. falciparum* and have been shown to inhibit both  $\beta$ -hematin formation and PfDHODH (an enzyme in the *de novo* pyrimidine biosynthetic).<sup>54,85,86</sup> In the HTS effort, several benzamides and pyridylbenzamides were identified which prompted further examination

of this scaffold. VU0003659 is both a pyridylbenzamide and phenylbenzamide and exhibits potent  $\beta$ -hematin inhibitory and in vitro antimalarial activity (Figure 27).



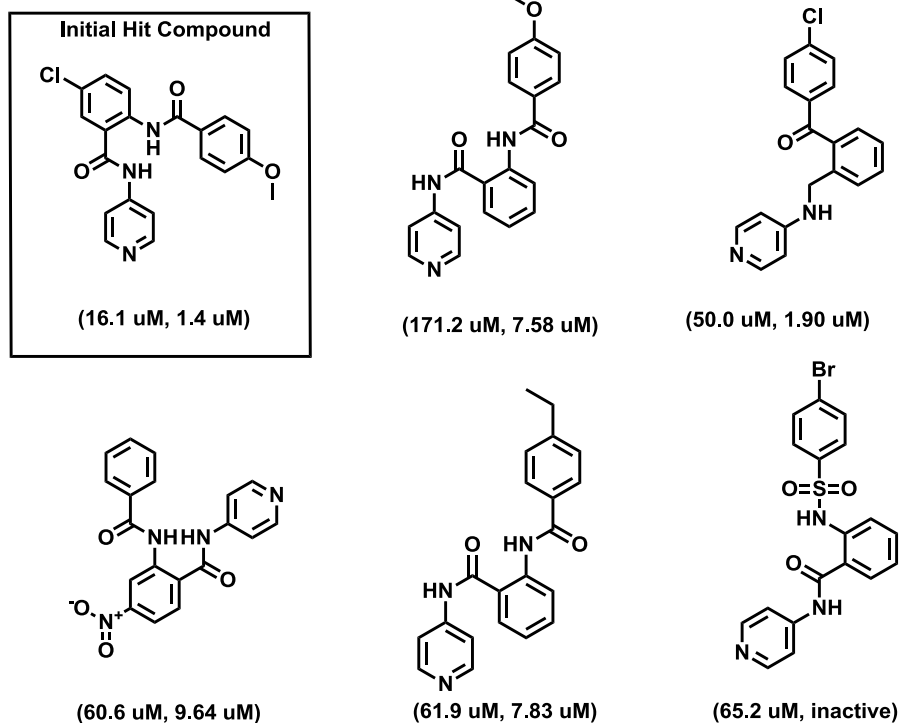
VU0003659

IC<sub>50</sub>  $\beta$ -hematin: 16.1  $\mu$ M

IC<sub>50</sub> *P. falciparum*: 1.4  $\mu$ M

**Figure 27.** VU0003659 was selected from the HTS results for further evaluation. The derivatives obtained preserved the pyridyl portion of the scaffold (black) while substituting the benzamide portion (blue).

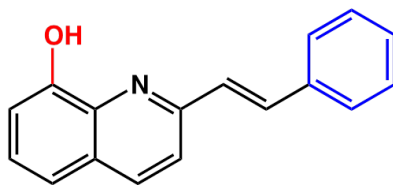
For this scaffold, the focus was to obtain derivatives that preserve the pyridylbenzamide moiety and focus on substituting the benzamide portion of the scaffold (blue, Figure 27). Consequently, a total of eleven derivatives were (Figure 28) obtained. Five of the compounds exhibited  $\beta$ -hematin inhibitory activity with IC<sub>50</sub> values ranging from 50.0 – 171  $\mu$ M. Four of the five  $\beta$ -hematin inhibitors retained activity against cultures of *P. falciparum* with IC<sub>50</sub> values ranging from 1.9 – 9.64  $\mu$ M.



**Figure 28.** A set of eleven pyridylbenzamides were. Parenthesis denote: ( $IC_{50}$   $\beta$ -hematin inhibitory activity,  $IC_{50}$   $\mu$ M in vitro antimalarial activity)

#### IV. Hydroxyquinoline

The HTS screening efforts revealed several hydroxyquinolines that were active against  $\beta$ -hematin formation and toxic to the parasite (Figure 29). This scaffold contains an ethene-bridged phenyl group to a quinoline, though the HTS screen revealed that a benzimidazole can substitute the quinoline ring as a scaffold. It is interesting that 8-hydroxyquinoline itself (the core scaffold) is not active against  $\beta$ -hematin formation. This suggests that the ethene-bridged phenyl ring plays a role in the activity of this scaffold.

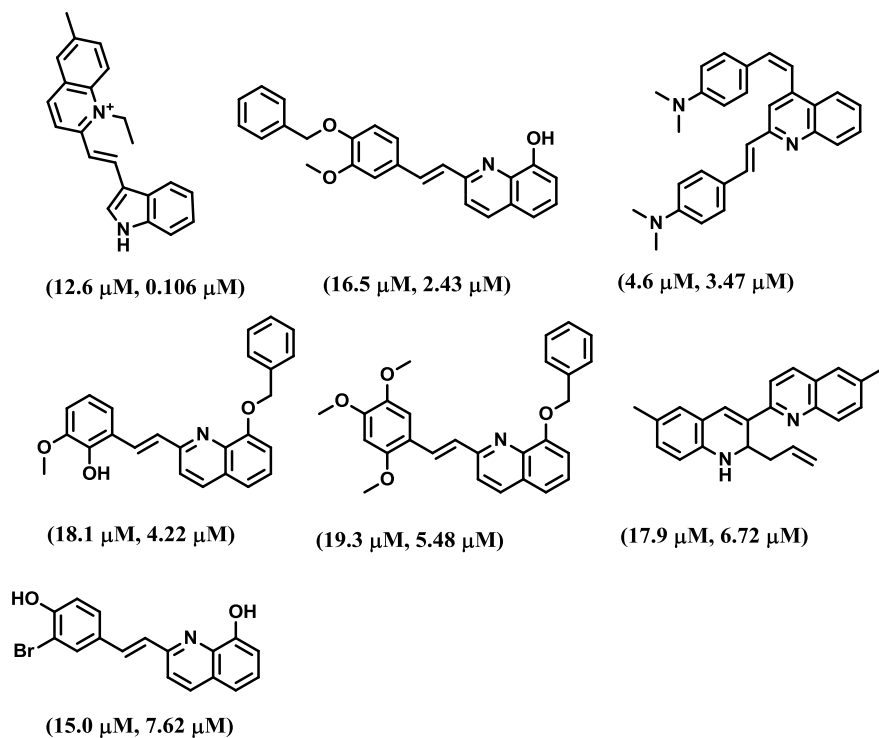


**Figure 29.** A set of six hydroxyquinolines were obtained in an effort to establish the effects of substitution at the hydroxyl (red) position or substitution of the phenyl ring (blue).

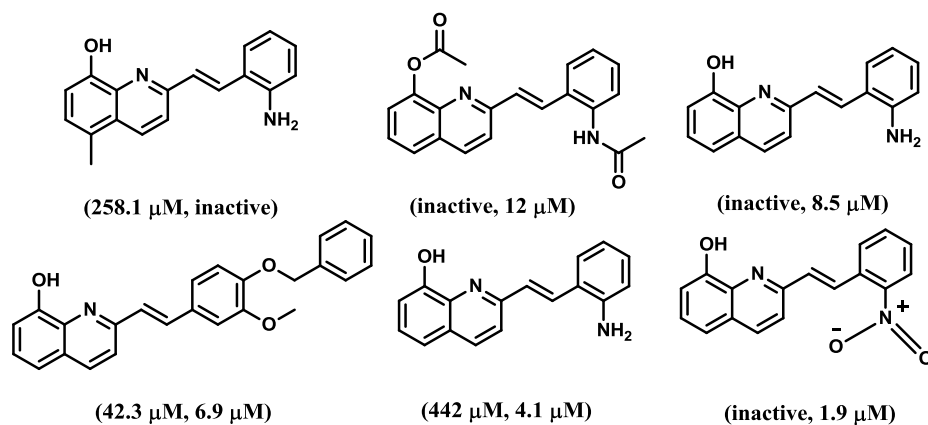
A moderate amount of structural diversity was observed for this scaffold in the HTS screen (Figure 30A). We therefore expected that manipulation of this scaffold would lead to derivatives where activity is retained. A set of six derivatives were obtained based on this scaffold. The primary focus was to establish the effects of 1) adding bulk to the 8-position of the quinoline ring and 2) substitutions at the ethene-bridged phenyl ring (Figure 30B). Three of the compounds exhibited  $\beta$ -hematin inhibitory activity with  $IC_{50}$  values ranging from 42.3 – 442  $\mu$ M. Interestingly, five of derivatives exhibited in vitro antimalarial activity with  $IC_{50}$  values ranging from 1.9 – 12  $\mu$ M. Since several of the compounds had no activity in the  $\beta$ -hematin formation assay, while maintaining activity against the malaria parasite suggests that this in vitro antimalarial activity is either the result of interaction with two distinct targets (one of which is possibly hemozoin formation) in *P. falciparum* or activity is due to another pathway altogether. Two independent targets could explain why three of the compounds with diminished activity against  $\beta$ -hematin formation is still toxic to the parasite. Indeed, a review of the literature reveals that in vitro antimalarial compounds containing this core scaffold also exhibits activity against multiple aminopeptidases that are present in the

digestive food vacuole of the parasite and play key roles in the process of hemoglobin digestion.

### A. HTS Compounds

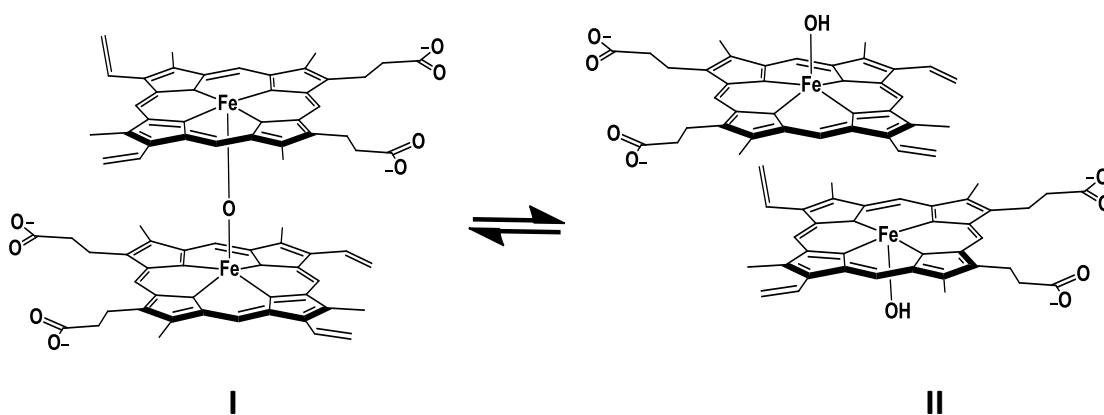


### B. Compounds Obtained



**Figure 30.** (A) Hydroxyquinolines identified in the HTS screen and (B) the set of 6 hydroxyquinolines that were obtained. Parenthesis denote: ( $IC_{50}$   $\beta$ -hematin inhibitory activity,  $IC_{50}$   $\mu\text{M}$  in vitro antimalarial activity)

A common feature of the hydroxyquinoline compounds exhibiting diminished activity in the  $\beta$ -hematin formation assay is the absence of O-containing functional groups on the ethene-bridged phenyl ring. There is potential that oxygen rich functional groups on this phenyl ring increase electron density and promote higher affinity interactions with free heme. Alternatively, the O atom itself could perhaps interact with the Fe(III) center of free heme, as is the case for the antimalarial halofantrine.<sup>88</sup> This hypothesis was examined by exploiting the sensitivity of heme to its environmental conditions (Figure 31).<sup>92</sup>

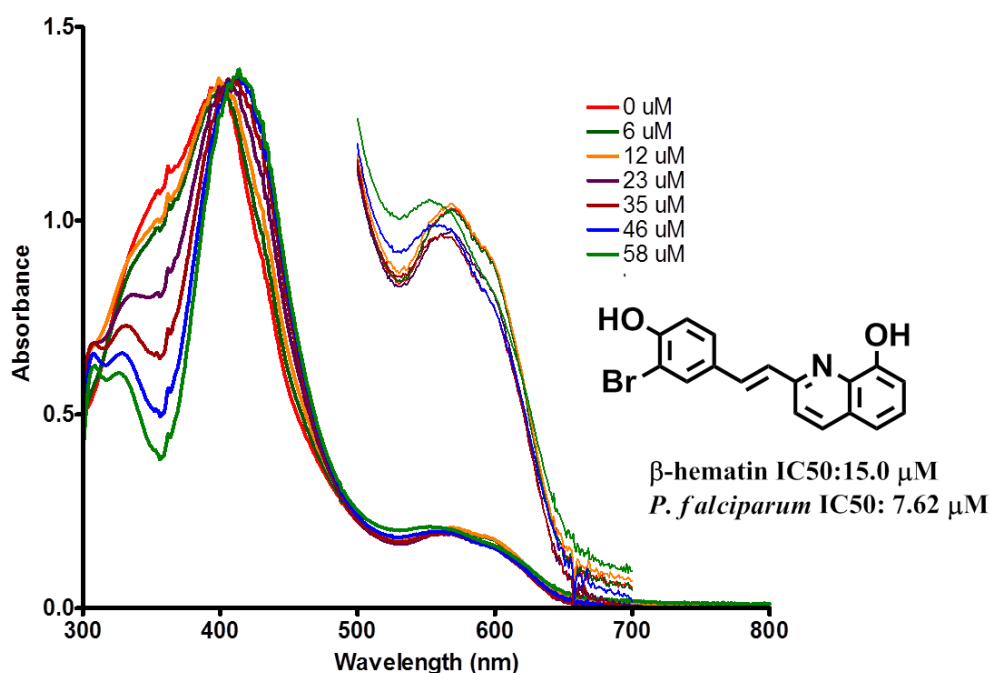


**Figure 31.** The speciation of free heme can be readily manipulated. (I) The  $\mu$ -oxo dimeric species of heme and (II) the  $\pi$ - $\pi$  dimeric species of heme can be controlled by the identity of the solvent.

Specifically, the  $\mu$ -oxo dimeric species of free heme was promoted by solubilization in 40% DMSO, pH 7.4. Under these conditions, the heme Soret band exhibits a characteristic shoulder peak ( $\sim 370$  nm) that is not observed in monomeric free heme or  $\pi$ - $\pi$  dimeric free heme when observed with UV-Vis spectrophotometry.<sup>92</sup> As a



five coordinate species, if a molecule binds to the Fe(III) center of free heme, the  $\mu$ -oxo dimeric linkage will be broken and the shoulder peak will no longer be observed. If a  $\beta$ -hematin inhibitor owes its activity to direct coordination to the Fe(III) center, the Fe-O-Fe linkage will be broken and the shape of the Soret band will change. As such, a representative hydroxyquinoline was analyzed using this approach. Figure 32 demonstrates that the shoulder peak of the heme Soret band decreases upon titration with the hydroxyquinoline  $\beta$ -hematin inhibitor. In fact, at 58  $\mu$ M concentration of the inhibitor, the Soret band now exhibits the characteristic shape of a pi-pi dimeric species. This is supportive of direct coordination of the hydroxyquinoline to the Fe(III) center of heme.



**Figure 32.** The hydroxyquinoline compound was titrated into a solution of  $\mu$ -oxo dimeric free heme. The shoulder-shift in Soret band as a function of increasing concentration of hydroxyquinoline suggests that this compound is outcompeting the  $\mu$ -oxo dimer linkage. This is indicative of coordination of the hydroxyquinoline to the Fe(III) center of heme, thereby inhibiting  $\beta$ -hematin formation.

## Conclusions and Future Directions

The HTS efforts discussed in Part I resulted in the identification of multiple scaffolds that have not previously been acknowledged as inhibitors of  $\beta$ -hematin formation and/or in vitro antimalarial compounds. The majority of these scaffolds have also never been evaluated for use as potential lead probe candidates. Therefore, four of these scaffolds were selected for a preliminary SAR analysis to determine the usefulness of each scaffold for optimization. The primary goal of this analysis was to determine if derivatives of each scaffold would retain  $\beta$ -hematin inhibitory and in vitro antimalarial activity. The four scaffolds were selected based upon the chemical tractability for synthetic chemistry, commercial availability and/or potency of in vitro antimalarial activity.

The triarylimidazole compound originally identified in the HTS effort exhibited more potent  $\beta$ -hematin inhibitory activity than either amodiaquine or CQ in this assay. This compound was also potent against both CQ-sensitive and multi-drug resistant strains of *P. falciparum* with  $IC_{50}$  values of 310 nM and 942 nM, respectively. Analysis of the eleven derivatives obtained for further study suggest that the presence of  $-OH$  or  $-OMe$  substituents on the phenyl ring contribute to the potency of this scaffold. This observation was also made for the hydroxyquinoline scaffold. Though the precise molecular interactions that are responsible for this activity are not yet known, two hypotheses are considered regarding the importance of oxygen substituents in the triarylimidazole and the hydroxyquinoline scaffold. 1) The oxygen atoms donate electron density to the phenyl ring. Since electron donating groups strengthen the cation-

$\pi$  interactions, we could expect the affinity between the –OH or –OMe substituted phenyl ring of the triarylimidazole or hydroxyquinoline with the Fe(III) center of heme to be increased.<sup>93</sup> 2) Alternatively, an oxygen atom could be coordinating directly to the Fe(III) center of heme as is the case of the antimalarial halofantrine.<sup>88</sup> For the hydroxyquinoline scaffold, spectrophotometric data was obtained in order to investigate hypothesis ‘2’. The results of this analysis demonstrate that the  $\mu$ -oxo dimeric species of heme is reduced upon titration with a hydroxyquinoline compound containing an –OH substituent on the phenyl ring. This is indicative of direct coordination to the Fe(III) center of heme. Future efforts will be necessary to validate that this interaction leads to the activity of the hydroxyquinoline. This analysis will also be necessary for the triarylimidazole.

Fewer than 50% of the pyridylbenzamide and benz-azole derivatives obtained retained  $\beta$ -hematin inhibitory or in vitro antimalarial activity. Since a small number of derivatives were obtained for these scaffolds, further investigation will be necessary before any conclusions regarding the usefulness of either scaffold for optimization can be made.

Our investigation has resulted in meaningful preliminary information regarding the triarylimidazole and hydroxyquinoline scaffolds. We will now focus on elucidating the specific molecular interactions that lead to  $\beta$ -hematin inhibitory activity. Specifically, the role of the –OH and –OMe substituents will be determined. If the oxygen containing substituents are verified to play a primary role in the observed activity, our focus can shift to optimizing the pharmacokinetic properties of the scaffolds while preserving the portion of the scaffold that leads to inhibitory activity. For the pyridylbenzamide and benz-azole

scaffolds, additional derivatives must be analyzed before any conclusions regarding the value of these two scaffolds as potential lead probe candidates can be made. Compounds that inhibit  $\beta$ -hematin formation from all four of the scaffolds will also be analyzed in cultures of *P. falciparum* in order to validate that hemozoin is the biological target leading to in vitro antimalarial activity.<sup>74</sup>

## **Part III: Identification of $\beta$ -Hematin Inhibitors from In vitro antimalarial Compounds Identified in Phenotypic Screens**

### Introduction

In antimalarial HTS, phenotypic assays are those that seek to identify small molecules that are capable of killing *P.falciparum*. Recently, phenotypic screens have been completed by GSK and Novartis against millions of compounds in their respective HTS collections.<sup>62,63</sup> These results were released to the public and identified thousands of chemical starting points for lead compound development. Importantly, these compounds are highly potent with IC<sub>50</sub> values of < 2  $\mu$ M in cultures of *P. falciparum*. The scientific community now has access to an arsenal of thousands of compounds that are highly toxic to the parasite, but the process of developing these hits into robust lead compounds will be challenging. It is reasonable to assume that identification of the molecular targets could aid in prioritization of these hits, while optimization steps could also potentially be decreased since the hit-target interactions could be directly studied, saving time, and money.

Recently, the Medicines for Malaria Venture (MMV) initiated a collaborative effort with GSK to identify the targets of the 13,231 in vitro antimalarial compounds reported as hits in the phenotypic screening effort. Here, we report the evaluation of the GSK compounds in the  $\beta$ -hematin formation assay.

## Experimental Methods

### NP-40 $\beta$ -Hematin Formation Assay

The NP-40  $\beta$ -hematin formation assay protocol was modified from previously reported method.<sup>54</sup> Solutions were added to the microtiter plate in the order of water (20  $\mu$ L), NP-40 stock solution (5  $\mu$ L), acetone (7  $\mu$ L) and heme suspension (25  $\mu$ L). Following the addition of water, the plate was shaken for 30 minutes to ensure solubilization of the test compound. The absorbance of each plate was then measured at 405 nm on a BioTek plate reader (pre-read, this ensures that background signal can be removed from the final plate reading upon completion of the assay). The NP-40 stock solution (348  $\mu$ M) was prepared in water. A 25 mM stock solution of hematin was prepared by dissolving hemin chloride in DMSO followed by one minute of sonication. The heme solution was then filtered through a 0.22  $\mu$ m PVDF membrane filter unit. From this solution, the heme suspension (228  $\mu$ M) was added to a 2 M acetate buffer at pH 4.9 and vortexed for ~ 5 sec. The plate was then incubated for six hours in a shaking water bath at 90 rpm and 37°C. Following incubation, the microtiter plate was removed from the water bath and the assay was analyzed using the pyridine-ferrochrome method. Following the addition of 15  $\mu$ L of acetone to each well of the plate, 8  $\mu$ L of pyridine solution was added (50% pyridine, 20% acetone, water and 200 mM HEPES, pH 7.4) so that the final concentration of pyridine was 5% (v/v). Following a 30 minute interval of shaking to facilitate the solubilization of free heme, the absorbance of the resulting complex was measured at 405 nm and the background signal from the pre-read absorbance was removed for each well.

### GSK Compound Analysis

Over 13,000 unique compounds were received from GSK in duplicate (125 nL volumes). Each compound was tested for inhibitory activity against  $\beta$ -hematin formation. Positive controls consisted of a 100  $\mu$ M final concentration of amodiaquine (dissolved in DMSO) and negative controls consisted of DMSO only. Controls were added to columns 6 (DMSO, added by GSK) and 18 (amodiaquine, added by Vanderbilt). Following addition of controls, the reagents of the  $\beta$ -hematin formation assay described above were added to the plate. Percent inhibitory activity of each test compound was calculated relative to positive and negative control wells added to each plate. The standard deviation of each plate was calculated relative to the negative controls where the highest deviation was observed.

### Target Confirmation in *P. falciparum*

In order to confirm hemozoin as the *in vivo* target of *in vitro* antimalarial activity, a heme speciation assay was used to measure the ratio of free heme:hemozoin present in the parasite. In this assay, tightly synchronized ring-stage parasite cultures (50 mL culture volume, 2% hematocrit, 5% parasitemia) are treated with a test compound and incubated for approximately 30 hours, allowing the rings to mature into schizonts where hemozoin formation is expected to be maximal. Following incubation at 37°C, the culture is transferred to 50 mL tubes and centrifuged at 1500 rpm for ten min. The culture media is removed and erythrocytes are lysed with a 0.05% solution of saponin, leaving trophozoites in the culture. Pyridine is then used to examine the concentration of

heme available as free heme. Sodium hydroxide is then used to solubilize and quantitate hemozoin.

## Results

The 13,231 in vitro antimalarial compounds were tested in duplicate in the  $\beta$ -hematin formation assay. Excellent  $Z'$  values were obtained with an average of 0.85. The average standard deviation of the negative controls was ~10%. Percent inhibitory activity was measured for each compound relative to positive and negative controls. The hits were prioritized into three sets:

- 1) >90% inhibitory activity, potent hits
- 2) 80% - 90% inhibitory activity, compounds with moderate activity
- 3) 50%-70% inhibitory activity, compounds with minimal activity

Inhibitory Activity	Number of compounds
50 – 70%	276
80 – 90%	293
>90%	250

**Table 7.**  $\beta$ -hematin inhibitors were prioritized based on % inhibitory activity.

In the original HTS screen discussed in Part I, compounds that inhibited >80% of  $\beta$ -hematin formation were considered hits. Using this definition of a hit, a hit-rate of

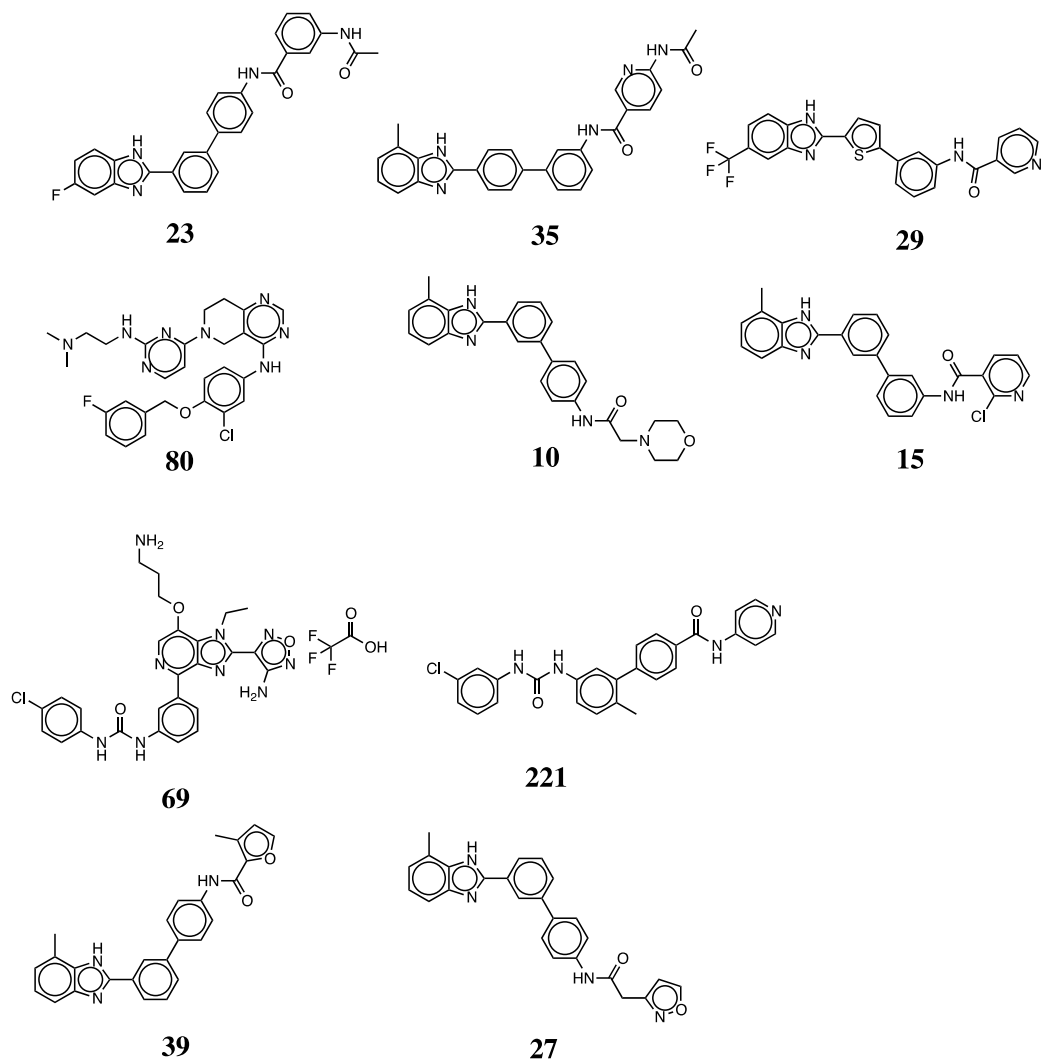


0.37% was obtained. In comparison, the GSK library contained a significantly higher number of active compounds. To maintain a reasonable hit-rate, the threshold that defines a hit was moved up to compounds exhibiting >90% inhibitory activity. This threshold resulted in a 1.9% hit-rate (250 hits). The enrichment in activity was not unexpected since the GSK library compounds are predetermined to have affinity toward targets present in *P. falciparum*.

The compounds in the GSK library were also prioritized based on cluster identity. We chose to perform this structural analysis for all compounds that exhibited >50% inhibitory activity. The threshold was lowered for this analysis so that the scaffolds that have enriched  $\beta$ -hematin inhibitory activity could be elucidated. The GSK library is comprised of 416 clusters. Ten of these clusters were identified where at least 50% of the members exhibited at >50% inhibitory activity (Table 8). Figure 33 identifies a representative compound from each of the ten clusters. It is clear that the 2-biphenyl benzimidazole represents the majority of active clusters.

Cluster #	hits	% of compounds in this cluster that are hits
23	25	76
80	7	70
69	8	67
39	13	65
35	14	64
10	37	61
221	6	60
27	15	56
29	14	54
15	21	51

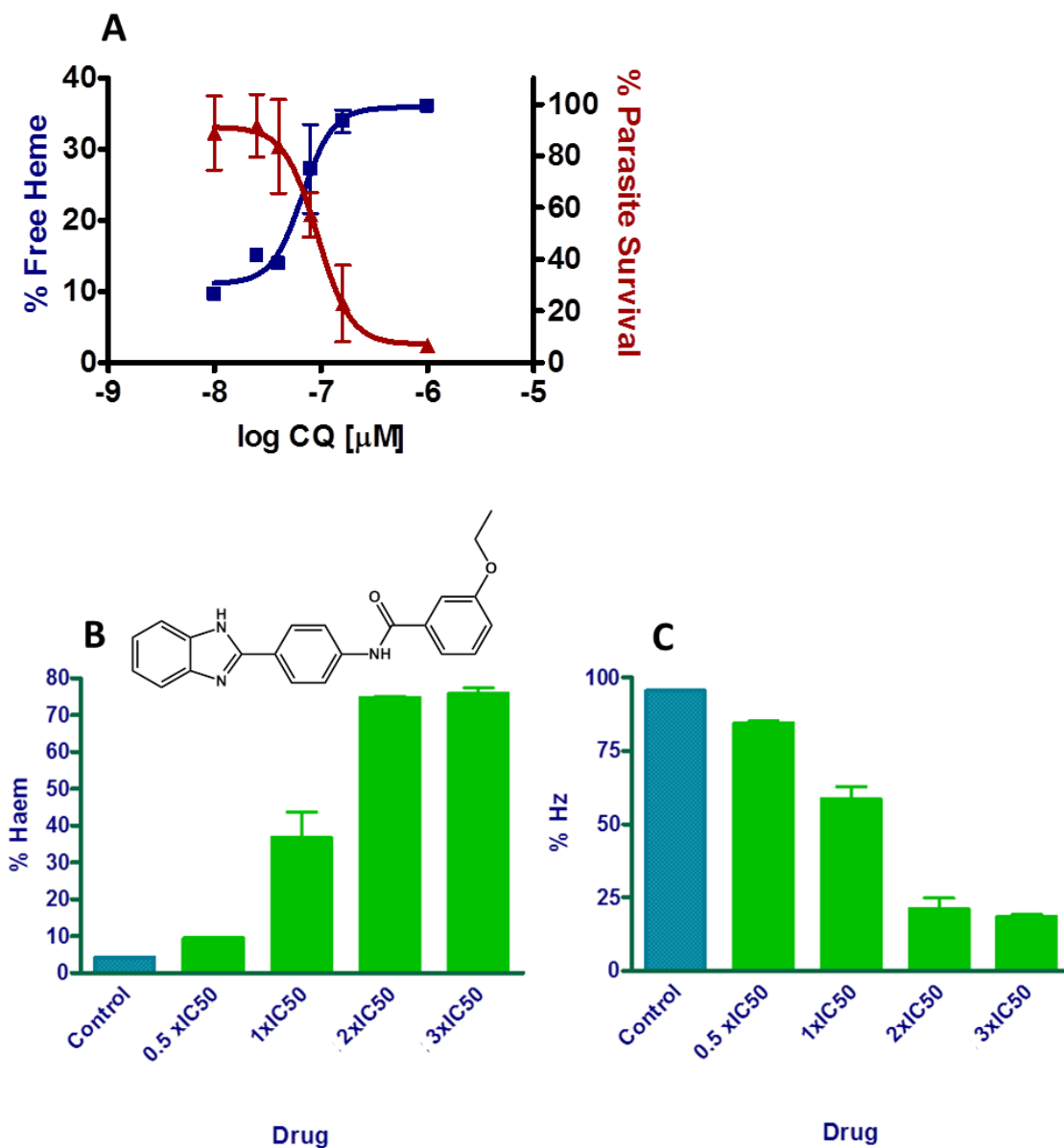
**Table 8.** Ten clusters were identified where more than half of the members exhibited >50% inhibitory activity.



**Figure 33.** Representative compounds from each cluster where >50% of members inhibit  $\beta$ -hematin formation.

As evident in the screening results, many of the *in vitro* antimalarial compounds identified by GSK were also active in the  $\beta$ -hematin formation assay, suggesting hemozoin as the target. In order to demonstrate that hemozoin is indeed the *in vivo* target of *in vitro* antimalarial activity, a heme speciation assay can be utilized which determines the ratio of free heme:hemozoin present in the parasite.<sup>74</sup> If a test compound truly targets

the hemozoin formation pathway, then the ratio of free heme should increase as a function of increasing drug concentration. In this assay, tightly synchronized ring-stage parasite cultures (50 mL culture volume, 1% hematocrit, 5% parasitemia) are treated with a  $\beta$ -hematin inhibitor and incubated for approximately 30 hours, allowing the rings to mature into schizonts where hemozoin formation is expected to be maximal. The ratio of free heme:hemozoin present in the parasite is then measured. Figure 34A shows the treatment of parasite cultures with CQ. From this plot, as the parasite dies (from increasing CQ concentration), there is an increase in the percentage of heme that is available as free heme. Therefore, as higher concentrations of CQ are added to the parasite culture, hemozoin formation is inhibited and there is a measurable increase in the percentage of heme that is available as “free heme”, thus implicating hemozoin as the primary molecular pathway responsible for parasite death. Using this assay, we have begun to evaluate each of the top 250 commercially available  $\beta$ -hematin inhibitors to validate hemozoin as the molecular pathway responsible for parasite death. For the  $\beta$ -hematin inhibitor identified in Figure 34, it is clear that the percentage of free heme increases as a function of increased inhibitor concentration.



**Figure 34.** Examination of the effects of  $\beta$ -hematin inhibitor on the heme:hemozoin ratio in *P. falciparum*. (A) Parasite culture treated with CQ. The  $\beta$ -hematin inhibitor identified in B was used to treat cultures of the parasite. (B)\* % of heme that is available as free heme and (C)\* % of heme that is incorporated into the hemozoin (Hz) crystal \*Data obtained by Jill Combrinck.

## Conclusions and Future Directions

Potent inhibitors of  $\beta$ -hematin formation have successfully been identified from the GSK library of in vitro antimalarial compounds. We will next analyze the top 250  $\beta$ -hematin inhibitors in a dose-response format. Using this information, a preliminary SAR analysis in collaboration with University of Cape Town (Cape Town, South Africa) will be performed in order to identify compounds that are worthy of lead optimization. SAR analysis will also be completed for the 2-biphenyl benzimidazole scaffold with enriched  $\beta$ -hematin inhibitory. Target validation of the top 250 commercially available  $\beta$ -hematin inhibitors is currently underway to determine if the molecular pathway responsible for parasite death is hemozoin inhibition.

## Acknowledgments

The data provided in this chapter is the result from multiple collaborations. **Part I.** Melissa Carter, Kathryn Wicht and Holly Carrell were involved with screening. Dave Weaver, Dan Dorset and Lisa Wright were helpful in the design and execution of the screening effort. The Walter Reed Army Institute of Research kindly provided training in culturing methods for *P. falciparum*. Tim Egan, Jill Combrinck and Kim Fong have performed follow-up experiments that confirm many of the  $\beta$ -hematin inhibitors identified in this screen are indeed hemozoin inhibitors in *P. falciparum*. **Part II.** The Vanderbilt University Chemical Synthesis Core assisted in obtaining/synthesizing compounds that were discussed in this section. **Part III.** The heme speciation analysis is

currently being performed with Jill Combrinck (Cape Town, South Africa) and Kim Fong (Vanderbilt University). Kim will also perform the follow-up dose-response analysis of the top 250  $\beta$ -hematin inhibitors.

## Chapter V

# APPLICATION OF MACHINE LEARNING TECHNIQUES REVEALS PATHWAY SPECIFIC INHIBITORS FOR $\beta$ -HEMATIN CRYSTALLIZATION IN *PLASMODIUM* *FALCIPARUM*<sup>124</sup>

## Introduction

The malaria eradication campaigns of the mid 1900's dramatically lowered infections worldwide through a combination of vector control methods and drug treatment using the antimalarial chloroquine (CQ).<sup>3</sup> After two decades the focus of these efforts shifted to a less ambitious goal of malaria control due in part to resistance and safety concerns. Recently, resurgence in malaria cases have been observed, primarily in underdeveloped countries and due in large part to the development of resistance mechanisms to nearly all affordable antimalarial drugs and insecticides.<sup>4,5</sup> Though it has been over 50 years since resistance to CQ was first reported, no affordable replacement has been developed.<sup>94,95</sup> Perhaps the primary reason that progress has been slow is because malaria is a disease of poverty.<sup>96</sup> With no market incentive, pharmaceutical companies have historically shown little interest in antimalarial drug development since R&D investments would not be recouped. There has also been a lack of public funding for tropical diseases, referred to as the '90/10 split', where 90% of the US health-related funding goes to research for only 10% of the worldwide disease burden.<sup>97</sup> Fortunately, interest in malaria control has increased in recent years, including an initiative announced



in 2007 by the Bill & Melinda Gates Foundation to eradicate malaria worldwide.

Furthermore, through the advent of public-private partnerships (PPP's), pharmaceutical companies are now collaborating with non-profit organizations to develop new antimalarial drugs.<sup>98</sup>

Although malaria has historically been a neglected disease, there is reason to be optimistic. Several significant advances have been made in antimalarial drug discovery, particularly in the past ten years. Perhaps one of the most exciting advancements has been the full genomic sequencing of *P. falciparum* and *P. vivax* which allows for the identification of new druggable targets.<sup>99,100</sup> Additionally, a more in-depth understanding of parasite biochemistry has allowed the introduction of high-throughput screening (HTS) techniques for both target-based and phenotypic assays. Successful target-based assays have been developed including those that target inhibitors of  $\beta$ -hematin formation, aminopeptidase activity, the mitochondrial electron transport chain, and pyrimidine biosynthesis. Phenotypic assays have also been developed to identify molecules that are toxic to parasite cultures. Recently, phenotypic screens have been completed by GSK and Novartis against millions of compounds in their respective HTS collections.<sup>62</sup> The results were released to the public and identified thousands of potent chemical starting points for lead compound development.

The scientific community now has access to an arsenal of thousands of compounds that are highly toxic to the parasite, but the process of developing these hits into robust lead compounds will be challenging. It is reasonable to assume that identification of the molecular targets could aid in prioritization of these hits, while optimization steps could also potentially be decreased since the hit-target interactions

could be directly studied, saving time, and money. While the experimental determination of targets is possible in some cases, it is time-consuming and expensive to develop and apply target-specific high-throughput screening (HTS) to large numbers of compounds.

Here we propose a more affordable *in silico* pre-screening of compounds to sort and prioritize according to their likelihood to interact with a specific target. The development of quantitative structure activity relationship (QSAR) models has shown practical value for *in silico* screening of potential hit compounds to identify novel chemical entities with a desired biological activity<sup>101-103</sup>. Hence, application of QSAR models to *in silico* screen drug-like small molecules enables the prioritization of focused libraries for acquisition and experimental verification. Further, such models can be applied in biomedical research for hit-to-lead or hit-to-probe optimization.

We test if ligand-based virtual screening approaches are able to streamline antimalarial drug discovery focusing on inhibition of  $\beta$ -hematin formation as target pathway. An in-house diverse small molecule library (144,330 total compounds) with an initial hit rate of 0.4% (530/144,330) was used as a knowledge-base to establish QSAR models. A theoretical enrichment of ~37 was established using an independent data set. These models were applied to virtually screen the publically available databases of in vitro antimalarial compounds. Experimentally, enrichment of ~44 fold was achieved for the GSK data set using a threshold cutoff of 70 $\mu$ M.

## Experimental Methods

### *$\beta$ -Hematin Formation HTS Assay*

The  $\beta$ -hematin formation assay has been described previously for use in HTS (Chapter IV, Part I). Briefly, over 140,000 10 mM library compounds originating from ChemBridge and ChemDiv were tested at 19.3  $\mu$ M. A bulk liquid dispenser was used to add water, NP-40 (30.55  $\mu$ M) and heme (100  $\mu$ M) suspended in a pH 4.9 acetate buffer (1 mM). The plates were incubated for five hours in a shaking water bath at 37°C. The pyridine-ferrochrome method of quantification was used to analyze the inhibitory activity of compounds by adding a solution containing 50% pyridine, 20% acetone, and water solution buffered with a 200 mM pH 7.4 HEPES buffer such that the final concentration in each well was 5% pyridine (vol/vol). From this method, we identified hits as those compounds exhibiting greater than 50% inhibitory activity. Follow-up dose-response curves were generated for all hits in order to eliminate false-positives and determine the potency of each hit.

### *QSAR model training (This section was kindly provided by Mariusz Butkiewicz)*

Quantitative structure activity relationships seek to correlate the often complex non-linear relations between chemical structure and biological activity for a specific protein target<sup>101,103</sup>. Modern QSAR techniques employ advanced 2D molecular fingerprints and 3D molecular descriptors coupled with machine learning<sup>104,105</sup>. The descriptors employed in this study (scalar, 2D/3D auto-correlation, radial distribution functions) are fragment-independent and translation/rotation invariant. Thus, the resultant

fingerprints are constant in length and independent from molecule orientation in space. A total of 1,284 numerical descriptors in 60 categories were implemented in this. 3D conformations were calculated for all molecules with CORINA<sup>106</sup>. A set of five machine learning algorithms was implemented in this study including Artificial Neural Networks<sup>107-109</sup>, Support Vector Machines<sup>110,111</sup>, kappa – Nearest Neighbors<sup>112,113</sup>, Kohonen networks<sup>114,115</sup>, and Decision Trees<sup>116,117</sup>. Machine learning models can adapt to complex interrelations and are capable of detecting even small signals at high noise levels. Hence, each of these methods is applied when no simple mathematical model can be assumed, many influencing factors interact, and the experimental uncertainty is high. The training data set had 80% of the data points employed in the actual training process. The number of training iterations was limited through early termination to counter “overfitting” of the machine learning model to the training data. A monitoring data set consisting of 10% of the data points was used to optimize all training parameters of the machine learning methods and to invoke early termination. The final 10% of the data points are set aside as an independent data set. It is not used in the training process, but used to evaluate the final model. There was no overlap of compounds between training, monitoring, and independent data sets. Sequential Forward Feature selection<sup>118,119</sup> was chosen to determine an optimized descriptor set for every combination of machine learning technique. Systematically, each data partition is chosen once as an independent dataset and cross-validated through machine learning model training<sup>120</sup>. The overall accuracy of all cross - validated QSAR models was evaluated by calculating a jury consensus of all predicted pIC<sub>50</sub> values for each independent data set iteration.

## Results

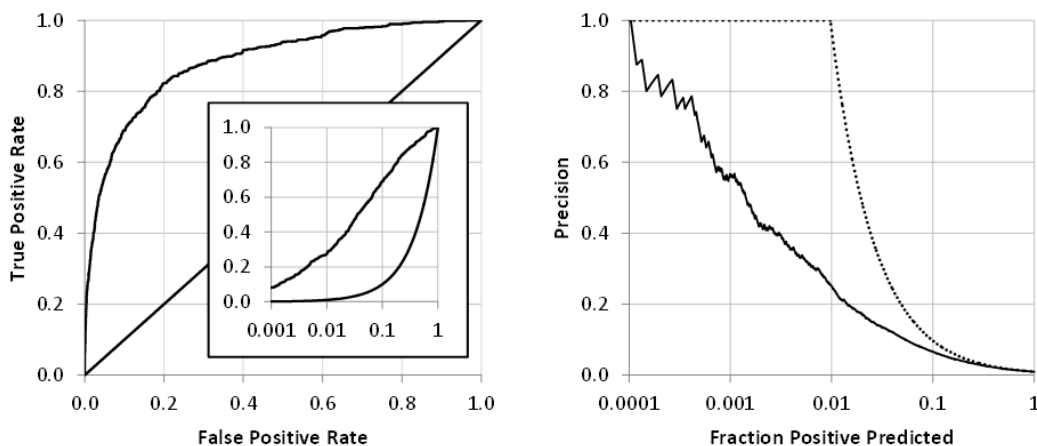
### Training Set

The heme detoxification biomineral, hemozoin, is the target of quinoline antimalarials. Resistance to these drugs is the result of efflux mechanisms developed by the parasite rather than changes to the pathway itself. For this reason, hemozoin remains a valid drug target for the development of new antimalarial probes. Recently, a  $\beta$ -hematin (synthetic hemozoin) formation assay was designed to mimic conditions present in the digestive food vacuole of the malaria parasite where hemozoin formation occurs. This assay was adapted for use in HTS and utilized to screen a library of over 144,000 compounds. The screening effort resulted in the identification of inhibitors of  $\beta$ -hematin formation (see Chapter IV). A follow-up dose-response assay was used to establish the potency of each hit, with all of the compounds having more potent activity in this assay than chloroquine. While the hits identified in this screening effort will be utilized for the identification of lead probe candidates, what can be learned from the set of over 142,000 compounds that are not active in this assay?

### QSAR model

Here, the results of the entire screening effort, both positives and negatives have been utilized to provide the knowledge-base for a target specific QSAR model by bcl::ChemInfo. Briefly: this *in silico* ligand based virtual screening suite applied a diverse set of orthogonal machine learning techniques to model nonlinear relations between the chemical structure of the ligand and its associated inhibitory concentration. It determines

an optimal set of numerical descriptors of chemical structure through feature forward selection (FFS) or feature backward elimination (FBE). The predictive power of the models was assessed determining for an independent dataset a variety of measures such as positive predictive value (PPV) and area under the curve (AUC) in receiver operator characteristics (ROCs). The best performing model was chosen by maximizing the PPV in the range critical for *in silico* screening and prioritization, here when selecting 0.1%-1.0% of compounds from a library. The final model achieved a PPV value of 0.69 for the top 0.1% to 1% of positive predicted compounds, i.e. 70% of the predicted active compounds are true actives. This corresponds to an enrichment of ~37 and was achieved using a cutoff of 1% false positive rate (see Figure ).



**Figure 35\*:** The final QSAR model is quantified by ROC curve analysis. The left graph shows a plot of false positive rate (FPR) compared to the true positive rate (TPR) achieving an area under the curve of 0.88. At an FPR cutoff of 5% an enrichment of 17 was achieved. The sub-graph shows the same roc curve on a logarithmic scale. On the right hand side, a plot of precision in respect to the fraction of positive predicted compounds is plotted on a logarithmic scale. The ideal precision trajectory is represented by the black dotted line. To recover all active compounds contained in the in-house screened library, the range from 0.0001 to 0.01 was evaluated with a precision integral of 0.58 in comparison to the ideal precision curve. To recover the top 100, 200, 300, and 400 compounds precision integral of 0.66, 0.69, 0.63, and 0.60 was achieved, respectively. \*Figure was kindly provided by Mariusz Butkiewicz

QSAR model prioritizes GlaxoSmithKline and Novartis compounds for inhibition of  $\beta$ -hematin pathway

GlaxoSmithKline (GSK) and Novartis have screened their corporate libraries and identified hit compounds acting against *in vitro* culture of the malaria parasite, *P. falciparum*. The targets of these potent *in vitro* antimalarial compounds are unknown and it would be far too expensive to order all of the commercially available compounds from these hits to test for activity against the  $\beta$ -hematin formation. In an effort to prioritize compounds most likely to have activity against this pathway, the QSAR model was

applied to virtually screen the active compounds published by GSK and Novartis. The output of the QSAR model is a predicted half maximal inhibition concentration (IC<sub>50</sub>) for  $\beta$ -hematin inhibition. Overlapping compounds between the training data and the GSK/Novartis data sets were taken out of the screened libraries to avoid re-identification of known actives. The remaining compounds were grouped into seven ‘Bins’ based on the potency of the predicted IC<sub>50</sub> values (0-70  $\mu$ M, 71 - 140  $\mu$ M, etc). The GSK library contained a total of 13,533 compounds of which 249 compounds (below 70  $\mu$ M) were predicted to express inhibitory effects *in silico* (see Table 9). The Novartis library contained 5,697 compounds and the computational model predicted 37 compounds as inhibitors with an IC<sub>50</sub> of below 70  $\mu$ M. This results yields an *in silico* hit rate of 1.8% and 0.6% for the GSK and Novartis compounds.

Bin	Predicted IC <sub>50</sub> values ( $\mu$ M)	Number of compounds in this bin (GSK)	Number of compounds in this bin (Novartis)
1	0-70	249	37
2	71-140	303	40
3	141-210	376	59
4	211-300	546	92
5	301-500	1549	241
6	501-700	1676	414
7	701-1200	4006	1644
8	1201-1800	2733	1662
9	1801+	1791	1513

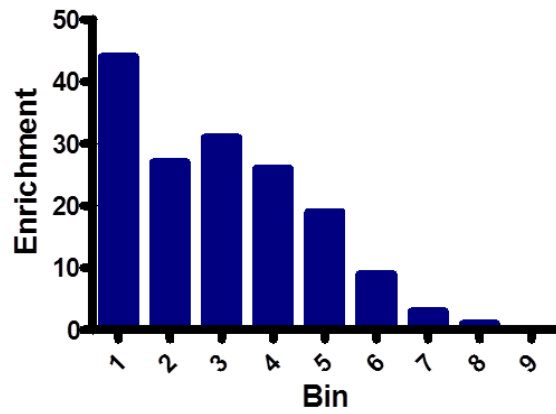
**Table 9.** Prioritization of the GSK and Novartis compounds based on predicted activity against  $\beta$ -hematin formation.



Experimental analysis of enrichment by predicted activity binning and structural similarity

The accuracy of the QSAR model to predict inhibitors of beta-hematin formation was experimentally validated using the GSK in vitro antimalarial data sets. Compounds were first pre-screened in the NP-40 detergent mediated  $\beta$ -hematin formation assay. Compounds inhibiting >80% of crystallization were considered hits, and were subsequently tested in a dose-response manner to establish potency. As evidenced in **Error! Reference source not found.**, the GSK data sets show a substantial increase in enrichment in Bin 1, where the hit-rate for the GSK set was 16%. Bin 2 also showed an increased degree of enrichment where 10% of the GSK compounds tested were active. The percentage of actives continues to decrease as a function of increasing Bin number, such that the largest ratio of active:inactive is observed in Bin 1, the bin predicted to contain the highest percentage of actives according to the QSAR model.

It is also worth noting that a small degree of enrichment is observed in bins 5-7. This is almost certainly due to the fact that the GSK and Novartis compounds are biased as they are known to inhibit some pathway within the parasite. As such, a higher hit-rate would be expected than that observed when screening a non-biased library, leading to some degree of enrichment.



**Figure 36.** Experimental evaluation of the GSK compounds reveals enrichment of activity in Bin 1.

## Discussion

The GSK and Novartis screening efforts have resulted in the identification of thousands of chemical starting points for lead probe identification, but the molecular targets of these active compounds are unknown. Leveraging this rich data source for the development of lead and probe compounds hinges on identification of pathway and target, a time-consuming and resource-intensive process. Hemozoin, a validated target specific to the parasite, has been studied in great detail and serves as an important pathway for future antimalarial development. One has to expect hemozoin inhibitors present in the data collected by GSK and Novartis. Therefore, one approach to select these compounds would be high-throughput screening the GSK and Novartis compounds for compounds that perturb the hemozoin formation pathway. To avoid testing all 20,000 active compounds, the challenge is to prioritize those that are most likely to inhibit hemozoin formation. This has been addressed by using a QSAR model to virtually screen the 20,000 compounds to prioritize those that are most likely to inhibit  $\beta$ -hematin formation – a process that also eliminates the need to have access to all 20,000 compounds.

The training set was provided by an HTS campaign that screened over 140,000 compounds to identify inhibitors of  $\beta$ -hematin formation (0.4% hit-rate). This method of developing a QSAR model takes advantage of the chemical space provided by both, active and inactive compounds. The resulting model was used to virtually screen the GSK and Novartis hits and prioritize the compounds based on predicted  $IC_{50}$ . When testing a subset of compounds predicted to inhibit of  $\beta$ -hematin formation with  $IC_{50}$

values better than 70  $\mu\text{M}$ , ~80% turned out to be active (PPV) representing an enrichment of >80 fold. We further demonstrate that PPV correlates tightly with predicted activity. Compounds with a low  $\text{pIC}_{50}$  value are predicted with a high confidence yielding a decrease of enrichment with increasing Bin number. Therefore, this method confidently filters for inhibitors of  $\beta$ -hematin formation. An analysis of the compounds in Bin 1 reveals that many diverse structural scaffolds are predicted to have activity against  $\beta$ -hematin formation. Among these actives are several quinoline, quinazoline, benzimidazole and carbazole scaffolds.

While the approach taken here has successfully filtered compounds to predict inhibitors of  $\beta$ -hematin formation, it is important to note that this approach for identifying target-specific activity is not limited to  $\beta$ -hematin, and can be applied to any pathway within the parasite given access to HTS data. In fact, multiple parasite-specific pathways have been the focus of target-based screening efforts in recent years. One such effort screened a 220,000 compounds library to identify inhibitors of *P. falciparum* pyrimidine biosynthetic enzyme dihydroorotate dehydrogenase (PfDHODH), resulting in the identification of 1249 hits. Perhaps a QSAR model for the results of the PfDHODH screening results would allow the delineation of pathway specific inhibitors of  $\beta$ -hematin formation and PfDHODH inhibitors. Alternatively, the model could be quite useful in identifying in vitro antimalarial compounds that have dual-targeting activity.

The QSAR approach developed here is not specific to the malaria parasite, and can be used for target-elucidation in other diseases as well. This is particularly applicable for use in neglected diseases where limited funding restricts the expensive and time-consuming process of target-elucidation. A further application of this model would be to

guide the selection of second generation compounds in the process of lead development. By creating a large list of possible second generation compounds, the model can prioritize a subset of compounds predicted to have more potent activity against the target.

### Acknowledgments

This work was a collaborative effort with the Meiler lab. Mariusz Butkiewicz was responsible for the computational portion of the QSAR model and will be co-author on the manuscript that results from this work. Kim Fong is currently working on pathway validation of the validated  $\beta$ -hematin inhibitors (from Bin1) in *P. falciparum*.

## CHAPTER VI

### FUTURE DIRECTIONS AND FINAL THOUGHTS

Herein, I have presented evidence that solidifies neutral lipid droplets as the site of hemozoin formation within the parasite, and identified the lipophilic detergent, NP-40, as a surrogate for these lipids. The NP-40 detergent-mediated assay has been utilized in HTS where 144,330 compounds were analyzed for  $\beta$ -hematin inhibitory activity. As a result, 530  $\beta$ -hematin inhibitors were identified, 171 of which exhibit *in vitro* antimalarial activity. With the HTS campaign complete, it is now time to begin the arduous process of lead identification and optimization.

#### Lead Identification

In order to identify robust, quality leads from the HTS results, the 171 *in vitro* antimalarial compounds must be effectively prioritized. We will prioritize compounds based on validation of hemozoin as the target, synthetic feasibility, preliminary SAR analysis, compound chemistry, PK properties, susceptibility for resistance to develop in *P. falciparum*, and activity against multiple stages of the parasite life cycle. Taken together, these experiments will guide the selection of a small number of hits to advance to the expensive and time-consuming process of lead optimization.

### Validation of Hemozoin Inhibition

The lipophilic detergent, NP-40, was selected as a surrogate for the biologically relevant neutral lipid droplets based on its similarity in assay performance. By utilizing an assay that successfully recapitulates the biological conditions within the digestive food vacuole of the parasite, 32% of the  $\beta$ -hematin inhibitors retained activity against cultures of *P. falciparum*, suggesting hemozoin formation as the pathway. Efforts are now underway to substantiate hemozoin inhibition as the molecular pathway responsible for parasite death. A powerful technique for quantitating heme accumulation and consequent parasite death as a function of drug dosing was recently reported (called the heme speciation assay).<sup>74</sup> This technique involves strenuous assay conditions that severely limit the number of compounds that can be analyzed in a reasonable amount of time (each compound currently takes 1-2 weeks to examine). To facilitate a more rapid analysis of hemozoin inhibition, the throughput of this assay must be increased.

In its current format, the heme speciation assay requires 10 mL of packed, parasitized erythrocytes containing highly synchronized rings. This large volume of culture is necessary for the quantitation of free heme and hemozoin using UV-Vis spectroscopy. An approach to reducing the volume of culture necessary is to utilize more sensitive spectroscopic techniques to detect heme. To address this, the Wright lab is currently validating the assay using inductively coupled plasma optical emission spectroscopy (ICP-OES) for heme quantification. With this approach, the heme speciation assay could be adapted for use in a 6-well plate, as opposed to a 50 mL flask, resulting in a significant increase in throughput.

If we cannot successfully increase the throughput of the heme speciation assay, we must have an approach to down-select the number of compounds that need to be validated using the current assay format. This will be necessary since testing all 171 *in vitro* antimalarials in the current format of the heme speciation assay would take approximately 6 years to complete (assuming one researcher is responsible for all experiments). One approach to identify off-target antimalarials is to monitor hemozoin formation using fluorescence microscopy. Specifically, the fluorescent properties of hemozoin can be exploited to monitor crystal formation in parasite cultures treated with the *in vitro* antimalarial  $\beta$ -hematin inhibitors identified in the screen. Hemozoin formation would be monitored (relative to drug-free controls) in 384-well plates to determine whether the test compound affects the crystallization process. A deviation in hemozoin formation would suggest crystallization as the target. If hemozoin formation occurs normally, then parasite death would be due to some other pathway. Using this approach to rapidly filter out compounds that do not interfere with hemozoin formation, fewer compounds would need to be validated in the heme speciation assay in its current, low-throughput format.

#### *Synthetic Amenability and SAR*

The synthetic amenability of validated hemozoin inhibitors will be analyzed to determine if a preliminary SAR analysis can be readily completed in a cost-effective manner. Primarily, we are interested to determine if the activity of the compound can be maintained following modifications to the core scaffold. If the compound loses activity following minor structural modifications, then the process of lead optimization would be



quite challenging. We previously completed this analysis based on the results of the pilot screen and selected several compounds for an SAR analysis (see Chapter IV, Part II).

The full results of the screening effort will now be reviewed in a similar manner.

For compounds selected as synthetically amenable, a collection of ~5-20 derivatives of each compound will be obtained from commercial resources or synthesized for a preliminary SAR analysis. This will not be necessary for all validated hemozoin inhibitors since 61% of these compounds share a substructure with at least four other compounds in the screening results. From this analysis, we aim to determine which molecular features give rise to  $\beta$ -hematin inhibitory and *in vitro* antimalarial activity. Since the presumptive target, heme, is well studied, this SAR analysis will be designed so that the interactions between target/inhibitor can be thoroughly analyzed.

### Antimalarial Properties

Validated hemozoin inhibitors will be further prioritized based on their selectivity for the parasite, activity against multiple strains of *P. falciparum*, rapid development of resistance, and activity against other stages of the parasite lifecycle. The first step will be to analyze the selectivity of each hemozoin inhibitor for the parasite. This will be accomplished by determining the toxicity in mammalian cell culture (HEP2).

Compounds should exhibit >ten-fold selectivity for the parasite toxicity versus mammalian cultures. Compounds showing selectivity for the parasite will then be tested in multiple multidrug-resistant strains of the parasite. By establishing the inhibitor dose-response in resistant strains, the resistance index ( $RI = IC_{50} \text{ multidrug-resistant strain} / IC_{50} \text{ drug sensitive strain}$ ) can be calculated for each compound to identify those that are

predisposed for resistance. We have completed this stage of the process for the 25 nanomolar potent hits identified in the screen. For 21 of the nanomolar-potent *in vitro* antimalarials identified, the calculated RI was < 3, indicating that these 21 compounds are approximately as effective against drug-resistant strains as they are against sensitive strains (Table 10).

VU identifier	BH formation IC50 (μM)	D6 IC50 (uM)	C235 IC50 (uM)	Resistance Index
VU0098755	12.6	0.106	0.127	1.2
VU0073687	6.3	0.185	0.551	3.0
VU0001281	5.9	0.194	0.174	0.9
VU0065708	16.2	0.198	0.184	0.9
VU0096505	8.8	0.238	0.217	0.9
VU0107282	17.0	0.290	0.540	1.9
VU0114785	13.4	0.346	4.8	13.9
VU0002101	14.3	0.348	0.412	1.2
VU0028177	13.3	0.350	0.465	1.3
VU0063971	8.9	0.384	0.833	2.2
VU0129813	26.8	0.396	0.294	0.7
VU0114734	22.1	0.461	1.1	2.5
VU0122653	24.5	0.550	0.900	1.6
VU0000264	2.0	0.593	0.248	0.4
VU0065892	6.2	0.611	0.693	1.1
VU0010690	25.0	0.673	1.5	2.3
VU0094619	2.4	0.700	0.284	0.4
VU0012464	7.3	0.708	0.923	1.3
VU0008057	9.6	0.730	1.5	2.1
VU0358149	8.3	0.778	19.1	24.5
VU0015078	1.1	0.810	5.7	7.1
VU0119324	21.5	0.845	0.186	0.2
VU0078364	5.3	0.922	2.0	2.1
VU0107278	11.8	0.951	3.9	4.1
VU0064165	15.4	0.993	1.0	1.0

**Table 10.** The RI values were calculated for each of the *in vitro* antimalarials that exhibited nanomolar potency.

Each compound with an RI of  $<3$  will be further tested to identify those compounds that are susceptible to accelerated resistance by the parasite. This will be accomplished by co-incubating validated hemozoin inhibitors at sub-lethal concentrations (5-20% of the  $IC_{50}$  concentration) in cultures of the D6 strain of the parasite. In one-week intervals, the  $IC_{50}$  of the hemozoin inhibitor will be established to determine if there is any increase in the concentration of test compound necessary to clear the parasite. Development of an antimalarial possessing activity against multiple stages of the parasite lifecycle is highly desirable. This includes activity against the liver stage and gametocytes (to block transmission).

Further considerations for hemozoin inhibitors that perform optimally in the above described assays will be taken into account for the selection of lead drug candidates including performance in typical PK assays. The chemistry of the subset of compounds must also be taken into account including properties such as solubility, stability and synthetic feasibility. According to the compound progression criteria used by the Medicines for Malaria Venture (MMV, a nonprofit organization focusing on the development of antimalarials), compounds should be soluble in PBS at  $>20 \mu\text{g/ml}$  and stable in solid form. Synthesis should be straightforward and cost-effective.

Superior compounds selected based on the criteria described above will be tested in the *P. berghei* mouse model of malaria in the 4 day suppressive Peters test (10mg/kg bodyweight). If parasite clearance is successful in the mouse model, further tests in the monkey model of human malaria will be performed. Compounds that meet the majority of the criteria discussed above and effectively clear the parasite from the mouse and

monkey model can then be submitted for lead optimization where the potency and drug properties of each hit will be improved.

### Lead Optimization

Several strategies for streamlining the process of lead optimization can be imagined based on our knowledge of the biology of the malaria parasite and the target, hemozoin. We can begin by considering the *in vivo* site of hemozoin formation, the neutral lipid body located within the digestive food vacuole. This localization of the target within a malaria-specific organelle presents an opportunity for increasing the potency of lead compounds. Specifically, leads can be modified to increase accumulation within the neutral lipid droplets that reside within the digestive food vacuole.

Chloroquine serves as an excellent example of increased potency based on drug accumulation. At cytosol pH, chloroquine exists in its neutral form and passes through lipid membranes, ultimately penetrating the parasitic digestive food vacuole. Upon entering this acidic (pH ~4.8) compartment, the weakly basic amine groups become protonated. In its protonated form, chloroquine becomes trapped, resulting in high local concentrations of the drug. This property of vacuolar concentration has been exploited in the development of the acridone antimalarials where the addition of weakly basic amine groups facilitated accumulation and increased potency.<sup>121</sup> Increasing digestive food vacuole accumulation is a clear strategy for the development of potent derivatives of the lead compounds. A second level of hemozoin targeting is possible by increasing the compound accumulation within neutral lipid droplets where free heme rapidly

accumulates and consequent hemozoin formation occurs. This level of optimization could be completed by analyzing the preferential partitioning of lead compounds into physiologically relevant neutral lipids (see Chapter II). Slight increases in the lipophilicity of leads could result in increased accumulation within the neutral lipid bodies. This accumulation of inhibitor at the site of hemozoin formation could result in increased potency of the lead compound.

### Target/Inhibitor Molecular Interactions

Hemozoin inhibition occurs either by 1) interactions with free heme or 2) capping of the hemozoin crystal. Either mode of interaction will ultimately result in parasite death due to heme-associated toxicity. However, by understanding the *precise* molecular interactions that occur, we can more effectively optimize leads that have increased affinity towards heme or hemozoin. Methods for determining the mode of interaction responsible for parasite death were presented in Chapter IV, Part II.

After establishing the mode of hemozoin inhibition, target/inhibitor interactions can be analyzed in detail using ITC, paramagnetic NMR and XRD. These tools will allow us to definitively identify the molecular interactions that occur between the inhibitor and target. This information facilitates the optimization of a lead compounds drug-like properties that maintain the features of the molecule that give rise to hemozoin inhibition.

An additional strategy for streamlining the lead optimization process utilizes the QSAR model presented in Chapter V. This model was shown to be a valid tool for

predicting  $\beta$ -hematin inhibitory activity. This model could also be used to guide the selection second generation derivatives of lead compounds.

## FINAL THOUGHTS

Since I began researching malaria in 2008, many significant advances have been made in the field of antimalarial drug discovery, including the identification of over 13,000 potent *in vitro* antimalarials by GSK.<sup>62</sup> There have been setbacks, as well. Foremost, artemisinin resistance was confirmed in Western Cambodia in 2009, and later in Thailand.<sup>73</sup> Alarmingly, these resistance mechanisms appear to have arisen independently, and artemisinin is the last line of defense we have against malaria. If artemisinin resistance spreads to or develops in endemic African countries, the consequences will be devastating. It is a critical time to prime the antimalarial pipeline with potential replacement drugs, and much of this work will be the responsibility of the academic community.

Drug discovery has long been the responsibility of the pharmaceutical industry, but times are changing. In the past ten years, academia has established an important role in drug discovery – particularly regarding neglected and tropical diseases. These diseases, including malaria, represent huge financial investments that will have zero return. Therefore, it has been the responsibility of academia to tackle malaria, particularly in unraveling the biology of *P. falciparum* which can then be exploited for the development of new drugs. Chapter II of this thesis, regarding the mechanism of

hemozoin formation, is a prime example of the role of academia in the drug discovery process.

Inhibition of hemozoin formation may not be a newly identified drug target, but it remains invaluable nonetheless. It is specific to the malaria parasite, essential for parasite survival, and we have a clear strategy for targeting the organelle in which hemozoin formation occurs. It is also a validated target. Chloroquine, which is perhaps the most successful antimalarial drug ever developed, targets the hemozoin formation pathway.<sup>74</sup> With the acknowledgment of hemozoin as such a valuable drug target, why are there no new drugs that exploit this pathway? A primary reason is that the biology of this target was, until recently, poorly understood. This changed in 2010, when we published data that reveals neutral lipid droplets (NLDs) as the location of free heme accumulation and a kinetically competent site for hemozoin formation.<sup>51</sup> This represents the first time that heme has been shown to rapidly accumulate *throughout* the NLDs *prior* to hemozoin formation. This small piece of knowledge represents an exciting opportunity for drug discovery. We can optimize hemozoin inhibitors to concentrate within the NLDs located in the digestive food vacuole by manipulating the lipophilicity of inhibitors. Drugs that more effectively target the site of hemozoin formation would be more potent and potentially have fewer side effects. In addition, by identifying NLDs as the site of hemozoin formation, we can mimic this process in assay format for the identification of novel hemozoin inhibitors.<sup>54</sup>

While it is true that the pharmaceutical industry has made outstanding efforts to identify *in vitro* antimalarial compounds in the past few years, the amount of time and money devoted to malaria compared to the profitable diseases of affluence is small.

Furthermore, the screens utilized by pharma were not novel, but had been previously developed by academia. This meant that the assay could be readily adapted and required minor assay validation and optimization steps. Pharma has never developed an assay for malaria, and is unlikely to in the future due to the enormous time and financial investment that is necessary. Fortunately, academia's newly established role in drug discovery has prompted the development of a number of assays that can be used in an HTS effort.

HTS in the academic setting has only recently been implemented at a few institutions, though this technique for drug discovery has been utilized by pharma for over 25 years. Though pharma has focused its use of HTS to financially rewarding diseases, many within the academic community have utilized HTS for tropical and neglected diseases.<sup>54,81,85</sup> Our lab has been fortunate enough to unite our advances in the understanding of hemozoin formation with the Vanderbilt HTS facility. Upon identifying the role of NLDs in hemozoin formation, we successfully developed an HTS assay to mimic this crystallization process (Chapter IV). Not only did we identify over 500 potent inhibitors, but the majority of these compounds have never been associated with activity against  $\beta$ -hematin formation. Upon testing these compounds against *P. falciparum*, we found that over 33% kill the parasite. While many of these *in vitro* antimalarials have previously been identified as toxic to the parasite, they have never been associated with  $\beta$ -hematin formation. Therefore, the results of our screen not only represent the discovery of novel  $\beta$ -hematin inhibitors, but give us the opportunity to utilize the structural data to more effectively analyze large phenotypic screens for compounds that are likely to be targeting hemozoin formation (Chapter V). This is a significant



advancement, since a limiting factor in the prioritization of large phenotypic screens is the identification of targets.

Our screening efforts represent the importance of developing an assay that is **biologically relevant**. Previous efforts by other groups to screen for hemozoin inhibitors have been abandoned, since so few (~1-2%) of their  $\beta$ -hematin inhibitors killed the parasite during the pilot screen.<sup>70</sup> Why did we succeed where others failed? Perhaps this success is due to the fact that we have more accurately recapitulated biological conditions where hemozoin formation occurs. Understanding the biological formation of hemozoin was time-consuming. We were not the first to develop a screen for  $\beta$ -hematin inhibitors, but we are the most successful. This is an important message for those hoping to develop target-based screens.

Here we have taken a systematic approach to exploit hemozoin formation as a pathway for drug discovery, accomplishing what the pharmaceutical industry would not and what most academic labs could not. The results of these efforts offer many novel chemical starting points for drug discovery. We are currently working to identify lead compounds to submit to the drug discovery pipeline. This is a critical time to enrich the antimalarial pipeline, since we are now on a race against time to develop a replacement for artemisinin before resistance is realized worldwide.

## BIBLIOGRAPHY

- (1) Large portions of this chapter were taken from: Sandlin, R. D.; Carrell, H. M.; Wright, D. W. In *Encyclopedia of Inorganic and Bioinorganic Chemistry*; John Wiley & Sons, Ltd: 2012.
- (2) Ricklefs, R. E.; Outlaw, D. C. *Science* **2010**, *329*, 226.
- (3) Carter, R.; Mendis, K. N. *Clinical Microbiology Reviews* **2002**, *15*, 564.
- (4) Marsh, K. *The Lancet* **1998**, *352*, 924.
- (5) White, N. J. *The Journal of Clinical Investigation* **2004**, *113*, 1084.
- (6) *Antimalarial Drug Combination Therapy: Report of a WHO Technical Consultation*, 2001.
- (7) Francis, S. E.; Sullivan, D. J., Jr.; Goldberg, D. E. *Annual Reviews of Microbiology* **1997**, *51*, 97.
- (8) Kumar, S.; Bandyopadhyay, U. **2005**, *157*, 175.
- (9) Kutty, R. K.; Daniel, R. F.; Ryan, D. E.; Levin, W.; Maines, M. D. *Archives of Biochemistry and Biophysics* **1988**, *260*, 638.
- (10) Sherman, I. W. *Bulletin of the World Health Organization* **1977**, *55*, 265.
- (11) Goldberg, D. E.; Slater, A. F.; Cerami, A.; Henderson, G. B. *PNAS* **1990**, *87*, 2931.
- (12) *Image obtained from Walter Reed Army Institute of Research.*
- (13) Gluzman, I. Y.; Francis, S. E.; Oksman, A.; Smith, C. E.; Duffin, K. L.; Goldberg, D. E. *The Journal of Clinical Investigation* **1994**, *93*, 1602.
- (14) Kolakovich, K. A.; Gluzman, I. Y.; Duffin, K. L.; Goldberg, D. E. *Molecular and Biochemical Parasitology* **1997**, *87*, 123.
- (15) Pisciotta, J. M.; Sullivan, D. *Parasitology International* **2008**, *57*, 89.
- (16) Fitch, C. D.; Chevli, R.; Kanjanangulpan, P.; Dutta, P.; Chevli, K.; Chou, A. C. *Blood* **1983**, *62*, 1165.

- (17) Becker, K.; Tilley, L.; Vennerstrom, J. L.; Roberts, D.; Rogerson, S.; Ginsburg, H. *International Journal for Parasitology* **2004**, *34*, 163.
- (18) Har-El, R.; Marva, E.; Chevion, M.; Golenser, J. *Free Radic Res Commun* **1993**, *18*, 279.
- (19) Egan, T. J.; Marques, H. M. *Coordination Chemistry Reviews* **1999**, *190-192*, 493.
- (20) Sullivan, D. J.; Gluzman, I. Y.; Russell, D. G.; Goldberg, D. E. *Proceedings of the National Academy of Sciences of the United States of America* **1996**, *93*, 11865.
- (21) Krogstad, D.; Gluzman, I.; Kyle, D.; Oduola, A.; Martin, S.; Milhous, W.; Schlesinger, P. *Science* **1987**, *238*, 1283.
- (22) Fidock, D. A.; Nomura, T.; Talley, A. K.; Cooper, R. A.; Dzekunov, S. M.; Ferdig, M. T.; Ursos, L. M. B.; Sidhu, A. B.; Naude, B.; Deitsch, K. W.; Su, X.-z.; Wootton, J. C.; Roepe, P. D.; Wellems, T. E. *Mol Cell* **2000**, *6*, 861.
- (23) Martin, R. E. **2012**.
- (24) Johnson, D. J.; Fidock, D. A.; Mungthin, M.; Lakshmanan, V.; Sidhu, A. B. S.; Bray, P., G.; Ward, S. A. *Molecular Cell* **2004**, *15*, 867.
- (25) Lancisi, G. M. *De Noxiis Paludum Effluviis Eorumque Remediis*; Salvioni, J. M.: Rome, 1717.
- (26) Golgi, C. *Verhandl des X Internat. Med. Cong. Berlin. Bd. II abth III*, 200.
- (27) Pagola, S.; Stephens, P. W.; Bohle, D. S.; Kosar, A. D.; Madsen, S. K. *Nature* **2000**, *404*, 307.
- (28) Pasternack, R. F.; Munda, B.; Bickford, A.; Gibbs, E. J.; Scolaro, L. M. *Journal of Inorganic Biochemistry* **2010**, *104*, 1119.
- (29) Slater, A. F.; Swiggard, W. J.; Orton, B. R.; Flitter, W. D.; Goldberg, D. E.; Cerami, A.; Henderson, G. B. *Proceedings of the National Academy of Sciences of the United States of America* **1991**, *88*, 325.
- (30) Bohle, S. D.; Debrunner, P.; Jordan, P., A.; Madsen, S. K.; Schulz, C. E. *Journal of the American Chemical Society* **1998**, *120*, 8255.
- (31) Klonis, N.; Dilanian, R.; Hanssen, E.; Darmanin, C.; Streltsov, V.; Deed, S.; Quiney, H.; Tilley, L. *Biochemistry* **2010**, *49*, 6804.
- (32) Downie, M. J.; Kirk, K.; Ben Mamoun, C. *Eukaryotic Cell* **2008**, *7*, 1231.

- (33) Ben Mamoun, C.; Prigge, S. T.; Vial, H. *Drug Dev Res* **2010**, *71*, 44.
- (34) Sato, S.; Clough, B.; Coates, L.; Wilson, R. J. *Protist* **2004**, *155*, 117.
- (35) Bergman, G. J. *Science Education* **1948**, *32*, 93.
- (36) Warhurst, D.; Craig, J.; Adagu, I.; Meyer, D.; Lee, S. *Malaria Journal* **2003**, *2*, 26.
- (37) Martin, R. E.; Marchetti, R. V.; Cowan, A. I.; Howitt, S. M.; Broer, S.; Kirk, K. *Science* **2009**, *325*, 1680.
- (38) Slater, A. F. G.; Cerami, A. *Nature* **1992**, *355*, 167.
- (39) Dorn, A.; Stoffel, R.; Matile, H.; Bubendorf, A.; Ridley, R. G. *Nature* **1995**, *374*, 269.
- (40) Bendrat, K.; Berger, B. J.; Cerami, A. *Nature* **1995**, *378*, 138.
- (41) Weissbuch, I.; Leiserowitz, L. *Chem. Rev.* **2008**, *108*, 4899.
- (42) Trager, W. *Trends in Parasitology* **2003**, *19*, 388.
- (43) Pisciotta, J.; Coppens, I.; Tripathi, A.; Scholl, P.; Shuman, J.; Bajad, S.; Shulaev, V.; Sullivan, D. *Biochem J* **2007**, *402*, 197.
- (44) Jackson, K. E.; Klonis, N.; Ferguson, D. J. P.; Adisa, A.; Dogovski, C.; Tilley, L. *Molecular Microbiology* **2004**, *54*, 109.
- (45) Egan, T. J.; Chen, J. Y.-J.; de Villiers, K. A.; Mabothe, T. E.; Naidoo, K. J.; Ncokazi, K. K.; Langford, S. J.; McNaughton, D.; Pandiancherri, S.; Wood, B. R. *FEBS Letters* **2006**, *580*, 5105.
- (46) Hoang, A. N.; Ncokazi, K. K.; de Villiers, K. A.; Wright, D. W.; Egan, T. J. *Dalton Transactions* **2010**, *39*, 1235.
- (47) Fitch, C. D.; Cai, G. Z.; Chen, Y. F.; Shoemaker, J. D. *Biochimica et Biophysica Acta* **1999**, *1454*, 31.
- (48) Egan, T. J. *Journal of Inorganic Biochemistry* **2008**, *102*, 1288.
- (49) Egan, T. J.; Combrinck, J. M.; Egan, J.; Hearne, G. R.; Marques, H. M.; Ntenti, S.; Sewell, B. T.; Smith, P. J.; Taylor, D.; van Schalkwyk, D. A.; Walden, J. C. *Biochem J* **2002**, *365*, 343.
- (50) Ncokazi, K. K.; Egan, T. J. *Anal Biochem* **2005**, *338*, 306.

- (51) Hoang, A. N.; Sandlin, R. D.; Omar, A.; Egan, T. J.; Wright, D. W. *Biochemistry* **2010**, *49*, 10107.
- (52) Kapishnikov, S.; Berthing, T.; Hviid, L.; Dierolf, M.; Menzel, A.; Pfeiffer, F.; Als-Nielsen, J.; Leiserowitz, L. *Proceedings of the National Academy of Sciences of the United States of America* **2012**, *109*, 11184.
- (53) Kapishnikov, S.; Weiner, A.; Shimoni, E.; Guttman, P.; Schneider, G.; Dahan-Pasternak, N.; Dzikowski, R.; Leiserowitz, L.; Elbaum, M. *Proceedings of the National Academy of Sciences of the United States of America* **2012**, *109*, 11188.
- (54) Large portions of this section were adapted from: Sandlin, R. D.; Carter, M. D.; Lee, P. J.; Auschwitz, J. M.; Leed, S. E.; Johnson, J. D.; Wright, D. W. *Antimicrobial Agents & Chemotherapy* **2011**, *55*, 3363.
- (55) Blauer, G.; Akkawi, M. *Archives of Biochemistry and Biophysics* **2002**, *398*, 7.
- (56) Huy, N. T.; Maeda, A.; Uyen, D. T.; Trang, D. T. X.; Sasai, M.; Shiono, T.; Oida, T.; Harada, S.; Kamei, K. *Acta Tropica* **2007**, *101*, 130.
- (57) Egan, T. J.; Mavuso, W. W.; Ncokazi, K. K. *Biochemistry* **2001**, *40*, 204.
- (58) Stiebler, R.; Hoang, A. N.; Egan, T. J.; Wright, D. W.; Oliveira, M. F. *PLoS One* **2010**, *5*.
- (59) Avrami, M. *Journal of Chemical Physics* **1939**, *7*, 1103.
- (60) Ambele, M. A.; Egan, T. J. *Malaria Journal* **2012**, *11*.
- (61) Egan, T. J.; Tshivhase, M. G. *Dalton Transactions* **2006**, 5024.
- (62) Gamo, F. J.; Sanz, L. M.; Vidal, J.; de Cozar, C.; Alvarez, E.; Lavandera, J. L.; Vanderwall, D. E.; Green, D. V. S.; Kumar, V.; Hasan, S.; Brown, J. R.; Peishoff, C. E.; Cardon, L. R.; Garcia-Bustos, J. F. *Nature* **2010**, *465*, 305.
- (63) Plouffe, D.; Brinker, A.; McNamara, C.; Henson, K.; Kato, N.; Kuhlen, K.; Nagle, A.; Adrian, F.; Matzen, J. T.; Anderson, P.; Nam, T.-g.; Gray, N. S.; Chatterjee, A.; Janes, J.; Yan, S. F.; Trager, R.; Caldwell, J. S.; Schultz, P. G.; Zhou, Y.; Winzeler, E. A. *Proceedings of the National Academy of Sciences of the United States of America* **2008**, *105*, 9059.
- (64) Guiguemde, W. A.; Shelat, A. A.; Bouck, D.; Duffy, S.; Crowther, G. J.; Davis, P. H.; Smithson, D. C.; Connelly, M.; Clark, J.; Zhu, F.; Jiménez-Díaz, M. B.; Martinez, M. S.; Wilson, E. B.; Tripathi, A. K.; Gut, J.; Sharlow, E. R.; Bathurst, I.;

- Mazouni, F. E.; Fowble, J. W.; Forquer, I.; McGinley, P. L.; Castro, S.; Angulo-Barturen, I.; Ferrer, S.; Rosenthal, P. J.; DeRisi, J. L.; Sullivan, D. J.; Lazo, J. S.; Roos, D. S.; Riscoe, M. K.; Phillips, M. A.; Rathod, P. K.; Van Voorhis, W. C.; Avery, V. M.; Guy, R. K. *Nature* **2010**, *465*, 311.
- (65) Kurosawa, Y.; Dorn, A.; Kitsuji-Shirane, M.; Shimada, H.; Satoh, T.; Matile, H.; Hofheinz, W.; Masciadri, R.; Kansy, M.; Ridley, R. G. *Antimicrobial Agents and Chemotherapy* **2000**, *44*, 2638.
- (66) Lucumi, E.; Darling, C.; Jo, H.; Napper, A. D.; Chandramohanadas, R.; Fisher, N.; Shone, A. E.; Jing, H.; Ward, S. A.; Biagini, G. A.; DeGrado, W. F.; Diamond, S. L.; Greenbaum, D. C. *Antimicrobial Agents and Chemotherapy* **2010**, *54*, 3597.
- (67) Tanaka, T. Q.; Williamson, K. C. *Molecular & Biochemical Parasitology* **2011**, *160*.
- (68) Baniecki, M. L.; Wirth, D. F.; Clardy, J. *Antimicrobial Agents and Chemotherapy* **2007**, *51*, 716.
- (69) Parapini, S.; Basilico, N.; Pasini, E.; Egan, T. J.; Olliaro, P.; Taramelli, D.; Monti, D. *Experimental Parasitology* **2000**, *96*, 249.
- (70) Rush, M. A.; Baniecki, M. L.; Mazitschek, R.; Cortese, J. F.; Wiegand, R.; Clardy, J.; Wirth, D. *Antimicrobial Agents and Chemotherapy* **2009**, *53*, 2564.
- (71) World Malaria Report 2008. [Online Early Access]. Published Online: 2008. <http://www.who.int>.
- (72) Noedl, H.; Se, Y.; Schaefer, K.; Smith, B. L.; Socheat, D.; Fukuda, M. M. *New England Journal of Medicine* **2008**, *359*, 2619.
- (73) Cheeseman, I. H.; Miller, B. A.; Nair, S.; Nkhoma, S.; Tan, A.; Tan, J. C.; Al Saai, S.; Phyto, A. P.; Moo, C. L.; Lwin, K. M.; McGready, R.; Ashley, E.; Imwong, M.; Stepniewska, K.; Yi, P.; Dondorp, A. M.; Mayxay, M.; Newton, P. N.; White, N. J.; Nosten, F.; Ferdig, M. T.; Anderson, T. J. *Science* **2012**, *336*, 79.
- (74) Combrinck, J. M.; Mabothe, T. E.; Ncokazi, K. K.; Ambele, M. A.; Taylor, D.; Smith, P. J.; Hoppe, H. C.; Egan, T. J. *ACS Chemical Biology* **2012**.
- (75) Iwaniuk, D. P.; Whetmore, E. D.; Rosa, N.; Ekoue-Kovi, K.; Alumasa, J.; de Dios, A. C.; Roepe, P. D.; Wolf, C. *Bioorganic Medicinal Chemistry* **2009**, *17*, 6560.
- (76) De, D.; Krogstad, F. M.; Cogswell, F. B.; Krogstad, D. J. *Am J Trop Med Hyg* **1996**, *55*, 579.

- (77) Carter, M. D.; Phelan, V. V.; Sandlin, R. D.; Bachmann, B. O.; Wright, D. W. *Combinatorial Chemistry & High Throughput Screening* **2010**, *13*, 285.
- (78) Zhang, J.-H.; Chung, T. D. Y.; Oldenburg, K. R. *J Biomol Screen* **1999**, *4*, 67.
- (79) Mossmann, T. *Journal of Immunological Methods* **1983**, *65*, 55.
- (80) Trager, W.; Jensen, J. B. *Science* **1976**, *193*, 673.
- (81) Johnson, J. D.; Denuff, R. A.; Gerena, L.; Lopez-Sanchez, M.; Roncal, N. E.; Waters, N. C. *Antimicrobial Agents and Chemotherapy* **2007**, *51*, 1926.
- (82) Seifoddini, H. K. **1989**, *16*, 419.
- (83) Godden, J. W.; Xue, L.; Bajorath, J. *Journal of Chemical Information and Modeling* **2000**, *40*, 163.
- (84) Ncokazi, K. K.; Egan, T. J. *Analytical Biochemistry* **2005**, *338*, 306.
- (85) Heikkila, T.; Ramsey, C.; Davies, M.; Galtier, C.; Stead, A. M. W.; Johnson, A. P.; Fishwick, C. W. G.; Boa, A. N.; McConkey, G. A. *Journal of Medicinal Chemistry* **2007**, *50*, 186.
- (86) Jung, M.; Park, W.-H.; Jung, J.-C.; Lee, Y.; Oh, S.; Moon, H.-I. *Chemical Biology & Drug Design* **2009**, *73*, 346.
- (87) Khan, M. S.; Siddiqui, S. A.; Siddiqui, M. S. R. A.; Goswami, U.; Khan, M. I. *Chemical Biology Drug Design* **2008**, *72*, 197.
- (88) Villiers, K. A. d.; Marques, H. M.; Egan, T. J. *Journal of Inorganic Biochemistry* **2008**, *102*, 1660.
- (89) McKellar, Q. A.; Scott, E. W. *Journal of Veterinary Pharmacology and Therapeutics* **1990**, *13*, 223.
- (90) Camacho, J.; Barazarte, A.; Gamboa, N.; Rodrigues, J.; Rojas, R.; Vaisberg, A.; Gilman, R.; Charris, J. *Bioorganic & Medicinal Chemistry* **2011**, *19*, 2023.
- (91) Egan, T. J.; Ross, D. C.; Adams, P. A. *FEBS Letters* **1994**, *352*, 54.
- (92) Asher, C.; de Villiers, K. A.; Egan, T. J. *Inorganic Chemistry* **2009**, *48*, 7994.
- (93) Hunter, C. A.; Low, C. M.; Rotger, C.; Vinter, J. G.; Zonta, C. *Proc Natl Acad Sci U S A* **2002**, *99*, 4873.

- (94) Wongsrichanalai, C.; Pickard, A. L.; Wernsdorfer, W. H.; Meshnick, S. R. *The Lancet Infectious Diseases* **2002**, *2*, 209.
- (95) Fidock, D. A.; Rosenthal, P. J.; Croft, S. L.; Brun, R.; Nwaka, S. *Nature Reviews Drug Discovery* **2004**, *3*, 509.
- (96) Sachs, J.; Malaney, P. *Nature* **2002**, *415*, 680.
- (97) Research, G. F. f. H. Global Forum for Health Research, Geneva, 2002.
- (98) Nwaka, S.; Ridley, R. G. *Nature Reviews Drug Discovery* **2003**, *2*, 919.
- (99) Gardner, M. J.; Hall, N.; Fung, E.; White, O.; Berriman, M.; Hyman, R. W.; Carlton, J. M.; Pain, A.; Nelson, K. E.; Bowman, S.; Paulsen, I. T.; James, K.; Eisen, J. A.; Rutherford, K.; Salzberg, S. L.; Craig, A.; Kyes, S.; Chan, M.-S.; Nene, V.; Shallom, S. J.; Suh, B.; Peterson, J.; Angiuoli, S.; Pertea, M.; Allen, J.; Selengut, J.; Haft, D.; Mather, M. W.; Vaidya, A. B.; Martin, D. M. A.; Fairlamb, A. H.; Fraunholz, M. J.; Roos, D. S.; Ralph, S. A.; McFadden, G. I.; Cummings, L. M.; Subramanian, G. M.; Mungall, C.; Venter, J. C.; Carucci, D. J.; Hoffman, S. L.; Newbold, C.; Davis, R. W.; Fraser, C. M.; Barrell, B. *Nature* **2002**, *419*, 498.
- (100) Carlton, J. M.; Adams, J. H.; Silva, J. C.; Bidwell, S. L.; Lorenzi, H.; Caler, E.; Crabtree, J.; Angiuoli, S. V.; Merino, E. F.; Amedeo, P.; Cheng, Q.; Coulson, R. M. R.; Crabb, B. S.; del Portillo, H. A.; Essien, K.; Feldblyum, T. V.; Fernandez-Becerra, C.; Gilson, P. R.; Gueye, A. H.; Guo, X.; Kang/'a, S.; Kooij, T. W. A.; Korsinczky, M.; Meyer, E. V. S.; Nene, V.; Paulsen, I.; White, O.; Ralph, S. A.; Ren, Q.; Sargeant, T. J.; Salzberg, S. L.; Stoeckert, C. J.; Sullivan, S. A.; Yamamoto, M. M.; Hoffman, S. L.; Wortman, J. R.; Gardner, M. J.; Galinski, M. R.; Barnwell, J. W.; Fraser-Liggett, C. M. *Nature* **2008**, *455*, 757.
- (101) Butkiewicz, M.; Mueller, R.; Selic, D.; Dawson, E.; Meiler, J.; Wiese, K. C., Ed.: Nashville, 2009, p 255.
- (102) Mueller, R.; Dawson, E. S.; Niswender, C. M.; Butkiewicz, M.; Hopkins, C. R.; Weaver, C. D.; Lindsley, C. W.; Conn, P. J.; Meiler, J. *J Mol Model* **2012**.
- (103) Mueller, R.; Rodriguez, A. L.; Dawson, E. S.; Butkiewicz, M.; Nguyen, T. T.; Oleszkiewicz, S.; Bleckmann, A.; Weaver, C. D.; Lindsley, C. W.; Conn, P. J.; Meiler, J. *ACS Chemical Neuroscience* **2010**.
- (104) Wild, D. J.; Blankley, C. J. *Journal of Chemical Information and Computer Sciences* **2000**, *40*, 155.



- (105) Verma, J.; Khedkar, V. M.; Coutinho, E. C. *Current Topics in Medicinal Chemistry* **2010**, *10*, 95.
- (106) Gasteiger, J.; Rudolph, C.; Sadowski, J. *Tetrahedron Computer Methodology* **1990**, *3*, 537.
- (107) Meiler, J. *Journal of Biomolecular NMR* **2003**, *26*, 25.
- (108) Tetko, I. V.; Kovalishyn, V. V.; Livingstone, D. J. *J. Med. Chem* **2001**, *44*, 2411.
- (109) Winkler, D. *Molecular Biotechnology* **2004**, *27*, 139.
- (110) Schoelkopf, B.; Smola, A. J. *Learning with Kernels*; The MIT Press: Cambridge, Massachusetts, 2002.
- (111) Alex, J. S.; Bernhard, S. *A tutorial on support vector regression*; Kluwer Academic Publishers, 2004; Vol. 14.
- (112) Song, Z.; Roussopoulos, N. *Advances in Spatial and Temporal Databases* **2001**, 79.
- (113) Dudani, S. A. *Systems, Man and Cybernetics, IEEE Transactions on* **1976**, 325.
- (114) Kohonen, T. *Self-Organization and Associative Memory, 100 figs. XV, 312 pages.. Springer-Verlag Berlin Heidelberg New York. Also Springer Series in Information Sciences, volume 8* **1988**, 1.
- (115) Kohonen, T. *Proceedings of the IEEE* **1990**, *78*, 1464.
- (116) Quinlan, J. R. *Machine Learning* **1986**, *1*, 81.
- (117) Dietterich, T. G. *Machine Learning* **2000**, *40*, 139.
- (118) Aha, D. W.; Bankert, R. L. *Learning from Data: Artificial Intelligence and Statistics V* **1995**, 199.
- (119) Mao, K. Z. *Systems, Man, and Cybernetics, Part B: Cybernetics, IEEE Transactions on* **2004**, *34*, 629.
- (120) Kohavi, R. 1995; Vol. 14, p 1137.
- (121) Kelly, J. X.; Smilkstein, M. J.; Cooper, R. A.; Lane, K. D.; Johnson, R. A.; Janowsky, A.; Dodean, R. A.; Hinrichs, D. J.; Winter, R.; Riscoe, M. *Antimicrobial Agents and Chemotherapy*. **2007**, *51*, 4133.

- (122) The data presented in this chapter has previously been published in: Hoang, A. N.; Sandlin, R. D.; Omar, A.; Egan, T. J.; Wright, D. W. *Biochemistry* **2010**, *49*, 10107.
- (123) The results presented in this chapter will be published as: Sandlin, *et al.* Investigations into Detergent-Mediated  $\beta$ -hematin Formation.
- (124) The results presented in this chapter will be published as: Butkiewicz, M.;\* Sandlin, R. D.;\* Meiler, J.; Wright, D. W. Application of Machine Learning Techniques Reveals Pathway Specific Inhibitors for  $\beta$ -Hematin Crystallization in *Plasmodium Falciparum*.

## Appendix A

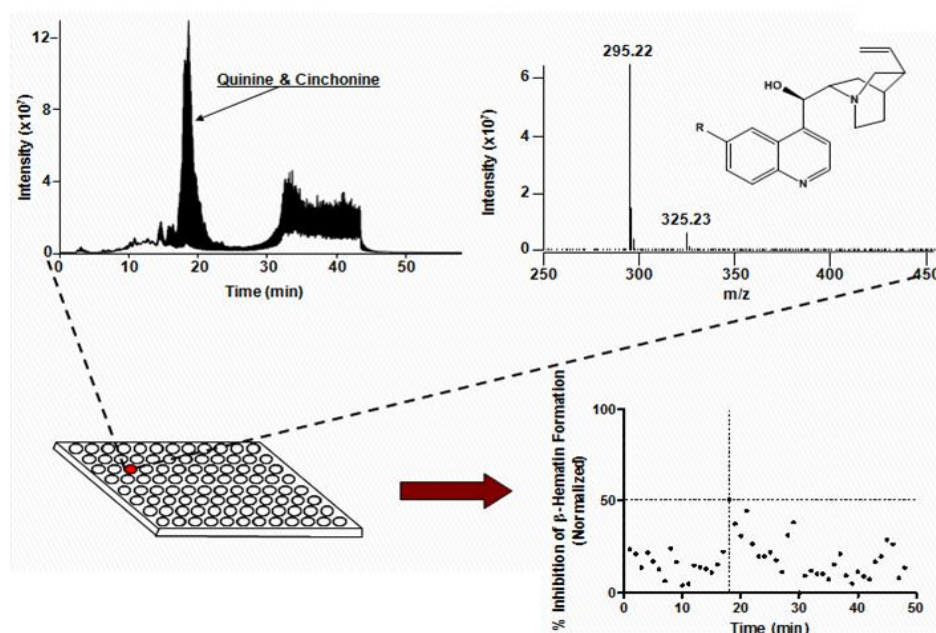
### Identification of Natural Product Extracts that Inhibit $\beta$ -Hematin Formation

While pharmaceutical companies primarily rely on the promise offered by screening small molecule libraries, natural products are now quite underutilized in this industry. Throughout history, natural resources have been used for their antimalarial effectiveness. In particular, the bark from the *Cinchona* tree was successfully used in the treatment of malaria, and later extracts identified the presence of quinine as the active drug component. Artemisinin, another effective antimalarial, is a natural product of the Wormwood shrub. Here, an underutilized resource, cave microorganisms, were analyzed in an attempt to identify new inhibitors of  $\beta$ -hematin formation. The state of Tennessee contains over 7,000 cave systems, six of which have been selected for the isolation of bacteria cultures by Brian Bachmann and coworkers. Cave microorganisms exist in a hypercompetitive environment where nutrient resources are limited, requiring organisms to evolve at a rapid rate, resulting in a rich resource for secondary metabolites. These metabolites can then be exploited by extraction methods followed by their incorporation into the detergent based  $\beta$ -hematin inhibition assay.

#### Proof of Concept: Analysis of Cinchona Bark

A real-world application was tested in attempt to rediscover the antimalarial  $\beta$ -hematin inhibitor, quinine. An ethanol extraction of *Cinchona* bark powdered supplement was fractioned onto a 96-well plate and separated by an acetonitrile:water

gradient using reverse phase liquid chromatography tandem mass spectrometry (RP-LC-MS/MS). One milliliter fractions of each sample were collected per minute in 96-deep well source plates and transferred to 96-well destination plates for screening, ensuring synchronization with the LC-MS/MS data to facilitate spectral identification of each well's compound(s). A compound capable of inhibiting 50% of  $\beta$ -hematin formation was identified and LC/MS data confirmed the presence of quinine in well 19 (**Figure 37**).



**Figure 37:** The extraction of quinine from cinchona bark.

#### Extraction of Metabolites from Cave Microorganisms

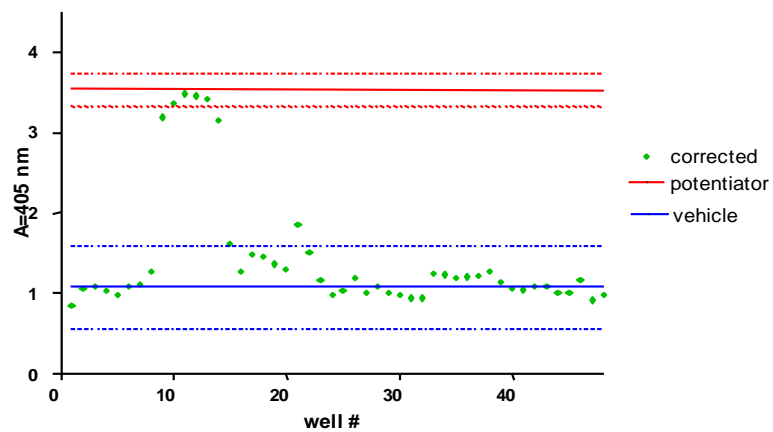
The NP-40 HTS assay was successfully adapted for use in screening natural product extracts from cave microorganisms. The substrate concentrations remain as previously reported, with the addition of acetonitrile (7.5% v/v) to suspend the fractioned extracts in a 96-well plate. The assay was completely validated and utilized to test the

bioactivity of a diverse library of bacterial extracts. The samples tested consisted of bacterial strains isolated from soil samples that were collected from three different caves. In order to further diversify the library of compounds, each purified strain was grown under six different media conditions to elicit a unique set of secondary metabolites from each bacterial strain. Isolated actinomycete strains were cultured under six unique media conditions followed by a series of extraction procedures. Metabolites were extracted from the mycelium using 100% methanol (h1) and 100% acetone (h2), resulting in two unique extracts from the cell mass. Activated HP-20 resin was then added to the supernatant of the fermentation broth and stirred for thirty minutes followed by three extractions using 20%, 60%, and 100% methanol (fractions h3-h5, respectively). For the extraction of nonpolar metabolites such as polyketides and oligosaccharides, ethyl acetate was added to a separate supernatant, shaken, then decanted and dried (e1). This resulted in two extracts taken directly from the cell mass, and four extracts taken from the supernatant. Extracts were then fractioned onto a 96-well plate and stored dry at -20 °C.

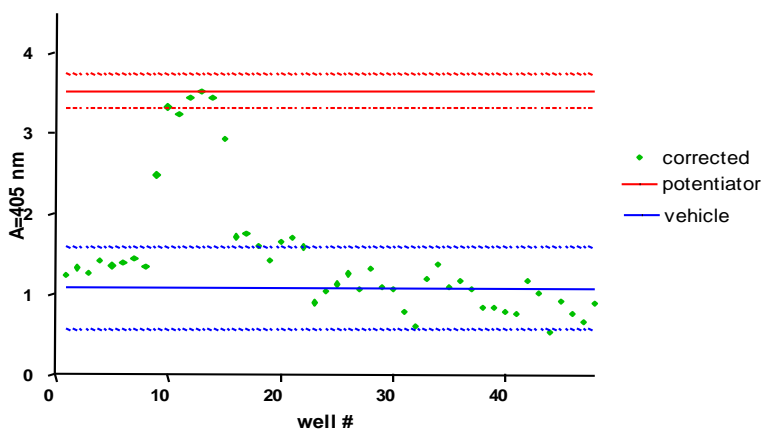
Plates containing fractions of the bacterial culture extracts were tested in a preliminary screen depicted in **Figure 37**. The  $2\sigma$  and  $3\sigma$  values are established based on a control plate containing the  $IC_{max}$  of amodiaquine (100  $\mu$ M). A value above  $3\sigma$  indicates an inhibitor that is within three standard deviations of the amodiaquine control and should be further analyzed for bioactivity. It should be noted that during the fractioning process, each well is characterized based on UV-Vis data, mass spectrometry analysis, and LC data such that each well is thoroughly analyzed during the fractioning process. In the plate at hand, there are three fractions that are within three standard deviations of the amodiaquine control

## Full Screening Results

The goal of screening 8,640 fractions was achieved with 199 active wells resulting in a hit rate of ~2.2% of screened fractions (Table 11). Figure 38 is a typical screen where green dots represent test compounds. The solid lines represent the average value of control wells, where the dashed lines include the absorbance values that are within three standard deviations of the corresponding control. Test compounds that are at least three standard deviations above the negative control are considered to have statistically significant activity. Test compounds that fall within the red lines are considered to be particularly potent, capable of inhibiting  $\beta$ -hematin formation to the same extent as the IC<sub>100</sub> amodiaquine control. Figure 38 represents a single actinomycete strain grown under two different media conditions and extracted using 100% methanol. The result is a clustering of compounds at elution times between 9-15 minutes. This was visualized in the natural products software developed by CFD Research Corporation, indicated by the red bars (Figure 39). This overlapping activity is common in the active strains tested thus far and is the result of either high concentrations of active compound that is carried into multiple wells, or a class of closely related compounds that display similar degrees of activity in the  $\beta$ -hematin formation assay.



A



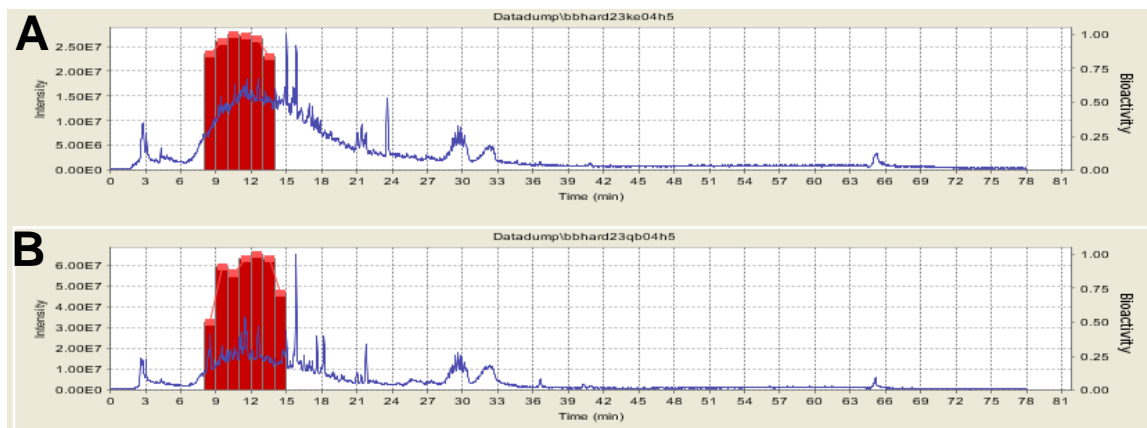
B

**Figure 38.** A single actinomycete strain grown under two different media conditions and extracted using 100% methanol. The result is a clustering of compounds at elution times between 9-15 minutes.

When viewing the positive ion MS data for the active fractions, the mass correlation feature of the software identified a common mass of 347.0 m/z in the active region of each plate. Though a promising correlation between mass and activity is observed, further analysis is required to determine if this common mass is in fact responsible for the  $\beta$ -hematin formation inhibition.

With the screening goals accomplished, activity guided fractionation will be used to positively identify active compounds. Briefly, a large scale culture (10 L) of the active actinomycete strain will be grown to ensure sufficient metabolite production. The extract will be fractionated on a Sephadex LH-20 column and tested for activity in the  $\beta$ -hematin formation assay. Active fractions will, then, be further purified using a C18 column and again tested for activity. If active fractions are sufficiently pure, then NMR will be used to positively identify the active compound(s) in each extract. This approach will be used to characterize those active compounds identified during screening.





**Figure 39.** This activity of actinomycete extracts presented in Figure 38 were visualized in the natural products software developed by CFD Research Corporation. Activity is indicated by the red bars.

**Table 11.** Extracts screened. Highlighted extracts are active in the  $\beta$ -hematin formation assay.

Strain Identifier	Growth Media	Extraction Protocol							Strain Identifier	Growth Media	Extraction Protocol						
		H1	H2	H3	H4	H5	E1	H7			H1	H2	H3	H4	H5	E1	H7
1	OA						X		13	BA	X		X	X	X	X	X
1	KE						X		13	KE	X			X			
1	KA						X		13	EA	X	X	X	X	X	X	
2	KE						X		13	QB	X	X				X	
2	ET						X		13	KA	X	X	X	X			X
2	BA						X		14	EA							X
2	EA						X		14	KA							X
3	OA						X		14	BA							X
4	OA							X	15	BA		X	X	X	X	X	X
4	KA							X	15	QB		X	X	X	X	X	
4	BA							X	15	OA		X	X	X	X	X	
4	QB							X	15	EA		X	X	X	X	X	
5	OA						X		15	KE		X	X	X	X	X	
5	KA							X	15	KA		X	X	X	X	X	
5	KE							X	16	QB							X
6	KE						X		17	QB	X	X	X	X	X	X	X
6	KA						X		17	KE	X	X				X	X
7	EA		X	X	X	X			17	BA	X	X	X	X	X	X	
7	OA		X	X	X	X			17	KA	X	X				X	
7	KA	X	X						17	OA	X	X	X	X	X	X	X
8	EA	X	X	X	X	X			17	EA	X	X	X	X	X	X	
8	QB	X	X	X	X				18	BA							X
8	KE	X		X	X	X			19	OA							X
8	KA	X	X	X		X			19	KA							X
8	OA	X	X	X	X	X			19	BA							X
8	BA	X		X	X	X			20	ET							X
9	OA						X		21	QB							X
10	BA						X		21	EA							X
10	KA						X		21	KA							X
10	OA						X		22	EA							X
10	QB						X		22	KE							X
11	QB						X		22	QB							X
11	KE						X		23	KA	X	X	X	X	X		
11	EA						X		23	OA			X			X	
11	KA						X		23	BA	X	X	X	X	X	X	
11	BA						X		23	EA	X	X	X	X	X		
12	KA						X		23	QB	X	X		X	X		
13	OA	X	X		X	X	X		23	KE	X	X		X	X		

## Appendix B

### Parasite Culturing Protocol

Schedule for one week culturing period:

- Day 1: Off
- Day 2: Change media
- Day 3: Subculture (split) parasite
- Day 4: Off
- Day 5: Change media, Add blood
- Day 6: Change media
- Day 7: Subculture (split) parasite

The schedule is critical to the survival of the parasite, as the parasite is very sensitive to media conditions. Ideally, parasite work should be done at roughly the same time each day. However, if you are occasionally a few hours early or late from the time you normally care for the parasite, it is ok.

#### **I. Reagent Preparation**

Preparation of RPMI basic medium (500 mL)

- Take one container of RPMI medium.
- Add 1 g glucose.
- Add 3 g HEPES.
- Gently shake contents in bottle until dissolved, then filter sterilize with filter. Store in refrigerator.

#### 1. Preparation of 1.45 mM hypoxanthine stock (200 ml)

- Dissolve 10.0 mg hypoxanthine in 50 ml distilled H<sub>2</sub>O.
- Heat for 10 min (until dissolved)
- Filter sterilize and store 4 °C.

#### 2. Preparation of TCM complete medium (100 mL)

- Take two sterile 50 mL tubes. To each, add the following:
- 42.5 mL RPMI.
- 5.25 mL plasma.

- 1.6 mL sodium bicarbonate.
- 1.0 mL hypoxanthine stock.
- Keep complete medium no longer than one week.

## **II Washing 50% HCT Blood**

- Place (15 mL) blood into 50 mL sterile conical tube.
- Place (15 mL) of RPMI in each tube containing the blood
- Spin at 3000 RPM for 8 minutes. Turn brake to '1' position to avoid resuspending the blood.
- Remove RPMI and buffy coat (a thick white coat on top of the blood layer)
- Repeat Steps 4-6
- After repeating step 6 add TCM to the blood so that you have a 50% Hct solution
- Use blood no longer than one week

## **III Parasite Care Routine**

For 25 mL flask culture:

- Carefully remove flasks from incubator. Let sit for 10 minutes to allow disturbed RBC's to settle to bottom of flask.
- Remove ~4mL of the media without removing RBCs
- Replace with 4 mL of TCM, if adding blood use 0.1 mL of 50% HCT Blood
- Gas culture with blood gas (90% N<sub>2</sub>, 5% O<sub>2</sub>, 5% CO<sub>2</sub> for 30 sec
- Place in 37°C Incubator

## **IV Subculture/Splitting Parasite**

Using a 25 mL flask:

- 4.5 mL of TCM
- 0.5 mL of 50% HCT Blood
- Depending on the split from previous cultures, do a 1/50 (if parasitemia is >5%) or 1/100 (if parasitemia is <5%) split: 1/50 split means adding 0.1 mL of old culture 1/100 split 0.05 mL of old culture
- Gas with Mixed Gas for 30 sec
- Place in 37°C Incubator

## Appendix C

### Malaria SYBR Green-I Assay

The malaria SYBR Green-I assay (MSF) is used to identify in vitro antimalarial compounds in 384-well plate format. This assay was adapted from Johnson *et al.*<sup>81</sup> This assay is performed on a ‘split’ day of the parasite culturing schedule (Appendix B).

#### **Optimal Parasite Culture:**

In order for the assay to perform optimally, the cultures should be healthy. In this instance healthy is defined as a culture that is growing as expected (5-8% parasitemia on a ‘split’ day) and shows no signs of being ‘stressed’ when viewed under the light microscope.

#### **Plate Preparation:**

Because the reagents used in this assay are sensitive to high O<sub>2</sub> concentrations, the assay should be setup quickly.

1. Prepare the drug plate
  - a. Add compound to be tested to the plate (384-well black, clear-bottom microtiter plate).
  - b. Add vehicle controls if necessary.
  - c. Add kill concentration of chloroquine (500 nM)
  - d. Add IC<sub>50</sub> concentrations for chloroquine. This is performed to ensure that parasite is healthy and responding to drug treatment as expected (~20 nM

for D6 strain and ~200 nM for C235 strain). While b-c need to be added to each plate, this step (d), can be added to a separate plate.

## 2. Prepare culture stock

Each well should contain 0.3 % parasitemia (from healthy culture), 2% Hct of fresh blood, 38  $\mu$ L of TCM and 4.25  $\mu$ L of RPMI. If test compounds are added using the ECHO delivery system (such that low volumes of test compound are present) then parasite, TCM, blood and RPMI can be premixed to facilitate quick and easy delivery of assay components. Alternatively, the test compound can be solubilized in RPMI and 4.25  $\mu$ L of this solution can be added to the plate. In this instance, the TCM, blood and parasite culture will be premixed and added to the plate (38  $\mu$ L).

## 3. Assay incubation

- a. The plate should be quickly transferred to a humidified incubator with a blood gas atmosphere (90% nitrogen, 5% oxygen and 5% carbon dioxide).
- b. Incubate plate for 72 hours. Do not disturb plate during this time.
- c. Remove plate from incubator

## 4 Addition of SYBR Green-I stock

- a) Prepare a stock solution of SYBR Green-I using Lysis Buffer (100 mM Tris HCl pH 7.5, 10 mM EDTA, 0.16% Saponin (w/v), 1.6% Triton X (v/v))

- b) Add 0.2  $\mu\text{L}$  SYBR Green-I (stock from Invitrogen, 10,000X) to 1 mL of lysis buffer or equivalent ratio. Note: SYBR Green-I does not respond well to freeze-thaw cycles so these should be avoided by freezing down small aliquots ( $\sim 30 \mu\text{L}/\text{tube}$ ).
- c) Add 38  $\mu\text{L}$  of this solution to each test well of the assay plate.
- d) Leave in dark drawer overnight.
- e) Read plate (BOTTOM READ only) at an excitation/emission wavelength of 488/522.
- f) Calculate inhibitory activity relative to the positive and negative control wells.

## Appendix D

### Full Results of Hits Identified in the HTS Screen

In the following pages, each of the compounds identified as a hit in the HTS screen (Chapter IV) is listed by the VU identifier. In addition to the VU number for each hit, the IC<sub>50</sub> values for  $\beta$ -hematin inhibition (BH), drug sensitive *P. falciparum* (D6) and the multi-drug resistant strain of *P. falciparum* (C235) are included where appropriate. ND = not determined. Inactive indicates that inhibitory activity >90% was not observed and therefore an IC<sub>50</sub> value was not determined.



VU identifier	Structure	BH IC50 (μM)	D6 IC50 (uM)	C235 IC50 (uM)	VU identifier	Structure	BH IC50 (μM)	D6 IC50 (uM)	C235 IC50 (uM)
VU0098755		12.6	0.106	0.127	VU0065892		6.2	0.611	0.693
VU0073687		6.3	0.185	0.551	VU0010690		25.0	0.673	1.5
VU0001281		5.9	0.194	0.174	VU0094619		2.4	0.700	0.284
VU0065708		16.2	0.198	0.184	VU0012464		7.3	0.708	0.923
VU0096505		8.8	0.238	0.217	VU0008057		9.6	0.730	1.5
VU0107282		17.0	0.290	0.540	VU0358149		8.3	0.778	19.1
VU0114785		13.4	0.346	4.8	VU0015078		1.1	0.810	5.7
VU0002101		14.3	0.348	0.412	VU0119324		21.5	0.845	0.186
VU0028177		13.3	0.350	0.465	VU0078364		5.3	0.922	2.0
VU0063971		8.9	0.384	0.833	VU0107278		11.8	0.951	3.9
VU0129813		26.8	0.396	0.294	VU0064165		15.4	0.993	1.0
VU0114734		22.1	0.461	1.1	VU0068266		18.3	1.0	ND
VU0122653		24.5	0.550	0.900	VU0359100		10.9	1.1	7.916
VU0000264		2.0	0.593	0.248	VU0013883		19.5	1.4	ND

VU identifier	Structure	BH IC50 (μM)	D6 IC50 (μM)	C235 IC50 (μM)	VU identifier	Structure	BH IC50 (μM)	D6 IC50 (μM)	C235 IC50 (μM)
VU0065413		16.5	1.4	ND	VU0043533		12.0	2.7	ND
VU0118945		22.5	1.5	ND	VU0033980		21.7	2.7	ND
VU0060841		17.3	1.5	ND	VU0133680		14.8	2.8	ND
VU0358549		7.2	1.6	ND	VU0073686		13.5	3.0	ND
VU0117011		10.4	1.7	ND	VU0064114		16.5	3.0	ND
VU0358176		2.4	1.7	ND	VU0077964		10.3	3.1	ND
VU0117080		11.4	1.7	ND	VU0106972		21.4	3.2	ND
VU0015069		10.4	1.9	ND	VU0000641		4.6	3.5	ND
VU0125795		16.2	2.0	ND	VU0054768		22.6	3.5	ND
VU0077944		25.6	2.2	ND	VU0042031		1.7	3.5	ND
VU0123773		12.7	2.2	ND	VU0066706		16.3	3.6	ND
VU0007713		10.3	2.3	ND	VU0021012		19.3	3.7	ND
VU0055392		13.7	2.3	ND	VU0123046		22.6	3.9	ND
VU0129734		18.7	2.4	ND	VU0077557		10.5	3.9	ND

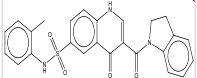
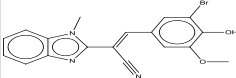
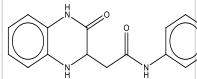
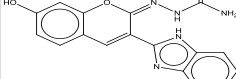
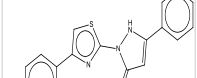
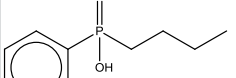
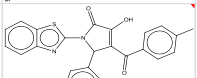
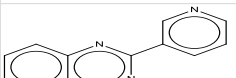
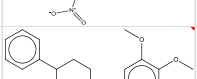
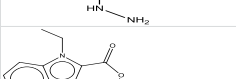
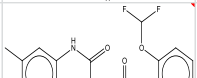
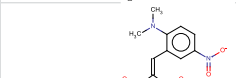
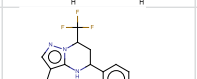
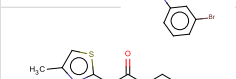

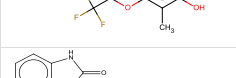
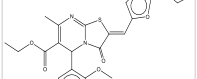
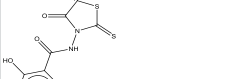
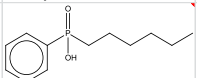
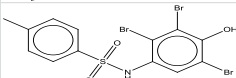

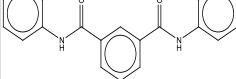
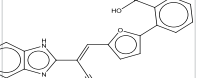
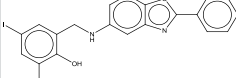
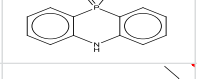
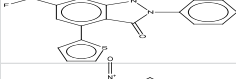
VU identifier	Structure	BH IC50 (μM)	D6 IC50 (nM)	C235 IC50 (nM)	VU identifier	Structure	BH IC50 (μM)	D6 IC50 (nM)	C235 IC50 (nM)
VU0002229		16.5	2.4	ND	VU0127450		17.3	4.7	ND
VU0060490		11.0	4.1	ND	VU0358764		9.0	4.8	ND
VU0068286		19.1	4.1	ND	VU0121735		11.0	5.0	ND
VU0066798		21.5	4.2	ND	VU0081577		24.4	5.1	ND
VU0116830		11.9	4.2	ND	VU0015041		19.9	5.1	ND
VU0358505		18.1	4.2	ND	VU0095273		21.7	5.1	ND
VU0073736		10.2	4.2	ND	VU0068227		23.7	5.1	ND
VU0359436		5.0	4.3	ND	VU0132168		13.8	5.2	ND
VU0060770		24.8	4.3	ND	VU0111491		16.5	5.3	ND
VU0073706		2.9	4.3	ND	VU0105653		20.0	5.3	ND
VU0122425		21.5	4.3	ND	VU0098496		19.3	5.5	ND
VU0358181		15.7	4.4	ND	VU0128298		11.5	5.5	ND
VU0116790		10.6	4.5	ND	VU0057475		18.6	5.5	ND

VU identifier	Structure	BH IC50 (μM)	D6 IC50 (uM)	C235 IC50 (uM)	VU identifier	Structure	BH IC50 (μM)	D6 IC50 (uM)	C235 IC50 (uM)
VU0054902		17.9	4.6	ND	VU0081575		21.3	5.6	ND
VU0124893		25.8	4.6	ND	VU0033455		26.8	5.9	ND
VU0057426		21.2	5.9	ND	VU0106991		18.2	6.2	ND
VU0124098		7.6	5.9	ND	VU0115413		15.8	6.3	ND
VU0077973		13.7	6.0	ND	VU0107331		21.9	6.3	ND
VU0056498		16.6	6.0	ND	VU0099400		15.4	6.4	ND
VU0068256		21.6	6.0	ND	VU0073509		6.9	6.5	ND
VU0116780		11.4	6.1	ND	VU0073498		10.1	6.6	ND
VU0066820		19.8	6.1	ND	VU0071259		17.9	6.7	ND
VU0066885		13.9	6.1	ND	VU0077935		23.6	6.8	ND
VU0194156		10.5	6.2	ND	VU0119224		21.5	6.8	12.38
VU0068276		21.3	6.2	ND	VU0012237		13.6	6.9	ND
VU0081548		22.3	6.2	ND	VU0007007		17.7	6.9	ND

VU identifier	Structure	BH IC50 (μM)	D6 IC50 (uM)	C235 IC50 (uM)	VU identifier	Structure	BH IC50 (μM)	D6 IC50 (uM)	C235 IC50 (uM)
VU0112087		20.2	7.0	ND	VU0129181		16.1	9.0	ND
VU0094315		17.6	7.1	ND	VU0099289		5.7	9.1	ND
VU0007691		9.7	7.2	ND	VU0054351		17.0	9.1	ND
VU0358440		15.4	7.3	ND	VU0140514		22.6	9.1	ND
VU0131684		15.0	7.6	ND	VU0116989		14.4	9.3	ND
VU0117249		7.9	7.7	ND	VU0002784		13.9	9.4	ND
VU0033649		21.5	7.7	ND	VU0358468		5.6	9.5	ND
VU0122447		17.3	7.9	ND	VU0069083		21.8	9.6	ND
VU0041098		7.8	7.9	ND	VU0063940		10.8	9.7	ND
VU0125966		23.2	8.2	ND	VU0358343		3.7	9.7	ND
VU0077962		10.6	8.5	ND	VU0060399		11.0	9.8	ND
VU0116770		13.6	8.5	ND	VU0118993		15.9	9.9	ND
VU0007694		10.0	8.7	ND	VU0117177		7.6	9.9	ND

VU identifier	Structure	BH IC50 (μM)	D6 IC50 (uM)	C235 IC50 (uM)	VU identifier	Structure	BH IC50 (μM)	D6 IC50 (uM)	C235 IC50 (uM)
VU0077946		10.3	9.9	ND	VU0073716		9.3	11.9	ND
VU0131034		14.5	10.4	ND	VU0126165		23.5	12.1	ND
VU0041052		3.4	10.4	ND	VU0012258		17.9	12.4	ND
VU0015715		21.9	10.4	ND	VU0114305		5.7	12.4	ND
VU0093477		10.3	10.4	ND	VU0059997		23.2	12.5	ND
VU0129123		7.3	10.5	ND	VU0081442		17.4	12.7	ND
VU0358483		19.3	11.0	ND	VU0005352		16.8	12.9	ND
VU0116748		10.9	11.1	ND	VU0077907		11.2	13.5	ND
VU0093551		11.0	11.1	ND	VU0066909		15.4	14.0	ND
VU0111471		15.3	11.2	ND	VU0004718		23.3	14.1	ND
VU0278601		12.5	11.3	ND	VU0060787		17.1	14.2	ND
VU0099279		10.0	11.7	ND	VU0116728		10.2	15.7	ND
VU0077577		7.2	11.9	ND	VU0056416		21.2	16.1	ND

VU identifier	Structure	BH IC50 (μM)	D6 IC50 (uM)	C235 IC50 (uM)	VU identifier	Structure	BH IC50 (μM)	D6 IC50 (uM)	C235 IC50 (uM)
VU0099202		11.0	16.2	ND	VU0112751		3.0	NA	NA
VU0065130		9.4	16.3	ND	VU0081492		11.0	NA	NA
VU0133817		21.2	16.3	ND	VU0115401		21.7	NA	NA
VU0097482		11.0	16.5	ND	VU0014981		0.4	NA	NA
VU0126567		21.3	16.5	ND	VU0114677		8.3	NA	NA
VU0120963		14.9	16.8	ND	VU0084736		9.0	NA	NA
VU0115374		12.2	17.0	ND	VU0130592		11.5	NA	NA
VU0057485		17.2	17.3	ND	VU0077974		12.1	NA	NA
VU0358463		8.6	17.5	ND	VU0000265		16.4	NA	NA
VU0120913		7.9	17.6	ND	VU0357676		17.3	NA	NA
VU0357882		8.9	17.8	ND	VU0012947		17.7	NA	NA
VU0077975		8.5	NA	NA	VU0144619		18.5	NA	NA
VU0060352		4.8	NA	NA	VU0137617		22.5	NA	NA

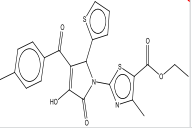
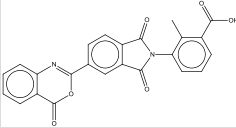
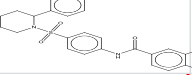
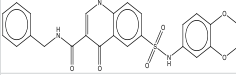
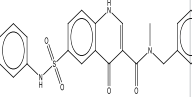
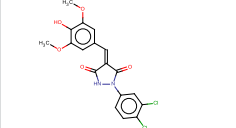
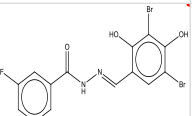
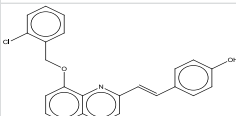
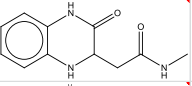
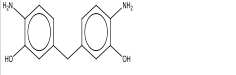
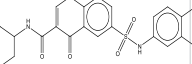
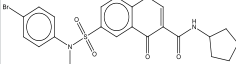
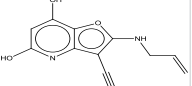
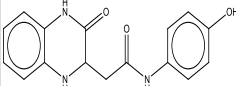
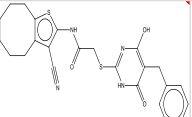
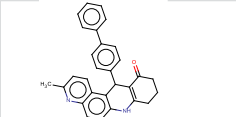
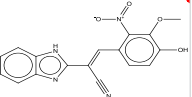
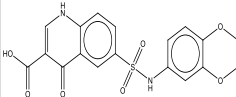
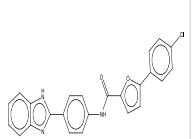
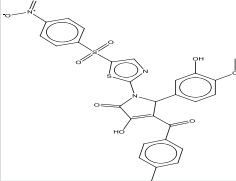
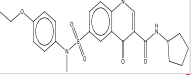
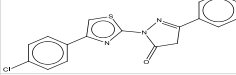
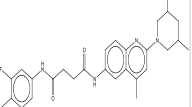
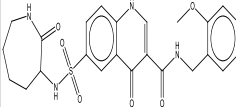
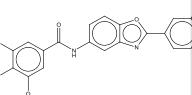
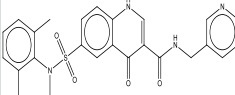
VU identifier	Structure	BH IC50 (μM)	D6 IC50 (uM)	C235 IC50 (uM)	VU identifier	Structure	BH IC50 (μM)	D6 IC50 (uM)	C235 IC50 (uM)
VU0116811		25.6	NA	NA	VU0358099		3.4	NA	NA
VU0032187		10.5	NA	NA	VU0357658		3.4	NA	NA
VU0014379		0.2	NA	NA	VU0012974		3.5	NA	NA
VU0063871		0.4	NA	NA	VU0000809		3.6	NA	NA
VU0020967		1.5	NA	NA	VU0358204		4.1	NA	NA
VU0099210		2.2	NA	NA	VU0031736		4.2	NA	NA
VU0123869		2.4	NA	NA	VU0357755		4.2	NA	NA
VU0001216		2.6	NA	NA	VU0016715		4.6	NA	NA
VU0013068		2.9	NA	NA	VU0008926		4.9	NA	NA
VU0000817		3.1	NA	NA	VU0007239		5.0	NA	NA
VU0357956		3.2	NA	NA	VU0081017		5.1	NA	NA
VU0009045		3.2	NA	NA	VU0040337		5.3	NA	NA
VU0073726		3.2	NA	NA	VU0101286		5.7	NA	NA



VU identifier	Structure	BH IC50 (μM)	D6 IC50 (uM)	C235 IC50 (uM)	VU identifier	Structure	BH IC50 (μM)	D6 IC50 (uM)	C235 IC50 (uM)
VU0129395		5.8	NA	NA	VU0357745		6.7	NA	NA
VU0005674		5.8	NA	NA	VU0032616		6.8	NA	NA
VU0358326		5.9	NA	NA	VU0012564		7.0	NA	NA
VU0358394		5.9	NA	NA	VU0358180		7.0	NA	NA
VU0004443		6.0	NA	NA	VU0006449		7.0	NA	NA
VU0357723		6.0	NA	NA	VU0111574		7.1	NA	NA
VU0111544		6.0	NA	NA	VU0005896		7.1	NA	NA
VU0070839		6.3	NA	NA	VU0072331		7.1	NA	NA
VU0112741		6.3	NA	NA	VU0358036		7.3	NA	NA
VU0078374		6.3	NA	NA	VU0117227		7.3	NA	NA
VU0098120		6.4	NA	NA	VU0069882		7.5	NA	NA
VU0114299		6.6	NA	NA	VU0002558		7.8	NA	NA
VU0127353		6.7	NA	NA	VU0032566		7.9	NA	NA

VU identifier	Structure	BH IC50 (μM)	D6 IC50 (uM)	C235 IC50 (uM)	VU identifier	Structure	BH IC50 (μM)	D6 IC50 (uM)	C235 IC50 (uM)
VU0111505		8.2	NA	NA	VU0122990		8.9	NA	NA
VU0111564		8.2	NA	NA	VU0118615		8.9	NA	NA
VU0002854		8.3	NA	NA	VU0017219		9.0	NA	NA
VU0114315		8.3	NA	NA	VU0112732		9.1	NA	NA
VU0358325		8.3	NA	NA	VU0049228		9.2	NA	NA
VU0032597		8.5	NA	NA	VU0077945		9.2	NA	NA
VU0117187		8.5	NA	NA	VU0117246		9.2	NA	NA
VU0358119		8.6	NA	NA	VU0359431		9.3	NA	NA
VU0114463		8.7	NA	NA	VU0069737		9.3	NA	NA
VU0007463		8.8	NA	NA	VU0046416		9.4	NA	NA
VU0003854		8.8	NA	NA	VU0014436		9.4	NA	NA
VU0118075		8.8	NA	NA	VU0099166		9.7	NA	NA
VU0014487		8.9	NA	NA	VU0130007		9.7	NA	NA

VU identifier	Structure	BH IC50 (μM)	D6 IC50 (uM)	C235 IC50 (uM)	VU identifier	Structure	BH IC50 (μM)	D6 IC50 (uM)	C235 IC50 (uM)
VU0003021		10.0	NA	NA	VU0130152		10.4	NA	NA
VU0116758		10.1	NA	NA	VU0077972		10.4	NA	NA
VU0106077		10.1	NA	NA	VU0101451		10.4	NA	NA
VU0003541		10.1	NA	NA	VU0358575		10.4	NA	NA
VU0071908		10.1	NA	NA	VU0077917		10.4	NA	NA
VU0085247		10.1	NA	NA	VU0002405		10.5	NA	NA
VU0084726		10.2	NA	NA	VU0103650		10.5	NA	NA
VU0077914		10.2	NA	NA	VU0111472		10.5	NA	NA
VU0132027		10.2	NA	NA	VU0111935		10.5	NA	NA
VU0114374		10.2	NA	NA	VU0116831		10.6	NA	NA
VU0072160		10.2	NA	NA	VU0116768		10.6	NA	NA
VU0054740		10.2	NA	NA	VU0115375		10.6	NA	NA
VU0359105		10.3	NA	NA	VU0117236		10.6	NA	NA

VU identifier	Structure	BH IC50 (μM)	D6 IC50 (uM)	C235 IC50 (uM)	VU identifier	Structure	BH IC50 (μM)	D6 IC50 (uM)	C235 IC50 (uM)
VU0040094		10.7	NA	NA	VU0066838		11.5	NA	NA
VU0114047		10.7	NA	NA	VU0116999		11.5	NA	NA
VU0077905		10.7	NA	NA	VU0027639		11.5	NA	NA
VU0014485		10.7	NA	NA	VU0002183		11.5	NA	NA
VU0127435		10.8	NA	NA	VU0007003		11.7	NA	NA
VU0116930		10.8	NA	NA	VU0118085		11.7	NA	NA
VU0069898		11.1	NA	NA	VU0127434		11.8	NA	NA
VU0003689		11.1	NA	NA	VU0071475		11.8	NA	NA
VU0278822		11.1	NA	NA	VU0108767		11.9	NA	NA
VU0121875		11.2	NA	NA	VU0124020		11.9	NA	NA
VU0084725		11.5	NA	NA	VU0032098		12.0	NA	NA
VU0075742		11.5	NA	NA	VU0081459		12.1	NA	NA
VU0121459		11.5	NA	NA	VU0115384		12.2	NA	NA

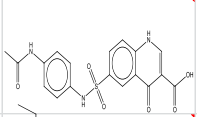
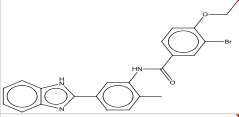
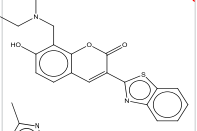
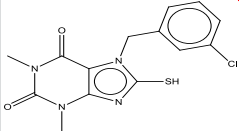
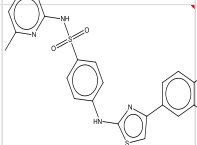
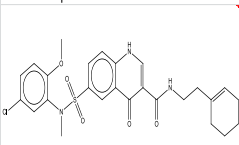
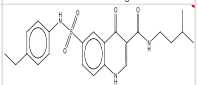
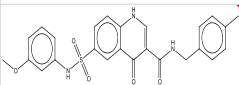
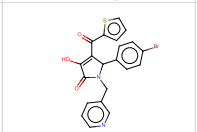
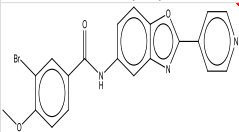
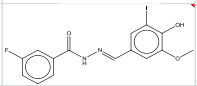
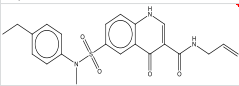
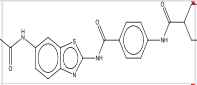
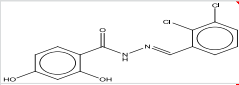
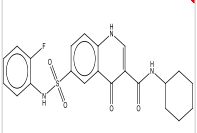
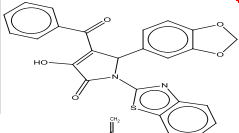
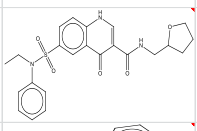
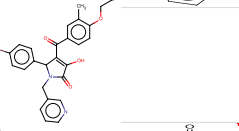
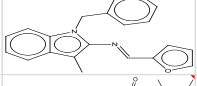
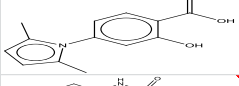
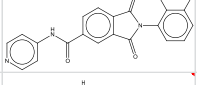
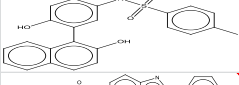
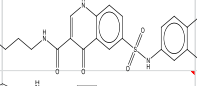
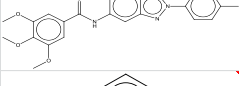
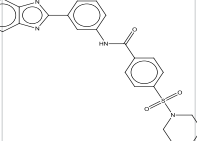
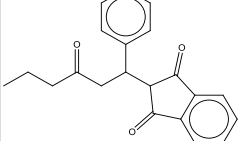
VU identifier	Structure	BH IC50 (μM)	D6 IC50 (uM)	C235 IC50 (uM)	VU identifier	Structure	BH IC50 (μM)	D6 IC50 (uM)	C235 IC50 (uM)
VU0012095		12.2	NA	NA	VU0130575		12.7	NA	NA
VU0131032		12.3	NA	NA	VU0114899		12.7	NA	NA
VU0096684		12.3	NA	NA	VU0116914		13.0	NA	NA
VU0001572		12.4	NA	NA	VU0036008		13.0	NA	NA
VU0081154		12.4	NA	NA	VU0009704		13.2	NA	NA
VU0126984		12.4	NA	NA	VU0093665		13.3	NA	NA
VU0081374		12.4	NA	NA	VU0117238		13.5	NA	NA
VU0002339		12.5	NA	NA	VU0043100		13.8	NA	NA
VU0107012		12.5	NA	NA	VU0117269		13.9	NA	NA
VU0044509		12.5	NA	NA	VU0096132		14.0	NA	NA
VU0129453		12.6	NA	NA	VU0129810		14.1	NA	NA
VU0033894		12.6	NA	NA	VU0079933		14.3	NA	NA
VU0085716		12.6	NA	NA	VU0359073		14.4	NA	NA

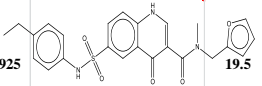
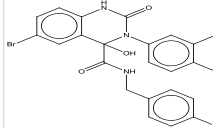
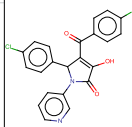
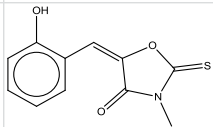
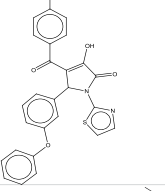
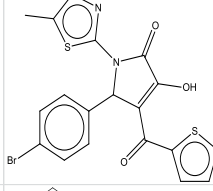
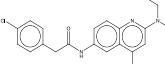
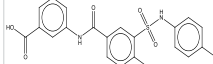
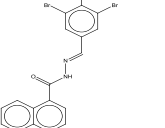
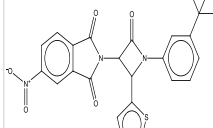
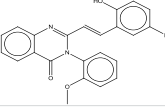
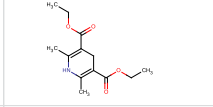
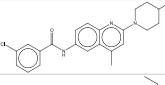
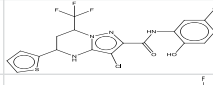
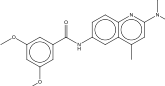
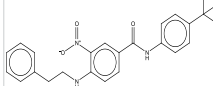
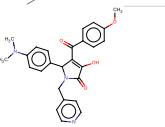
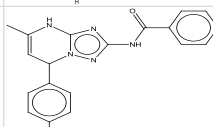
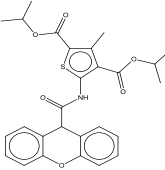
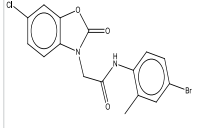
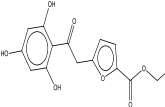
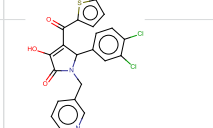
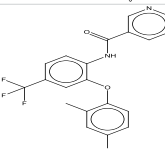
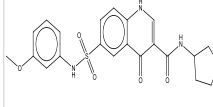
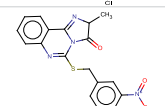
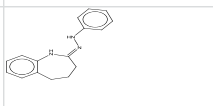
VU identifier	Structure	BH IC50 (μM)	D6 IC50 (uM)	C235 IC50 (uM)	VU identifier	Structure	BH IC50 (μM)	D6 IC50 (uM)	C235 IC50 (uM)
VU0111889		14.4	NA	NA	VU0056471		15.4	NA	NA
VU0081419		14.4	NA	NA	VU0144620		15.4	NA	NA
VU0129383		14.6	NA	NA	VU0077916		15.4	NA	NA
VU0144628		14.7	NA	NA	VU0107256		15.5	NA	NA
VU0085220		14.8	NA	NA	VU0041101		15.5	NA	NA
VU0012439		14.8	NA	NA	VU0117228		15.5	NA	NA
VU0059085		14.9	NA	NA	VU0034663		15.6	NA	NA
VU0111482		15.0	NA	NA	VU0115410		15.6	NA	NA
VU0021348		15.1	NA	NA	VU0118489		15.7	NA	NA
VU0020915		15.1	NA	NA	VU0011772		15.7	NA	NA
VU0106675		15.1	NA	NA	VU0063881		15.7	NA	NA
VU0002175		15.3	NA	NA	VU0056490		15.7	NA	NA
VU0115364		15.4	NA	NA	VU0107321		15.7	NA	NA

VU identifier	Structure	BH IC50 (μM)	D6 IC50 (uM)	C235 IC50 (uM)	VU identifier	Structure	BH IC50 (μM)	D6 IC50 (uM)	C235 IC50 (uM)
VU0065728		15.8	NA	NA	VU0126679		16.3	NA	NA
VU0118468		15.8	NA	NA	VU0130142		16.3	NA	NA
VU0065261		15.9	NA	NA	VU0027357		16.3	NA	NA
VU0068296		16.0	NA	NA	VU0119378		16.5	NA	NA
VU0115403		16.0	NA	NA	VU0064134		16.5	NA	NA
VU0038391		16.0	NA	NA	VU0121592		16.5	NA	NA
VU0021346		16.1	NA	NA	VU0144631		16.5	NA	NA
VU0113028		16.1	NA	NA	VU0124726		16.6	NA	NA
VU0126071		16.1	NA	NA	VU0122285		16.6	NA	NA
VU0085686		16.1	NA	NA	VU0111422		16.7	NA	NA
VU0013761		16.2	NA	NA	VU0012266		16.8	NA	NA
VU0126098		16.2	NA	NA	VU0142474		16.8	NA	NA
VU0039845		16.3	NA	NA	VU0094292		16.8	NA	NA

VU identifier	Structure	BH IC50 (μM)	D6 IC50 (uM)	C235 IC50 (uM)	VU identifier	Structure	BH IC50 (μM)	D6 IC50 (uM)	C235 IC50 (uM)
VU0119875		16.8	NA	NA	VU0114368		17.7	NA	NA
VU0115363		16.8	NA	NA	VU0073649		17.7	NA	NA
VU0066848		16.9	NA	NA	VU0116810		17.7	NA	NA
VU0081336		16.9	NA	NA	VU0004714		17.8	NA	NA
VU0117912		16.9	NA	NA	VU0040765		17.8	NA	NA
VU0121430		17.0	NA	NA	VU0144658		17.9	NA	NA
VU0032772		17.1	NA	NA	VU0111492		17.9	NA	NA
VU0122624		17.2	NA	NA	VU0115411		18.0	NA	NA
VU0007148		17.2	NA	NA	VU0100428		18.0	NA	NA
VU0079952		17.5	NA	NA	VU0105577		18.0	NA	NA
VU0014378		17.5	NA	NA	VU0112701		18.1	NA	NA
VU0081509		17.5	NA	NA	VU0056444		18.1	NA	NA
VU0129851		17.6	NA	NA	VU0032672		18.1	NA	NA

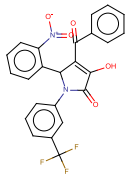
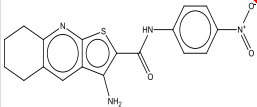
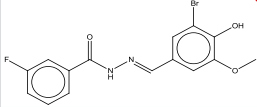
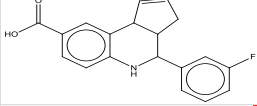
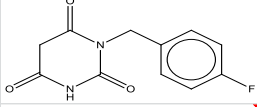
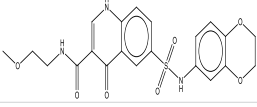


VU identifier	Structure	BH IC50 (μM)	D6 IC50 (uM)	C235 IC50 (uM)	VU identifier	Structure	BH IC50 (μM)	D6 IC50 (uM)	C235 IC50 (uM)
VU0108788		18.1	NA	NA	VU0098218		18.7	NA	NA
VU0036021		18.3	NA	NA	VU0126775		18.8	NA	NA
VU0099192		18.3	NA	NA	VU0115402		18.8	NA	NA
VU0116788		18.3	NA	NA	VU0144648		18.8	NA	NA
VU0039979		18.3	NA	NA	VU0063850		18.9	NA	NA
VU0014482		18.4	NA	NA	VU0115337		19.0	NA	NA
VU0123289		18.4	NA	NA	VU0013754		19.1	NA	NA
VU0111452		18.5	NA	NA	VU0096454		19.1	NA	NA
VU0117197		18.5	NA	NA	VU0129861		19.1	NA	NA
VU0006754		18.6	NA	NA	VU0123064		19.1	NA	NA
VU0003020		18.6	NA	NA	VU0096640		19.2	NA	NA
VU0111483		18.6	NA	NA	VU0121419		19.4	NA	NA
VU0124864		18.7	NA	NA	VU0013046		19.4	NA	NA

VU identifier	Structure	BH IC50 ( $\mu$ M)	D6 IC50 ( $\mu$ M)	C235 IC50 ( $\mu$ M)	VU identifier	Structure	BH IC50 ( $\mu$ M)	D6 IC50 ( $\mu$ M)	C235 IC50 ( $\mu$ M)
VU0077925		19.5	NA	NA	VU0073548		21.1	NA	NA
VU0126110		19.8	NA	NA	VU0006654		21.2	NA	NA
VU0129368		19.9	NA	NA	VU0129435		21.2	NA	NA
VU0107217		19.9	NA	NA	VU0052922		21.3	NA	NA
VU0012474		20.0	NA	NA	VU0123478		21.3	NA	NA
VU0122895		20.1	NA	NA	VU0007198		21.4	NA	NA
VU0140504		20.1	NA	NA	VU0057227		21.4	NA	NA
VU0107207		20.1	NA	NA	VU0081513		21.4	NA	NA
VU0096208		20.3	NA	NA	VU0098283		21.5	NA	NA
VU0101667		20.6	NA	NA	VU0117902		21.5	NA	NA
VU0121695		20.7	NA	NA	VU0040105		21.5	NA	NA
VU0103752		21.1	NA	NA	VU0144638		21.5	NA	NA
VU0113020		21.1	NA	NA	VU0009666		21.6	NA	NA

VU identifier	Structure	BH IC50 ( $\mu$ M)	D6 IC50 ( $\mu$ M)	C235 IC50 ( $\mu$ M)	VU identifier	Structure	BH IC50 ( $\mu$ M)	D6 IC50 ( $\mu$ M)	C235 IC50 ( $\mu$ M)
VU0126100		21.6	NA	NA	VU0074030		22.5	NA	NA
VU0079943		21.6	NA	NA	VU0096096		22.8	NA	NA
VU0116821		21.7	NA	NA	VU0144689		22.9	NA	NA
VU0073595		21.8	NA	NA	VU0041042		22.9	NA	NA
VU0138061		21.8	NA	NA	VU0098292		22.9	NA	NA
VU0034579		21.9	NA	NA	VU0131180		22.9	NA	NA
VU0017272		21.9	NA	NA	VU0145035		22.9	NA	NA
VU0096660		22.0	NA	NA	VU0100692		23.0	NA	NA
VU0129392		22.2	NA	NA	VU0073581		23.1	NA	NA
VU0118672		22.2	NA	NA	VU0073600		23.2	NA	NA
VU0123062		22.2	NA	NA	VU0034723		23.3	NA	NA
VU0146006		22.3	NA	NA	VU0138545		23.3	NA	NA
VU0144670		22.4	NA	NA	VU0122993		23.4	NA	NA

VU identifier	Structure	BH IC50 (μM)	D6 IC50 (uM)	C235 IC50 (uM)	VU identifier	Structure	BH IC50 (μM)	D6 IC50 (uM)	C235 IC50 (uM)
VU0006922		23.5	NA	NA	VU0039282		24.9	NA	NA
VU0013989		23.5	NA	NA	VU0107063		24.9	NA	NA
VU0002472		23.5	NA	NA	VU0108757		24.9	NA	NA
VU0129358		23.6	NA	NA	VU0126155		25.1	NA	NA
VU0072340		24.0	NA	NA	VU0101576		25.1	NA	NA
VU0068654		24.1	NA	NA	VU0117005		25.4	NA	NA
VU0077976		24.1	NA	NA	VU0142741		25.5	NA	NA
VU0010417		24.2	NA	NA	VU0358733		25.6	NA	NA
VU0006925		24.3	NA	NA	VU0112721		25.7	NA	NA
VU0115360		24.6	NA	NA	VU0111442		25.9	NA	NA
VU0034696		24.8	NA	NA	VU0115383		26.0	NA	NA
VU0129961		24.8	NA	NA	VU0039141		26.2	NA	NA
VU0138186		24.8	NA	NA	VU0005198		26.4	NA	NA

VU identifier	Structure	BH IC50 ( $\mu$ M)	D6 IC50 ( $\mu$ M)	C235 IC50 ( $\mu$ M)
VU0070650		26.6		ND
VU0126943		26.7		ND
VU0014486		26.9		ND
VU0069013		26.9		ND
VU0017645		26.9		ND
VU0077927		27.0		ND

## Appendix E

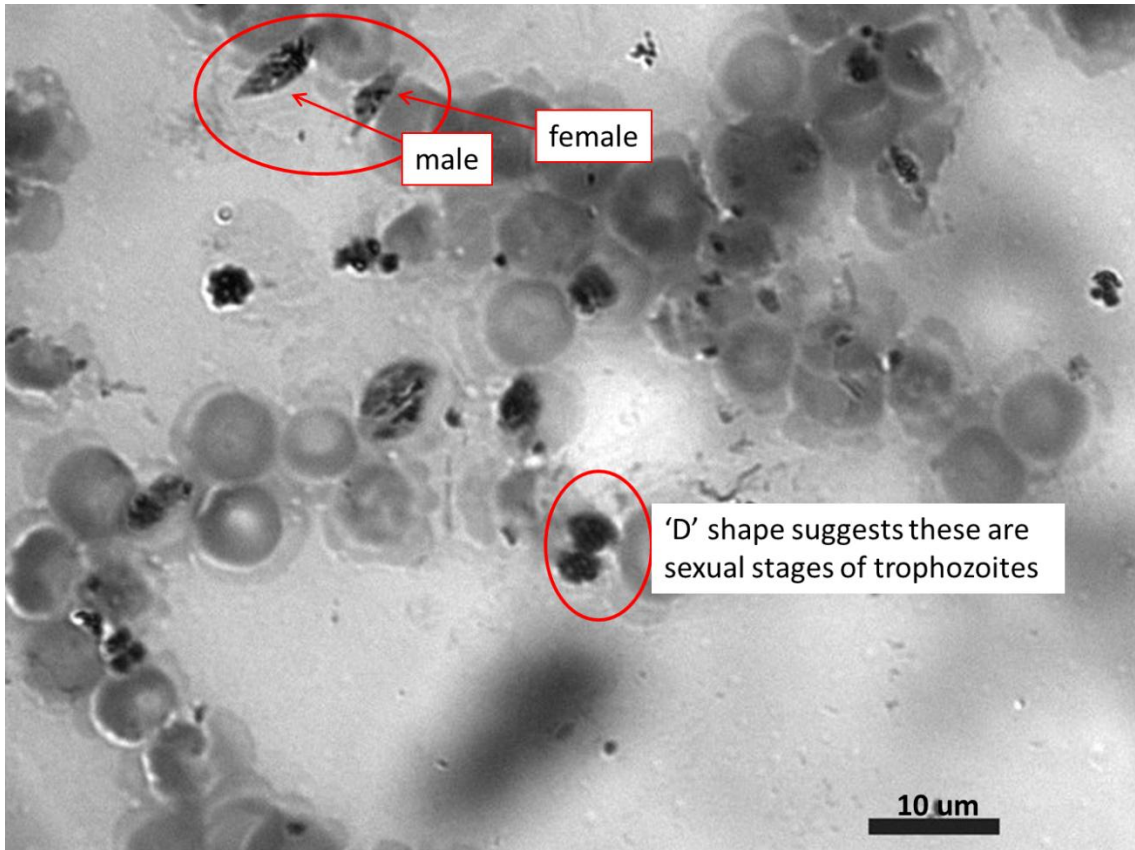
### Gametocyte Culturing Protocol

Under normal culturing conditions (Appendix B), the parasite is observed almost exclusively in the asexual form. However, procedures exist that allow manipulation of culture conditions to encourage sexual forms of the parasite to dominate.<sup>67</sup> The D6 strain was successfully cultured to promote gametocyte development using a combination of different reported methods. The idea is to take advantage of the differential life cycles of sexual v asexual forms. Asexual forms of the parasite complete a life cycle every 48 h, whereas sexual forms (gametocytes) take 7-10 days to mature. Since merozoites do not reinfect old red blood cells very well, the sexual form of the parasite will slowly start to dominate as the asexual form begins to die.

Culture medium and 50% Hct blood should be prepared as described in Appendix B except rather than adding 4.5 mL of medium, 7 mL of medium should be added (Final volume of 7.5 mL). *The blood should be as fresh as possible, preferably obtained from a donor no more than 7 days from beginning the gametocyte culture schedule.* To promote gametocyte production/survival, medium must be prewarmed to 37°C and exchanged daily at the same time each day. Medium exchange must be performed quickly as a decrease in culture temperature will compromise gametocyte survival. Also, after day 5, be careful not to agitate the erythrocytes in the bottom of the flask.

After five days of exchanging the medium, the culture should be stained every other day to monitor gametocyte production. Also, the amount of media in culture was

reduced from 7.5 mL to 5mL. Using the procedure described here, the first gametocyte was observed on day 9 (day 1 = the day cultures were initiated). The gametocytes are elongated relative to asexual forms of the parasite and exist as stage I-V gametocytes. (*Note* - Stage I-III gametocytes resemble the asexual form of the parasite) The population of gametocytes increased and by day 16, both male and female gametocytes were observed. Importantly, mature gametocytes (Stage IV, Figure 40) were observed on this day. As CQ is not toxic to mature gametocytes, the culture was treated with 50 nm CQ overnight to selectively kill the asexual forms of the parasite without disturbing the gametocytes.



DAY 16

**Figure 40.** On day 16, gametocytes were the primary form of the parasite in culture. The blobs that do not resemble the parasite are crystals of hemozoin which visible accumulated in the culture flask by Day 9.

On day 18 of using this protocol, gametocytes dominated the culture and 50% parasitemia was observed.



## Appendix F

### Top 250 $\beta$ -Hematin Inhibitors Identified in the GSK In vitro antimalarial Library

The compounds inhibiting >90%  $\beta$ -hematin formation are listed here and identified by the TCMDC number supplied by GSK. The % Inhibitory activity of each compound in the  $\beta$ -hematin formation assay is included. SMILES information for each of the TCMDC identifiers is available free online at:

<http://www.nature.com/nature/journal/v465/n7296/full/nature09107.html#/supplementary-information>)

Refer to supplementary Table 1 for a complete list.

Identifier	Average % Inhibition in beta-hematin assay	uM Parasite Activity (reported in ChemBL)	Identifier	Average % Inhibition in beta-hematin assay	uM Parasite Activity (reported in ChemBL)
TCMDC-140344	104	0.514	TCMDC-132862	100	0.910
TCMDC-124423	104	0.378	TCMDC-136243	100	0.888
TCMDC-139205	103	0.530	TCMDC-137983	100	0.395
TCMDC-137481	103	0.152	TCMDC-132558	100	0.194
TCMDC-137869	103	0.168	TCMDC-132135	100	0.633
TCMDC-123680	103	0.267	TCMDC-138432	100	0.237
TCMDC-134493	103	0.860	TCMDC-125364	100	0.646
TCMDC-137446	102	0.628	TCMDC-141388	100	0.121
TCMDC-137059	102	0.735	TCMDC-132846	100	0.119
TCMDC-137072	102	0.651	TCMDC-140319	100	1.168
TCMDC-140347	102	0.894	TCMDC-125274	100	1.090
TCMDC-141560	102	0.801	TCMDC-138898	100	0.925
TCMDC-123692	102	0.814	TCMDC-132571	100	0.396
TCMDC-138197	102	0.174	TCMDC-135405	100	0.138
TCMDC-136853	102	1.087	TCMDC-141338	100	0.978
TCMDC-141332	102	1.321	TCMDC-136152	100	0.828
TCMDC-125530	102	0.659	TCMDC-141609	100	0.272
TCMDC-132178	102	0.793	TCMDC-138486	100	0.132
TCMDC-132167	102	0.313	TCMDC-139550	100	0.114
TCMDC-132419	101	0.090	TCMDC-138911	100	0.751
TCMDC-141585	101	0.531	TCMDC-137092	100	0.958
TCMDC-138391	101	0.208	TCMDC-136781	100	0.731
TCMDC-132130	101	0.161	TCMDC-137212	100	0.035
TCMDC-125671	101	0.614	TCMDC-142308	100	0.873
TCMDC-133941	101	0.153	TCMDC-136965	100	0.236
TCMDC-136993	101	0.627	TCMDC-135688	100	0.832
TCMDC-136966	101	0.497	TCMDC-135945	100	0.840
TCMDC-132201	101	0.410	TCMDC-136287	100	0.122
TCMDC-138752	101	0.278	TCMDC-138696	99	0.716
TCMDC-136862	101	0.733	TCMDC-132192	99	0.323
TCMDC-136831	101	0.265	TCMDC-135250	99	0.975
TCMDC-138520	101	0.335	TCMDC-124969	99	0.647
TCMDC-138446	101	0.110	TCMDC-132141	99	0.789
TCMDC-139618	101	0.788	TCMDC-137180	99	1.477
TCMDC-139725	101	0.117	TCMDC-139008	99	1.161
TCMDC-141612	101	0.736	TCMDC-136998	99	0.596
TCMDC-125788	101	0.761	TCMDC-136145	99	0.804
TCMDC-137087	101	0.630	TCMDC-136859	99	0.585
TCMDC-139498	101	0.314	TCMDC-141611	99	0.859
TCMDC-132710	100	0.148	TCMDC-138557	99	0.776
TCMDC-132159	100	0.302	TCMDC-125505	99	0.774
TCMDC-124421	100	0.718	TCMDC-136830	99	0.065
TCMDC-131238	100	0.927	TCMDC-123466	99	0.277
TCMDC-137063	100	0.167	TCMDC-133257	99	0.630

Identifier	Average % Inhibition in beta-hematin assay	uM Parasite Activity (reported in ChemBL)	Identifier	Average % Inhibition in beta-hematin assay	uM Parasite Activity (reported in ChemBL)
TCMDC-136923	99	0.612	TCMDC-133194	98	0.104
TCMDC-138451	99	0.186	TCMDC-141399	97	0.762
TCMDC-135507	99	0.174	TCMDC-137135	97	0.715
TCMDC-124526	99	1.588	TCMDC-137125	97	0.182
TCMDC-136194	99	1.510	TCMDC-139410	97	0.256
TCMDC-141000	99	0.135	TCMDC-136195	97	0.669
TCMDC-138298	99	0.048	TCMDC-132915	97	0.062
TCMDC-136382	99	0.621	TCMDC-132131	97	0.889
TCMDC-132898	99	0.184	TCMDC-135373	97	0.616
TCMDC-125529	99	0.830	TCMDC-132829	97	0.772
TCMDC-132729	99	0.130	TCMDC-141610	97	0.287
TCMDC-132753	99	0.956	TCMDC-138430	97	0.770
TCMDC-132910	99	0.200	TCMDC-136906	97	1.088
TCMDC-133171	99	0.756	TCMDC-136951	97	0.688
TCMDC-139502	99	0.063	TCMDC-135456	97	0.832
TCMDC-137120	99	0.552	TCMDC-133699	97	0.738
TCMDC-135054	99	0.930	TCMDC-124972	97	1.054
TCMDC-137137	99	0.505	TCMDC-135305	97	0.213
TCMDC-133702	99	0.534	TCMDC-136992	97	0.635
TCMDC-132188	98	0.577	TCMDC-139871	96	0.776
TCMDC-138686	98	0.818	TCMDC-141978	96	0.983
TCMDC-125577	98	0.524	TCMDC-133935	96	0.147
TCMDC-133932	98	0.142	TCMDC-133940	96	0.142
TCMDC-132145	98	0.452	TCMDC-137503	96	0.661
TCMDC-137034	98	0.857	TCMDC-132997	96	0.867
TCMDC-137582	98	0.104	TCMDC-136922	96	0.363
TCMDC-133009	98	0.308	TCMDC-123506	96	0.134
TCMDC-140797	98	0.895	TCMDC-132897	96	0.138
TCMDC-137094	98	0.289	TCMDC-137902	96	0.376
TCMDC-124146	98	0.871	TCMDC-136820	96	0.204
TCMDC-136837	98	0.726	TCMDC-132160	96	0.557
TCMDC-142040	98	0.202	TCMDC-123486	95	0.512
TCMDC-132405	98	0.119	TCMDC-125415	95	0.258
TCMDC-136193	98	0.941	TCMDC-137131	95	0.232
TCMDC-140681	98	0.464	TCMDC-140367	95	0.734
TCMDC-139268	98	0.158	TCMDC-133007	95	0.167
TCMDC-137480	98	0.104	TCMDC-134151	95	0.149
TCMDC-132566	98	0.255	TCMDC-141392	95	0.617
TCMDC-137129	98	0.185	TCMDC-132844	95	0.139
TCMDC-138205	98	0.111	TCMDC-133042	95	0.146
TCMDC-139559	98	1.006	TCMDC-125600	95	0.168
TCMDC-132189	98	0.829	TCMDC-132849	95	0.117
TCMDC-133701	98	0.240	TCMDC-136940	95	1.025
TCMDC-132320	98	0.519	TCMDC-132028	95	0.167

Identifier	Average % Inhibition in beta-hematin assay	uM Parasite Activity (reported in ChemBL)	Identifier	Average % Inhibition in beta-hematin assay	uM Parasite Activity (reported in ChemBL)
TCMDC-136818	95	0.990	TCMDC-139406	92	0.695
TCMDC-135557	95	0.279	TCMDC-131914	92	0.601
TCMDC-138256	94	0.445	TCMDC-140827	92	0.759
TCMDC-133460	94	0.978	TCMDC-133136	92	0.170
TCMDC-132845	94	0.099	TCMDC-136824	92	0.134
TCMDC-142335	94	0.253	TCMDC-136954	92	0.789
TCMDC-138660	94	0.608	TCMDC-140540	91	0.684
TCMDC-124127	94	1.117	TCMDC-137037	91	0.581
TCMDC-133422	94	0.086	TCMDC-132821	91	0.607
TCMDC-133550	94	0.837	TCMDC-137793	91	0.143
TCMDC-133705	94	0.572	TCMDC-135248	91	0.570
TCMDC-133044	94	0.140	TCMDC-133052	91	0.215
TCMDC-135478	94	0.197	TCMDC-134161	91	0.981
TCMDC-132143	94	1.743	TCMDC-133155	91	0.715
TCMDC-132906	94	0.156	TCMDC-124822	91	0.874
TCMDC-142048	94	0.030	TCMDC-136941	91	0.797
TCMDC-125220	94	0.799	TCMDC-123601	91	0.890
TCMDC-136913	94	0.643	TCMDC-135542	91	0.109
TCMDC-139383	93	0.573	TCMDC-136927	91	0.228
TCMDC-136970	93	1.045	TCMDC-137067	91	0.670
TCMDC-138659	93	0.915	TCMDC-137110	90	0.413
TCMDC-137068	93	0.645	TCMDC-132695	90	0.907
TCMDC-133135	93	0.277	TCMDC-136819	90	0.238
TCMDC-140218	93	0.911	TCMDC-140889	90	1.172
TCMDC-141561	93	1.018	TCMDC-136960	90	0.681
TCMDC-141584	93	0.344	TCMDC-133158	90	0.231
TCMDC-132958	93	0.157	TCMDC-136957	90	0.719
TCMDC-135406	93	0.111	TCMDC-132840	90	0.670
TCMDC-138467	93	0.557	TCMDC-140648	90	1.120
TCMDC-136914	92	0.454	TCMDC-133177	90	0.199
TCMDC-132144	92	0.767			
TCMDC-137136	92	0.388			
TCMDC-135912	92	0.754			
TCMDC-132854	92	0.115			
TCMDC-132947	92	0.156			
TCMDC-137304	92	1.144			
TCMDC-135247	92	0.698			
TCMDC-136946	92	0.806			
TCMDC-132120	92	1.244			
TCMDC-135360	92	0.906			
TCMDC-132857	92	0.170			
TCMDC-136961	92	0.278			
TCMDC-133210	92	0.351			
TCMDC-137065	92	0.560			

200 11<sup>th</sup> Avenue N., Apt. 420  
Nashville, TN 37203

rebecca.sandlin@vanderbilt.edu  
Cell: (615) 415-1882

---

### EDUCATION

---

**Doctor of Philosophy, Chemistry** 2012  
Vanderbilt University (Nashville, TN) Advisor: David W. Wright

**Bachelor of Science, Chemistry and Mathematics** 2007  
Western Kentucky University (Bowling Green, KY) Advisor: Kevin M. Williams

---

### RESEARCH EXPERIENCE

---

Vanderbilt University, Nashville, TN Dept. of Chemistry  
2008 - current  
Graduate Research Assistant

Western Kentucky University, Bowling Green, KY Dept. of Chemistry  
2004-2007  
Research Assistant

---

### PUBLICATIONS

---

1. **Sandlin, Rebecca D.**; Wicht, Kathryn; Wright, Egan, Timothy; David W. Identification of  $\beta$ -Hematin Inhibitors in a High-Throughput Screening Effort Reveals Scaffolds with *In Vitro* Antimalarial Activity. *Submitted*
2. **Sandlin, Rebecca D.**; Carrell, Holly; Wright, David W. Hemozoin: Crystal Engineering Survivability. *Wiley Encyclopedia of Inorganic and Bioinorganic Chemistry* (2012), *Accepted*.
3. **Sandlin, Rebecca D.**; Whelan, Celia J.; Bradley, M. S.; Williams, Kevin M. Effects of amine ligand bulk and hydrogen bonding on the rate of reaction of platinum(II) diamine complexes with key nucleotide and amino acid residues (2012). *Inorganica Chimica Acta*, doi: 10.1016/j.ica.2012.05.008
4. **Sandlin, Rebecca D.**; Carter, Melissa D.; Lee, Patricia J.; Auschwitz, Jennifer M.; Leed, Susan E.; Johnson, Jacob D.; Wright, David W. Use of the NP-40 detergent-mediated assay in discovery of inhibitors of  $\beta$ -hematin crystallization. *Antimicrobial Agents and Chemotherapy*, 55(7), 3363-3369 (2011).
5. **Sandlin, Rebecca D.**; Starling, Michael P.; Williams, Kevin M. A bulky platinum triamine complex that reacts faster with guanosine 5'-monophosphate than with N-acetylmethionine. *Journal of Inorganic Biochemistry*, 104(2), 214-216 (2010).

6. Slocum, D.; Reinscheld, T.; White, C.; Timmons, M.; Shelton, P.; Slocum, M.; **Sandlin, Rebecca D.**; *et al.* ortho-Lithiations Reassessed; the Advantages of Deficiency Catalysis in Hydrocarbon Media. *Organometallics*. *Accepted* (2013)
7. Hoang, Anh N.; **Sandlin, Rebecca D.**; Omar, Aneesa; Egan, Timothy J.; Wright, David W. The neutral lipid composition present in the digestive vacuole of *Plasmodium falciparum* concentrates heme and mediates  $\beta$ -hematin formation with an unusually low activation energy. *Biochemistry*, 49(47), 10107-10116 (2010).
8. Carter, Melissa D.; Phelan, Vanessa V.; **Sandlin, Rebecca D.**; Bachmann, Brian O.; Wright, David W. Lipophilic mediated assays for  $\beta$ -hematin inhibitors. *Combinatorial Chemistry & High Throughput Screening*, 13(3), 285-292 (2010).
9. Slocum, D. W.; Reece, Troy L.; **Sandlin, Rebecca D.**; Reinscheld, Thomas K.; Whitley, Paul E. Metalations utilizing aryllithiums; ortho-functionalization of *p*-bromoanisole (pBrA). *Tetrahedron Letters*, 50(14), 1593-1595 (2009).

#### PUBLICATIONS IN PREPARATION

10. Butkiewicz, Mariusz;\* **Sandlin, Rebecca D.**;\* Meiler, Jens; Wright, David W. Application of Machine Learning Techniques Reveals Pathway Specific Inhibitors for  $\beta$ -Hematin Crystallization in *Plasmodium falciparum*.
11. **Sandlin, Rebecca D.**; Wicht, Kathryn; Wright, David W. SAR Analysis of Benzimidazole Inhibitors of  $\beta$ - Hematin Formation.
12. **Sandlin, Rebecca D.**; Stiebler, Renata; Oliviera, Marcus; Wright, David W. Analysis of Detergent-Mediated  $\beta$ -Hematin Formation.
13. Butkiewicz, Mariusz;\* **Sandlin, Rebecca D.**;\* Meiler, Jens; Wright, David W. Self-Organizing Maps Reveal Pathway Specific Antiplasmodials.
14. **Sandlin, Rebecca D.**;\* Kim Fong\*, Omar, Aneesa; Wright, David W.; Egan, Timothy. Identification of  $\beta$ -Hematin Inhibitors in the TCAMS Data Set.

\* Authors contributes equally

#### HONORS AND AWARDS

Vanderbilt University Chemical Biology Research Symposium, Poster Award	2012
Keystone Symposia Conference (J1), Award for Poster	2012
Keystone Symposia Conference (J1), Travel Grant	2012
Selected as a Graduate Teaching Fellow, Vanderbilt University	2010
Outstanding Graduating Senior in Chemistry	2007
Sigma Xi Student Research Conference, 1 <sup>st</sup> place, oral presentation	2007
Kentucky Academy of Sciences Meeting, 2 <sup>nd</sup> place, oral presentation	2006
Sigma Xi Student Research Conference, 2 <sup>nd</sup> place, oral presentation	2006
C.P. McNally award for most outstanding chemistry undergraduate	2006
Sigma Xi Student Research Conference, 2 <sup>nd</sup> place, poster presentation	2005
Elected to Pi Mu Epsilon Mathematics Society	2005

## TEACHING

---

### Vanderbilt University (Nashville, TN)

- Teaching Fellow, Undergraduate Chemistry Recitation, Fall 2009 – Spring 2010
- General Chemistry Laboratory Fall 2008- Spring 2009.

## PRESENTATIONS

---

1. R. D. Sandlin et al. Finding the Pathway: New Machine Learning Paradigms for the Identification of Lead Compound Targets from Phenotypic Antimalarial Assays. *Keystone Symposia (J1), Santa Fe, NM, USA 2012*. Poster presentation.
2. R. D. Sandlin et al. A Virtual High-Throughput Approach to the Identification of Antiplasmodial Hemozoin Inhibitors. *15th International Conference for Biological Inorganic Chemistry, Vancouver, BC, Canada; 2011*. Poster presentation.
3. R. D. Sandlin et al. Factors affecting the rate of reaction of platinum anticancer drug models with DNA and protein targets. *37th annual student research conference, Bowling Green, KY, USA 2007*. Oral presentation.
4. R. D. Sandlin et al. Factors affecting the rate of reaction of platinum(II) complexes with DNA and protein targets. *233rd Annual American Chemical Society Meeting, Chicago, IL, USA 2007*. Poster presentation.
5. R. D. Sandlin et al. "Factors affecting the rate of reaction of platinum(II) complexes with DNA and protein targets". *92nd Annual Kentucky Academy of Science Meeting, Morehead, KY, USA, 2006*. Oral presentation
6. R. D. Sandlin et al. Effects of amine ligand bulk on the rate of reaction of platinum(II) diamine complexes with guanine and methionine residues. *36th annual student research conference, Bowling Green, KY, USA 2006*. Oral presentation.
7. R. D. Sandlin et al. Effects of amine ligand bulk on the rate of reaction of platinum(II) diamine complexes with guanine and methionine residues. *231st Annual American Chemical Society Meeting, Atlanta, GA, USA 2006*. Poster presentation.
8. R. D. Sandlin et al. Effects of amine ligand bulk on the rate of reaction of platinum(II) diamine complexes with guanine and methionine residues. *91st Annual Kentucky Academy of Science Meeting, Richmond, KY, USA 2005*. Oral Presentation
9. R. D. Sandlin et al. Effects of amine ligand bulk in platinum diamine complexes on the rate of reaction with DNA and protein residues. *35th annual student research conference, Bowling Green, KY, USA, 2005*. Poster presentation.
10. R. D. Sandlin et al. Effects of amine ligand bulk in platinum diamine complexes on the rate of reaction with DNA and protein residues. *229th Annual American Chemical Society Meeting, San Diego, CA, USA, 2005*. Poster presentation.
11. R. D. Sandlin et al. Effects of Amine Ligand Bulk on the Rate of Reaction with DNA and Protein Residues by Platinum Complexes. *90th Annual Kentucky Academy of Science Meeting, Murray, KY, USA, 2004*. Poster presentation.